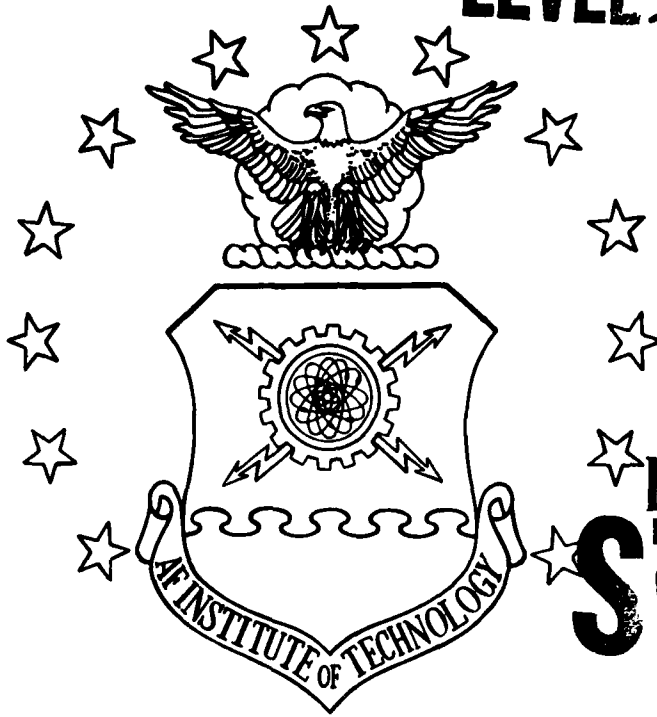


LEVEL II

①

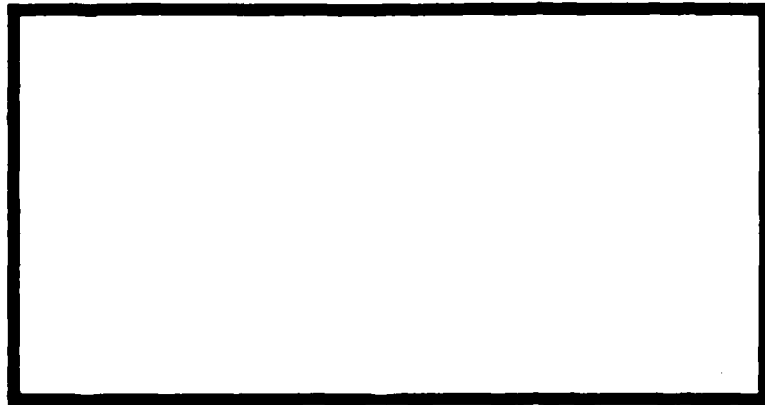
AD A111122



DTIC
 ELECTE
 FEB 19 1982

S

E



DTIC FILE COPY

UNITED STATES AIR FORCE
 AIR UNIVERSITY
 AIR FORCE INSTITUTE OF TECHNOLOGY
 Wright-Patterson Air Force Base, Ohio

82 02 18 074

This document has been approved
 for public release and sale; its
 distribution is unlimited.

AFIT/GAE/AA/81D-10

ELASTIC-PLASTIC FINITE ELEMENT
MODEL COMPARISONS IN
FRACTURE MECHANICS

THESIS

AFIT/GAE/AA/81D-10

Howard D. Gans
2nd Lt USAF

Approved for public release; distribution unlimited

Acknowledgments

I would like to express my deepest gratitude to Professor A. N. Palazotto for his patience, technical guidance and encouragement during the course of this work, and for suggesting the topic. I would also like to thank Dr. T. Nicholas of the Air Force Wright Aeronautical Laboratory for his helpful suggestions, for sponsoring this study, and for supplying the computer resources that were necessary to complete this thesis. Thanks also go to Capt. H. C. Briggs and Capt. J. Marsh for their valuable suggestions and interest in the topic. Appreciation is extended to Capt. T. Hinnerichs and Dr. A. Jalese for the use of their programs, their careful explanations and helpful suggestions.

I especially want to express my deepest appreciation to my wife, Hillary, for her loving support, encouragement, and understanding.

Contents

	Page
Acknowledgments	ii
List of Figures	iv
List of Tables	vii
List of Symbols	viii
Abstract	xi
I. Introduction	1
II. Objective	3
III. Theoretical Formulation	9
Theory of Plasticity	9
Elastic-Plastic Solution Technique	14
Viscoplastic Material Models	16
Viscoplastic Solution Procedure	21
Fracture Mechanics	25
Linear Elastic Fracture Mechanics (LEFM)	25
The Crack Tip Element	26
Plasticity within the Singularity Elements	29
IV. Results and Discussion	32
Time Independence vs. Time Dependence	32
Mesh Arrangement	33
Elastic Analysis-Stress Intensity Factor	46
Numerical Evaluation of K_I	48
Plastic Analysis	52
Computational Comparisons	74
V. Conclusions	78
Bibliography	81
Appendix A: The Finite Element Method	83
Appendix B: Calculation of Equivalent Nodal Forces	106
Appendix C: Users Guide for JALESE	112
Vita	119

List of Figures

Figure		Page
1	Stress vs. Strain Curve for an Elastic, Perfectly Plastic Material	4
2	Stress vs. Strain Curve for an Elastic-Plastic Material with Strain Hardening	5
3	Center-Cracked Plate Specimen	7
4	Uniaxial Stress vs. Strain Curve for IN-100	11
5	Steps in the Initial Stress Method	17
6	Initial Stress Method for a Uniaxial Specimen	18
7	General 8-Noded Quadrilateral with Midside Nodes Moved to 1/4-Chord	27
8	General Crack Tip Element	27
9	Crack Tip Surrounded with Crack Tip Elements	30
10	Two Triangular Elements Uniaxial Verification Mesh	34
11	One Eight-Noded Element Uniaxial Verification Mesh	35
12	Crack Tip Element Test Mesh	37
13	8-Noded Element Test Mesh	38
14	Crack Tip Element Fine Mesh	39
15	8-Noded Element Fine Mesh	40
16	CST Fine Mesh	41
17	Crack Tip Region - Crack Element, Fine Mesh	42
18	Crack Tip Region - 8-Noded Element, Fine Mesh	42
19	Crack Tip Region - CST, Fine Mesh	43
20	Crack Tip Region - Crack Element, Coarse Mesh	47

List of Figures (Continued)

Figure		Page
21	Crack Tip Region - 8-Noded Element, Coarse Mesh	47
22	Elastic Analysis (\bar{K}_I), Coarse Meshes	49
23	Elastic Analysis (\bar{K}_I), Fine Meshes	50
24	Stress Profiles, $\theta=7.5^\circ$, $P=10.896$ klb	53
25	Stress Profiles, $\theta=7.5^\circ$, $P=16.060$ klb	54
26	Stress Profiles, $\theta=45^\circ$, $P=10.896$ klb	55
27	Stress Profiles, $\theta=45^\circ$, $P=16.060$ klb	56
28	Stress Profiles, $\theta=75^\circ$, $P=10.896$ klb	57
29	Stress Profiles, $\theta=75^\circ$, $P=16.060$ klb	58
30	Stress Profiles, $\theta=112.5^\circ$, $P=10.896$ klb	59
31	Stress Profiles, $\theta=112.5^\circ$, $P=16.060$ klb	60
32	Stress Profiles, $\theta=157.5^\circ$, $P=10.896$ klb	61
33	Stress Profiles, $\theta=157.5^\circ$, $P=16.060$ klb	62
34	Plastic Region, Crack Element, Fine Mesh, $P=10.896$ klb	63
35	Plastic Region, Crack Element, Fine Mesh, $P=16.060$ klb	63
36	Plastic Region, 8-Noded Element, Fine Mesh, $P=10.896$ klb	64
37	Plastic Region, 8-Noded Element, Fine Mesh, $P=16.060$ klb	64
38	Plastic Region, CST, Fine Mesh, $P=10.896$ klb	65
39	Plastic Region, CST, Fine Mesh, $P=16.060$ klb	65
40	Displacement Profiles, $\theta=0^\circ$, $P=10.896$ klb	68
41	Displacement Profiles, $\theta=0^\circ$, $P=16.060$ klb	69

List of Figures (Concluded)

Figure		Page
42	Convergence of Coarse to Fine Mesh, Crack Tip Element Mesh	71
43	Convergence of Coarse to Fine Mesh, 8-Noded Element Mesh	72
A-1	Triangular Element and Nodal Displacements in x-y Space	84
A-2	Distorted Isoparametric Element in x-y Space	91
A-3	8-Noded Isoparametric Element in Space	93
A-4	Zero Energy Mode for an 8-Noded Isoparametric Element	102
A-5	Gaussian Integration Stations of an 8-Noded Isoparametric Element in ξ - η Space	104
B-1	Example of the Calculation of Equivalent Nodal Forces for the CST	108
B-2	8-Noded Element at the Boundary Under Loading	110
B-3	Example of the Calculation of Equivalent Nodal Forces for the 8-Noded Isoparametric Element	111
C-1	Plotting Subroutine for the JALESE Program. .	115

List of Tables

Table		Page
I	Regions and Degrees of Freedom, Fine Meshes	45
II	Elastic Analysis, Values of \bar{K}_I for Fine and Coarse Meshes	51
III	Strains Near the Crack Tip, $\theta=0^\circ$, Fine Meshes	67
IV	Computational Resource Usage Comparisons, Two Triangular Elements, Uniaxial Test, JALESE and VISCO	76
A-I	Weight Coefficients and Abscissae of Gaussian Quadrature Formula	105

List of Symbols

a	Half crack length (center cracked plate)
\underline{a}^e	Vector of nodal displacements
a_i	Parameters for Constant Strain Triangle (CST)
\underline{B}	Matrix relating total strain to nodal displacement
b	Half-width of specimen
b_i	Parameters for CST
c_i	Parameters for CST
dt^i	The i th time step
dt_m	Maximum stable time step for Malvern model
$d\epsilon_{ij}$	Incremental component of total strain
$d\epsilon_{ij}^p$	Incremental component of plastic strain
$d\sigma$	Stress increment
$d\sigma_o$	Overstress in initial stress method
\underline{D}	Elastic material matrix relating stress to total strain
\underline{D}_{EP}	Elastic-plastic strain to stress matrix
E_{mnpq}	Tensor relating elastic strain to stress
E	Young's Modulus
\underline{F}	Generalized force vector
\underline{F}^{eq}	Equivalent nodal force vector
G	Shear modulus
H'	Slope of stress vs. plastic strain curve
i, j	Indices
J_2	Second invariant of deviatoric stress
\underline{J}	Jacobian matrix
K	Stress intensity factor

List of Symbols (Continued)

$\underline{\underline{K}}$	Global stiffness matrix
$\underline{\underline{K}}_e$	Elastic stiffness matrix
N_i	Shape functions
P	Maximum value of P_σ or P_ϵ at any given time/applied pressure/applied load
\dot{P}	Applied force rate
P_ϵ	Strain tolerance parameter
P_σ	Stress tolerance parameter
\underline{P}	Applied load vector
\underline{Q}	Plastic load vector
q	Applied loading
q^e	Equivalent nodal load vector
R/A	Ratio of radial distance from crack tip to half-crack length
r	Radial distance from crack tip
$\underline{\underline{S}}_e$	Stress recovery matrix
S_{ij}	Deviatoric stress
t	Time
u	Displacement in x-direction
U_d	Distortion energy
v	Displacement in y-direction
w	Width of specimen
x,y	Cartesian coordinates
α_i	Shape parameters for CST
γ_i	Fluidity constant in Norton Creep Law
γ_p	Fluidity constant in Malvern Flow Law
δ_{ij}	Kronecker's delta
ϵ	Total uniaxial strain

List of Symbols (Concluded)

$\underline{\epsilon}_0$	Initial stress vector
ϵ_{ij}	Components of total strain
ϵ_{ij}^E	Elastic components of strain tensor
ϵ_{ij}^P	Plastic components of total strain
$\dot{\epsilon}_{ij}^P$	Plastic strain rate tensor
ϵ_e^P	Total effective plastic strain
ϵ_{tol}	Strain tolerance
η	Local coordinate
θ	Angular measure from crack tip
λ	Positive scalar constant
ν	Poisson's ratio
ξ	Local coordinate
σ	Uniaxial stress
$\underline{\sigma}_0$	Initial stress vector
σ_{ij}	Components of stress
σ_e	Effective stress
$\bar{\sigma}$	Strain hardening yield stress
$\bar{\sigma}_0$	Initial yield stress
σ_{tol}	Stress tolerance

Abstract

Stress near a crack tip in plasticity was analyzed using three different finite element modelings; a constant strain viscoplastic triangle, an eight-noded elastic-plastic quadrilateral and a crack tip elastic-plastic singularity element. The specimen under consideration was a center cracked plate made from IN-100. The half-crack length was 0.1367 in (3.472 mm). An elastic solution was formulated and two different loadings to generate plasticity were considered. Fine mesh and coarse mesh solutions for the higher order elements were generated and compared. Comparisons were made based on an equal number of degrees of freedom in two specific regions referred to as the near field and the far field regions.

It was determined that the elements whose elastic solutions conformed best to linear elastic fracture mechanics predictions were the constant strain triangle and the eight-noded quadrilateral in a fine mesh. The crack tip element did not perform as well as was expected. For the plastic analysis, the constant strain triangle exhibited the largest plastic region and gave the most accurate stress profiles. The eight-noded isoparametric element came within fifteen percent of the stress levels generated from the constant strain triangle. The stress singularity that is characteristic of the crack tip element forced that element to behave unnaturally stiff in plasticity.

Because it is not as stiff as either the crack tip element or the eight-noded element, the constant strain triangle offered the most accurate solutions. The CST solution required the least amount of computational resources. Though the isoparametric element mesh was easier to formulate and gave fairly accurate answers elastically and plastically, it was determined that the constant strain triangle in a fine mesh offered the best solution to elastic-plastic finite element problems for the center cracked plate.

I. Introduction

The United States Air Force has a vital interest in the effects of cracks on airframe components. Prior to 1969, the Air Force determined the "safe life" of an aircraft by first assuming a defect-free structure. Mean life fatigue analysis was then used in which the projected lifetime of the aircraft was divided by a safety factor.

The "safe life" approach had several disadvantages. The manufacturing process invariably results in cracking, thus invalidating the hypotheses of a defect-free structure. Ordinary wear, maintenance, and battle damage also create discontinuities in the structure. The service failures of the F-111 and C-5A emphasized the poor correlation between the safe life model and actual aircraft durability. A new method of estimating aircraft life was needed.

Structural engineers have turned to Linear Elastic Fracture Mechanics (LEFM) to determine the stresses caused by cracks in a structure. LEFM has worked well; unfortunately, it too has its limitations. LEFM assumes that a material will behave with perfect elasticity until it reaches its failure load. As a consequence, brittle failure will result. Real materials exhibit plasticity after the elastic yield load has been reached. Higher loads result in more plasticity and greater deviations from LEFM predictions.

Plasticity occurs around the tip of a crack on a material under loading due to unusually high stress concentration near the crack. Plastic behavior is nonlinear, and this results in irrecoverable strains in the material.

Plastic behavior greatly alters the material properties in the region near the crack tip. In order to accurately determine the survivability and durability of cracked material under loading, elastic-plastic or elastic-viscoplastic fracture mechanics must be utilized.

The primary method for numerically analyzing stress in the vicinity of a crack is the "Finite Element Method". To accomplish this, programs have been written incorporating various finite elements and the laws of plastic flow. The major purpose of this thesis is to determine which of the three different finite element models considered is the most accurate and easiest to use.

The study of crack growth is also essential in the accurate prediction of the structural lifetime of many aircrafts. Linear elastic fracture mechanics does not accurately predict crack growth and, therefore, a plastic analysis must be performed. The study of plastic crack growth is beyond the scope of this thesis. However, the information gained from this finite element modeling of plasticity study will be useful in future analyses of crack growth.

II. Objective

Plasticity may be studied in several ways. A material may deform plastically by the singular or combined effects of load, time or temperature. A specimen could be elastic-perfectly plastic, where the stress level is the same for a given plastic strain (see Fig. 1), or it could exhibit strain hardening, where stress will increase with strain (see Fig. 2). The model to be selected will depend upon the desired complexity of the analysis.

Stress analysis in a cracked plate is accomplished today by the use of finite element computer programs. Since there are many finite element programs available for elastic-plastic stress evaluation, it would seem to be an easy matter to select a program, punch up data cards, and perform the analysis. However, not all finite element programs or finite element modelings are alike. The structural engineer must determine how accurate his model and program are. He also must minimize the consumption of resources in analysis and this includes computer processor time, memory usage, and his own time in setting up the problem. The engineer is easily bewildered by the proliferation of programs and models. As previously stated, the primary purpose of this thesis is to determine which one of the available finite element formulations best describes a typical cracked plate problem, in terms of accurate results, least amount of computer time, and ease of use.

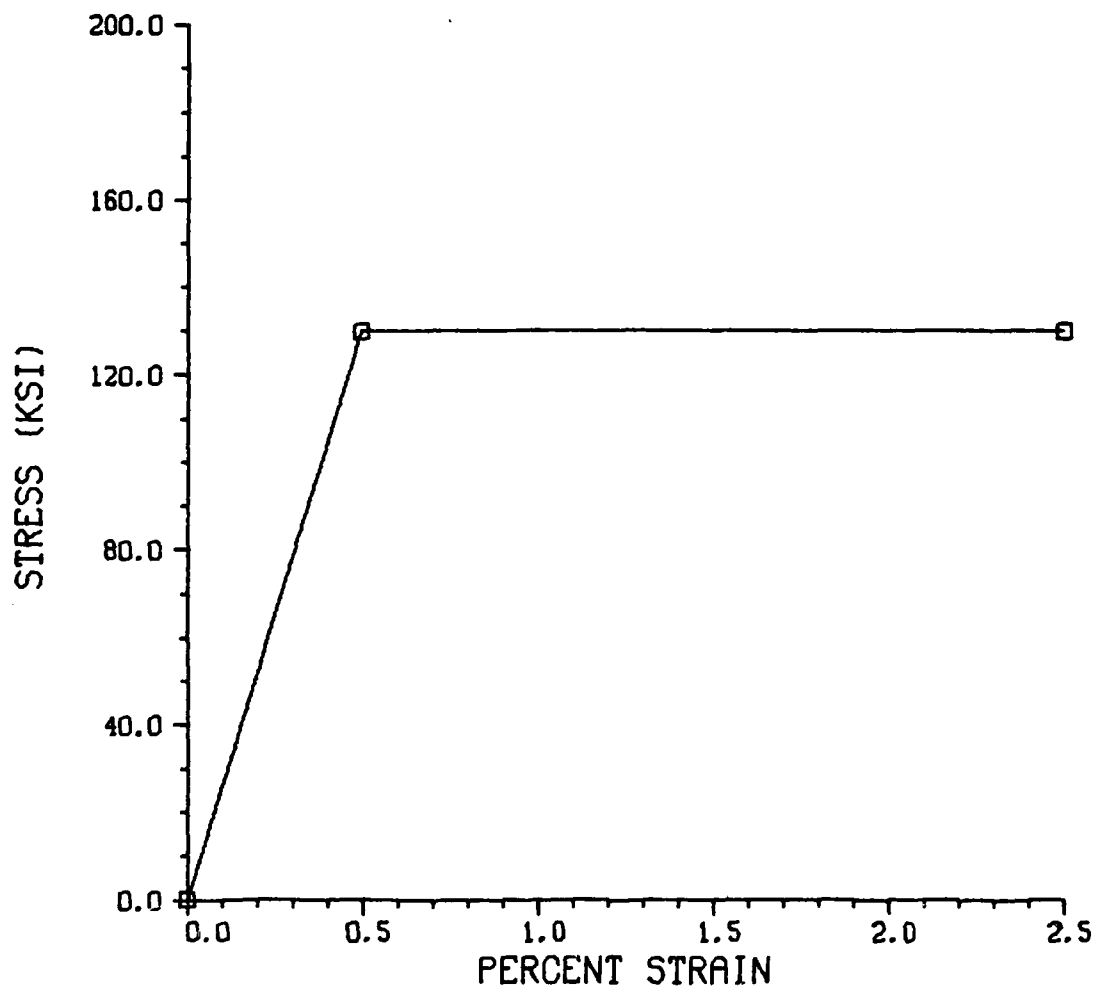


Figure 1. Stress vs. Strain Curve for an Elastic-Perfectly Plastic Material

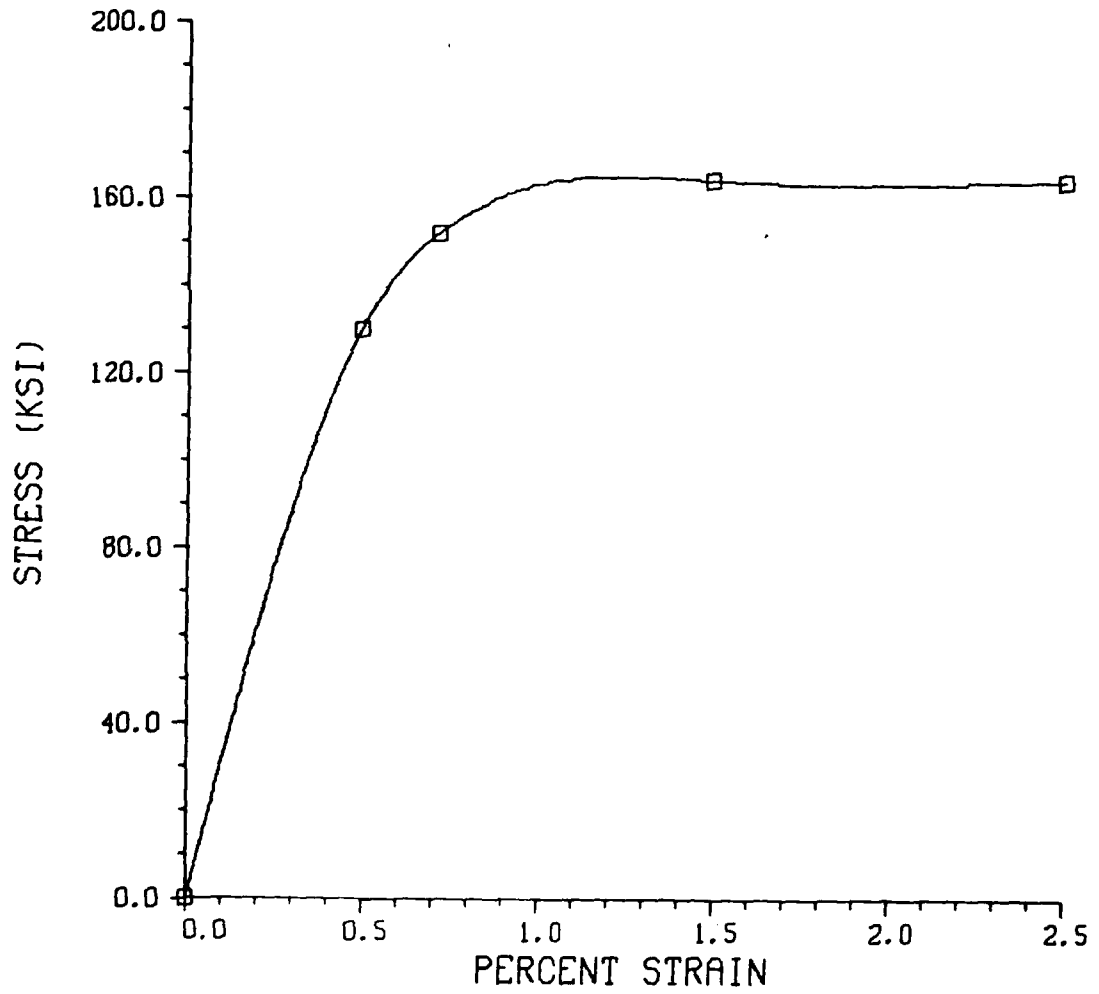


Figure 2. Stress vs. Strain Curve for an Elastic-Plastic Material with Strain Hardening

To accomplish this, three different types of elements were considered; a constant strain triangle (CST), an eight-noded rectangular element, and a crack tip singularity element. Two different programs were applied to the problem; the VISCO program written by Captain Terry Hinrichs, USAF, and a program written by Jalese Ahmad and V. Papaspyropoulos of Battelle Corporation, Columbus, Ohio, which shall be referred to as JALESE. JALESE utilizes the 8-noded and crack elements and VISCO incorporates the constant strain triangle (CST).

The material under consideration was IN-100 at 1350°F (731.2°C). The specimen to be modeled measured 1 inch (0.0254 m) in height, 1.4 in. (0.0356 m) in width, and 0.3 in. (0.00762 m) in thickness (see Fig. 3). Young's modulus for IN-100 was taken to be 26.3×10^3 ksi (181.2×10^3 MPa), Poisson's ratio was assumed to be 0.3, and the yield stress was 130.0 ksi (895.9 MPa). Because the specimen and loading were symmetric, only the top quarter of the geometry was analyzed. Appropriate boundary conditions were applied to insure symmetry.

The ratio of the material thickness, t , to the width of the specimen, $2b$, was 0.21. This indicated that the material was relatively thin as compared to its width. Therefore, a plane stress solution was used.

To guarantee the applicability of the results, the number of degrees of freedom in the crack tip region and the mesh as a whole was kept within a few percent. For

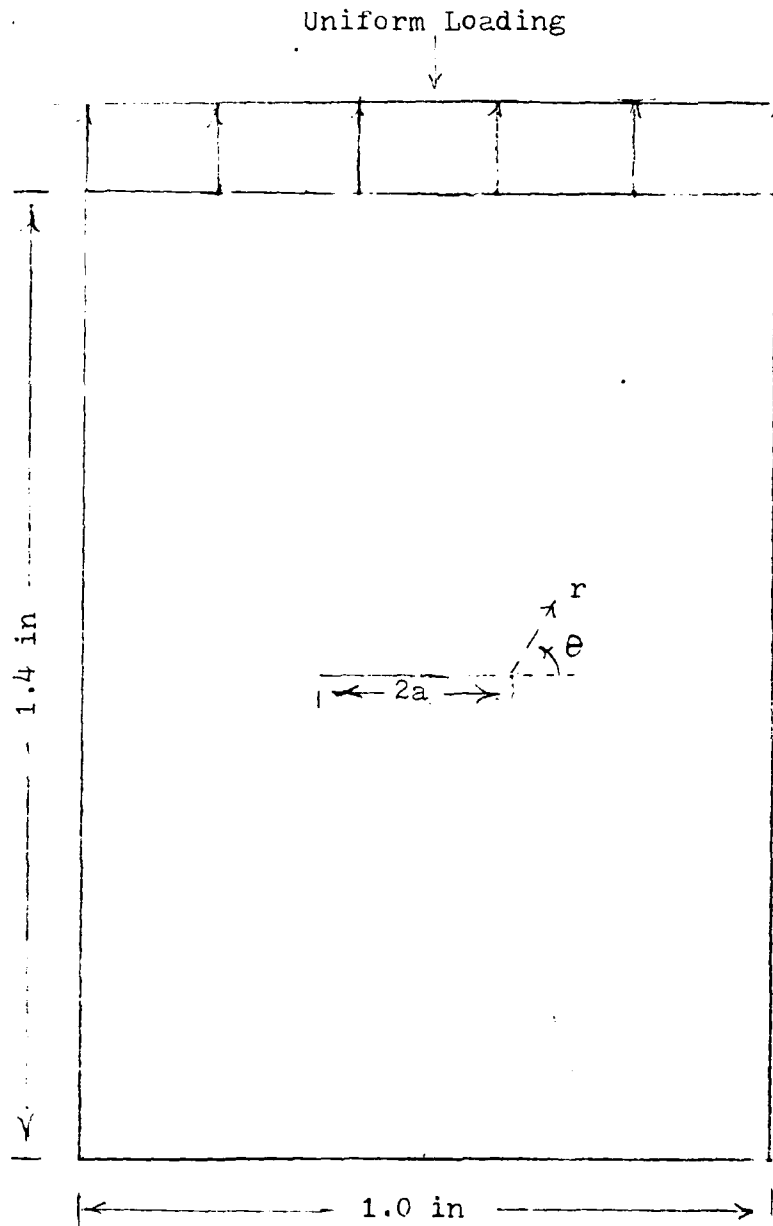


Figure 3. Center-Cracked Plate Specimen.

comparison purposes, a coarse mesh for the 8-noded and crack element in which the number of degrees of freedom in the crack tip region was halved was also run. Convergence of the coarse mesh solution to the fine mesh solution was also investigated.

An elastic analysis was first performed on the specimen, using the different finite element models. A stress intensity factor was obtained and comparisons were made between the finite element modelings and results from linear elastic fracture mechanics. Plastic runs were then accomplished, using two different loadings. Regions of plasticity and stress profiles were used for comparison. Criteria for program efficiency were central processor time, core memory usage, and various subjective factors, such as ease of use.

III. Theoretical Formulation

Theory of Plasticity

The generalized relationship between the elastic stress tensor and the elastic strain tensor may be written as:

$$\sigma_{mn} = E_{mnpr} \epsilon_{pr} \quad (1)$$

where σ_{mn} is the elastic stress tensor, ϵ_{pr} is the elastic strain tensor, and E_{mnpr} are the elastic constants. For an isotropic material, that is a material whose elastic properties are completely independent of the orientation of the axes, such as IN-100, the 81 components of E_{mnpr} reduce down to only two independent constants. Those constants are E , Young's modulus, taken to be 26.3×10^3 ksi (181.2×10^3 MPa) and ν , Poisson's ratio, which was taken to be 0.3.

In compact tensor form, the equation for strain versus stress for an isotropic material can be written as (Ref 3):

$$\epsilon_{mn} = \frac{1}{E} [(1+\nu)\sigma_{mn} - \nu\delta_{mn}\sigma_{rr}] \quad (2)$$

where δ_{mn} is Kronecker's delta.

One would believe that the above elastic equation could be used for any level of stress. Unfortunately, this is not true. At a certain value of stress, called the "yield stress", the material behavior deviates from elastic behavior. The material then begins to exhibit plasticity. For IN-100, yielding will occur at 130.0 ksi (895.9 MPa).

For a uniaxial test, the material will yield when the applied load equals the yield stress, and the specimen will behave according to its uniaxial stress-strain curve. The uniaxial stress-strain curve for IN-100 is shown in Fig. 4. However, for multiaxial stress situations, such as the cracked plate problem, it is necessary to determine the combination of stresses that will cause yielding. The yield criterion indicates when plasticity has begun (Ref 9).

One of the most widely used yield criterion is the one postulated by von Mises (Ref 9). This criterion states that yield in tension is caused by maximum distortion energy. The distortion energy is given by:

$$U_d = \frac{1}{2G} J_2 \quad (3)$$

where U_d equals distortion energy, G equals the shear modulus, and J_2 is the second invariant of the deviatoric stress (Ref 11), defined as

$$J_2 = \frac{1}{2} s_{ij} s_{ij} \quad (4)$$

where s_{ij} are the components of the deviatoric stress tensor.

This criterion can also be viewed as stating that yielding will occur when J_2 reaches a critical value, which is the yield stress. For IN-100, the yield stress in compression equals the yield stress in tension. This is a characteristic of isotropic materials. Therefore, the von Mises criterion can be used in either situation.

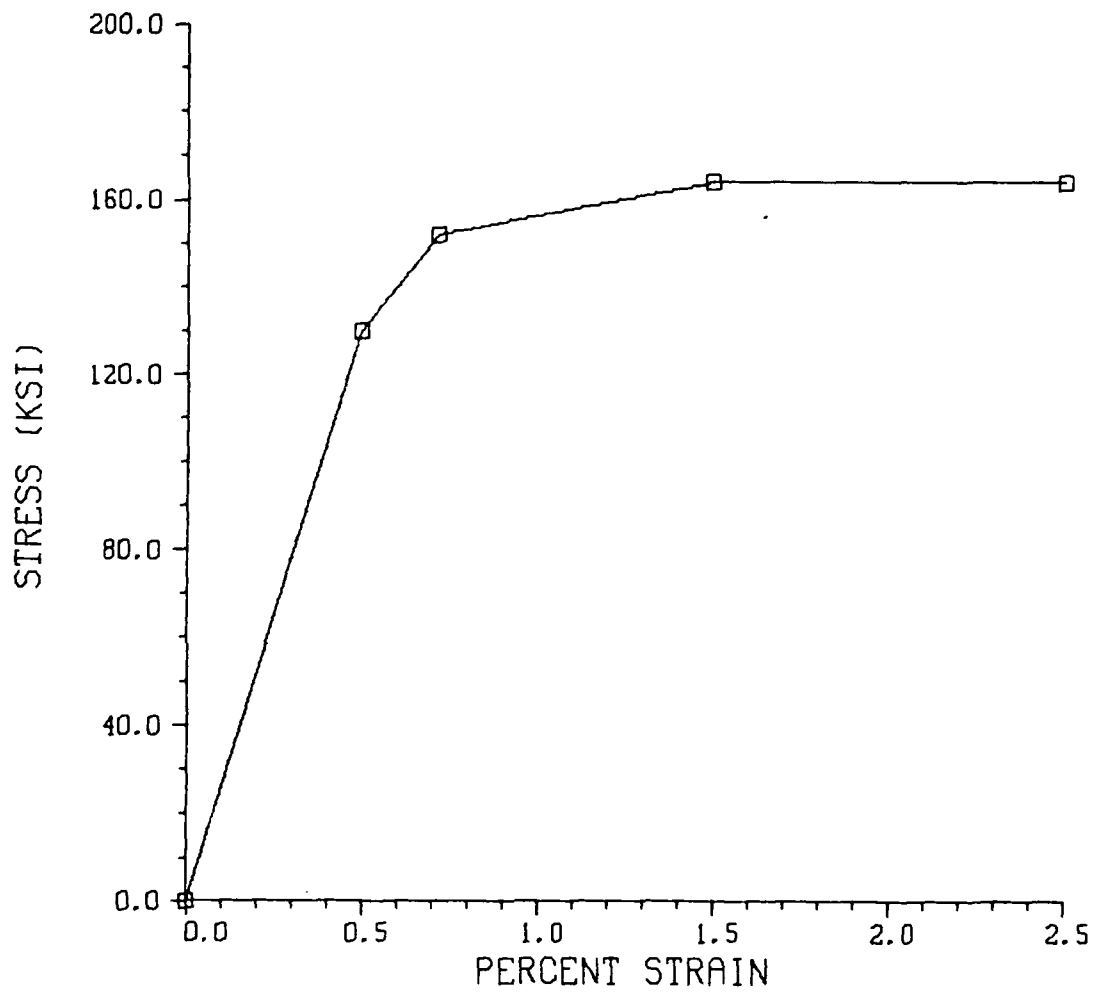


Figure 4. Uniaxial Stress vs. Strain Curve
for IN-100

The von Mises yield criterion can be stated as follows:

$$F\{\sigma\} = [(\sigma_x + \sigma_y + \sigma_z)^2 + 3(\tau_{xy}^2 + \tau_{yz}^2 + \tau_{zx}^2) - (\sigma_x\sigma_y + \sigma_y\sigma_z + \sigma_z\sigma_x)]^{1/2} - \sigma_0 \quad (5)$$

where σ_0 is the uniaxial yield stress, then yielding will occur when $F(\sigma) \geq 0$. The formulation of the von Mises yield criterion is presented in Mendelson (Ref 9).

For isotropic strain hardening, the yield stress is a function of effective plastic strain and may be expressed as a segmental linear function of ϵ_e^P :

$$\bar{\sigma}(\epsilon_e^P) = \sigma_0 + H' \epsilon_e^P \quad (6)$$

where σ_0 is the uniaxial yield stress of the material, which is the stress necessary to produce yielding, ϵ_e^P is the effective plastic strain, ϵ_0 , and H' is the slope of the uniaxial stress-strain curve. The effective plastic stress is defined incrementally by $d\epsilon^P$ (see Eq. 10).

If one has exceeded the uniaxial yield stress of a material, the total strain, ϵ_{mn} , can be expressed as the sum of its plastic and elastic parts.

$$\epsilon_{mn} = \epsilon_{mn}^E + \epsilon_{mn}^P \quad (7)$$

where ϵ_{mn}^E equals the elastic strain tensor and ϵ_{mn}^P is the plastic strain tensor. A plastic flow theory which is consistent with the von Mises criterion is that the ratio of the increment of plastic strain to deviatoric strain remains constant, or

$$\frac{d\epsilon_{ij}^P}{S_{ij}} = d\lambda \quad (8)$$

It can be shown (Ref 3) that

$$d\lambda = \frac{\frac{3}{2}d\epsilon^P}{\sigma_{ij}} \quad (9)$$

where $d\epsilon^P$ is the incremental effective plastic strain, defined as

$$d\epsilon^P = \sqrt{\frac{2}{3}d\epsilon_{ij}d\epsilon_{ij}} \quad (10)$$

Therefore, one can write:

$$d\epsilon_{ij}^P = \frac{3}{2} \frac{d\epsilon^P}{\sigma_e} S_{ij} \quad (11)$$

where σ_e , called the effective stress, is expressed as:

$$\sigma_e = \sqrt{3J_2} \quad (12)$$

Eq. 11 is called the Prandtl-Reuss equation for plastic flow. For isotropic strain hardening, the Prandtl-Reuss equation becomes:

$$d\epsilon_{ij}^P = \frac{3}{2} \frac{d\sigma_e}{H'\sigma_e} S_{ij} \quad (13)$$

where H' is the slope of the uniaxial stress-strain curve.

This equation allows one to solve for the differential change in plastic stress using known quantities. However, since $d\epsilon_{ij}^P$ cannot usually be calculated explicitly, an iterative solution technique must be used.

Elastic-Plastic Solution Technique

There are two methods available for solving elastic-plastic problems incrementally using a finite element computer program. The first, called the tangent modulus method, requires a stiffness matrix, $[K]$, be constantly updated to account for the effects of plasticity. Since recalculating K requires much computer time, a second method for computing the plastic strain is desired (Ref 13).

The second method of calculating plastic strains is to divide the total force vector into a plastic load vector and an elastic load vector. This technique, called the residual force method, avoids repeated modifications of the stiffness matrix. The residual force method was used in effect for both the VISCO and JALESE programs.

When using the residual force approach, the basic equation of equilibrium for the finite element method can be expressed as

$$\{F\} = [K]\{U\} \quad (14)$$

where $\{F\}$ is the generalized force vector, $[K]$ is the stiffness matrix, and $\{U\}$ is the generalized displacement vector and is broken up as follows:

$$[K_e]\{U\}^i = \{P\}^i + \{Q\}^i \quad (15)$$

where K_e is the elastic stiffness matrix, P is the applied load vector, and Q is the effective plastic load vector for the elements in plasticity.

An incremental solution process, denoted by the i superscripts, is used and there are two possible incremental procedures. Both methods apply an incremental load and calculate the associated values of stress and strain. The initial stress method approaches equilibrium by iterating the initial stress increments. The initial strain method approaches compatibility by iterating the initial strain increments. The JALESE program uses the initial stress method to compute the elastic and plastic strains. The VISCO program uses a time dependent form of the initial strain technique and is described in Ref 7. Therefore, the initial stress method will now be examined in detail (Ref 15).

The initial stress method for the solution of elastic-plastic problems is accomplished by first applying the total load vector and examining for plasticity by the yield criterion. If no yielding has occurred, one has a perfectly elastic problem. If plasticity is indeed present, then one solves for the elastic and plastic strains by first solving a purely elastic problem for the total applied load, dP . In this first step, $d\epsilon^i$ is determined by the elastic solution. Note that the superscript i denotes the current increment and $i-1$ denotes the preceding increment. The subscript I denotes the current iteration and $I-1$ denotes the preceding iteration.

The corresponding elastic stress, $d\sigma_{EI}$ is calculated from $d\epsilon$. Then, an initial stress, $d\sigma_0$ is calculated, where

$$d\sigma_o = d\sigma_E - d\sigma_o \quad (16)$$

This initial stress is the stress required to maintain compatibility with the uniaxial stress-strain curve. The resulting "balancing" force from the initial stress is calculated by:

$$\underline{dQ} = \int \underline{B}^T d\underline{\sigma}_o d(\text{vol}) \quad (17)$$

\underline{dQ} is added to the applied load, \underline{dP} , and the iterative process starts over. A stable solution that satisfies compatibility and equilibrium is reached when the change in $\underline{dQ}_i \approx 0$.

Figure 5 shows the steps in the initial stress algorithm. Note that \underline{D}_{EP} is the strain to stress matrix for elastic-plastic solutions. A diagram for a uniaxial initial stress solution is shown in Fig. 6.

Viscoplastic Material Models

Another phenomenon associated with problems in plasticity is creep. Creep includes all time-dependent effects and results in creep strains, which are developed at a finite rate. Time-independent permanent plastic strains are lumped together into the generalized term "plasticity". The combination of time-dependent and time-independent effects into a unified plastic flow law is called "viscoplasticity" (Ref 14).

In deriving the flow law for viscoplasticity, one must first decompose the total strain rate into its elastic and plastic strain rate components.

For each load increment dP in the plastic range:

$$1. \quad \underline{dU}_I = \underline{K}^{-1} (\underline{dP} + \underline{dQ}_{I-1})$$

$$2. \quad \underline{d\varepsilon}_I = \underline{B} \underline{dU}_I$$

$$3. \quad \underline{d\sigma}_{EI} = \underline{D} \underline{d\varepsilon}_I$$

$$4. \quad \underline{\sigma}'_I = \underline{\sigma}_{I-1} + \underline{d\sigma}_{EI}$$

$$5. \quad \underline{d\sigma}_I = \underline{D}_{EI-1} \underline{d\varepsilon}_I$$

$$6. \quad \underline{d\sigma}_O = \underline{d\sigma}_{EI} - \underline{d\sigma}_I$$

$$7. \quad \underline{\sigma}_I = \underline{\sigma}'_I - \underline{d\sigma}_O$$

$$\underline{\varepsilon}_I = \underline{\varepsilon}_{I-1} + \underline{d\varepsilon}_I$$

$$8. \quad \underline{dQ} = \int \underline{B}^T \underline{d\sigma}_O \underline{d}(\text{vol})$$

Process is terminated when $\underline{dQ}_I = \underline{dQ}_{I-1}$

Figure 5. Steps in the Initial Stress Method (Ref 7)

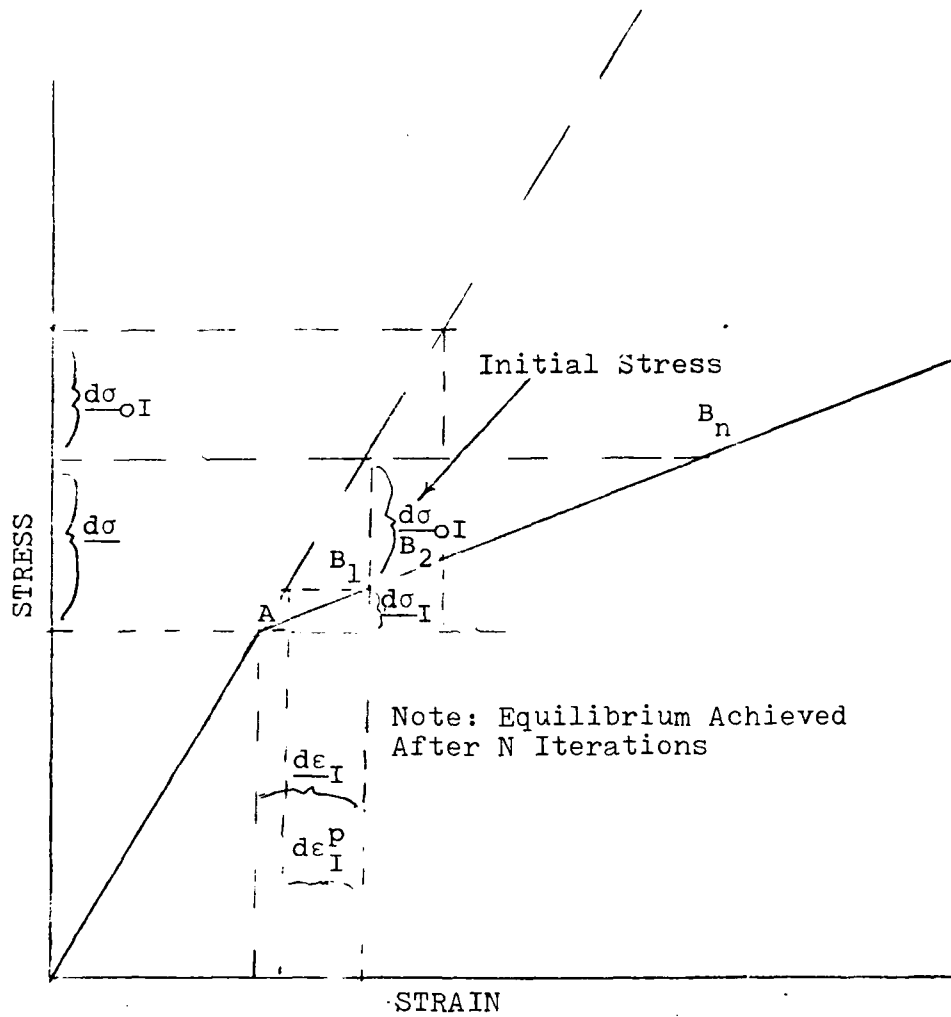


Figure 6. Initial Stress Method for a Uniaxial Specimen

$$\dot{\epsilon}_{ij} = \dot{\epsilon}_{ij}^E + \dot{\epsilon}_{ij}^P \quad (18)$$

where $\dot{\epsilon}_{ij}$ is the total strain rate, $\dot{\epsilon}_{ij}^E$ is the elastic strain rate and $\dot{\epsilon}_{ij}^P$ is the plastic strain rate. The elastic strain rate versus stress rate equation is obtained from the time derivative of Hooke's law of elasticity. The plastic strain rate tensor is related to stress rate by the time derivative form of the Prandtl-Reuss equation (Ref 14):

$$\dot{\epsilon}_{ij}^P = \lambda S_{ij} \quad (19)$$

where S_{ij} are the components of the deviatoric stress tensor. Once again, incompressibility and isotropy have been assumed.

It is not entirely correct to treat separately the plastic strain due to creep and the plastic strain caused instantaneously by loading. However, the superposition of Malvern's overstress law with Norton's law for secondary creep has been proposed as a unified viscoplastic flow law (Ref 14) into a finite element program referred to as VISCO (Ref 7).

Creep may be described as time-dependent deformation occurring under a constant strain (Ref 13). The constitutive law for creep is in the form of a strain rate. The creep law used in the VISCO program is Norton's law and may be expressed as (Ref 14):

$$\dot{\epsilon}_{ij}^{P, \text{creep}} = \frac{d\epsilon_{ij}^{P, \text{creep}}}{dt} = \gamma_c (\sigma_e)^B \frac{3}{2} \frac{S_{ij}}{\sigma_e} \quad (20)$$

where $\dot{\epsilon}_{ij}^p$ creep is the creep strain rate, ϵ_{ij}^p creep is the creep strain, γ_c is the creep coefficient, and B is the creep exponent. γ_c and B are constants determined from uniaxial creep test results.

The Malvern overstress equation relates the instantaneous plastic strain rate tensor to stress, and may be written as follows:

$$\dot{\epsilon}_{ij}^p = \gamma_p \left[\frac{\sigma_e}{\bar{\sigma}(\epsilon_e^p)} - 1 \right] \frac{3}{2} \frac{S_{ij}}{\sigma_e} \quad (21)$$

where γ_p is a fluidity constant, σ_e is the effective stress, and $\bar{\sigma}(\epsilon_e^p)$ is the strain hardening yield stress which has been defined in Eq. 6. Of course, this equation is only valid if yield has been exceeded, that is, if the effective stress is greater than the strain hardening yield stress. If yield has not been exceeded, then $\dot{\epsilon}_{ij}^p$ equals zero.

The Malvern model can be adapted for time-independent elastic-plastic solutions. When this is done, γ_p may take on any non-zero positive value. The elastic-plastic solution is the steady state value of the stresses, strains and displacements after the total load has been applied. Therefore, if one multiplies both sides of Eq. 21 by dt, the resulting expression acting as the coefficient of $\frac{3}{2} \frac{S_{ij}}{\sigma_e}$, reduces to the coefficient for time-independent plasticity (Eq. 13).

VISCO utilizes an Euler linear extrapolation scheme to integrate the viscoplastic strain rate expressions. The equations for the Euler extrapolation may be written as follows:

$$\{\dot{\epsilon}_{ij}^p\}^i = \begin{cases} 0 & \text{if } \sigma_e^{i-1} < \bar{\sigma}(\epsilon_e^p)^{i-1} \\ \gamma_p \left[\frac{\sigma_e^{i-1}}{\bar{\sigma}(\epsilon_e^p)^{i-1}} - 1 \right] \frac{3}{2} \frac{\{S_{ij}\}^{i-1}}{\sigma_e^{i-1}} & \text{if } \sigma_e^{i-1} > \bar{\sigma}(\epsilon_e^p)^{i-1} \end{cases} \quad (22)$$

$$\{d\epsilon_{ij}^p\} = \{\dot{\epsilon}_{ij}^p\} dT$$

$$(\epsilon_e^p)^i = (\epsilon_e^p)^{i-1} + \sqrt{\frac{2}{3}} \{d\epsilon_{ij}^p\}^i \{d\epsilon_{ij}^p\}^i \quad (23)$$

$$\bar{\sigma}(\epsilon_e^p)^i = \bar{\sigma}_0 + H' (\epsilon_e^p)^i \quad (24)$$

The superscript i refers to the time step and the subscript i refers to specific components of stress or strain (Ref 7).

Viscoplastic Solution Procedure

There are two generalized techniques available for solving the viscoplasticity problem. These are the same two procedures that were used to solve the time-independent analysis. In the first method, the tangential stiffness matrix must be constantly updated. It has previously been stated that this method is inappropriate for use in a finite element computer program. The second solution procedure uses a constant elastic stiffness matrix to iteratively correct the "residual forces" obtained from the difference of elastic and plastic stresses calculated. In

the elastic-plastic analysis, load was incremented directly to satisfy the yield condition and the plastic flow law was used. In the elastic-viscoplastic solution technique, time is incremented directly and load, stress, and strain are incremented indirectly. Zienkiewicz and Cormeau present the viscoplastic solution procedure, and it may be summarized as follows:

First, the time increment, dt^i , is added to the preceding time t^{i-1} to obtain the current total time, t^i . Then, the increments of the plastic strain tensor are computed by the equation:

$$\{d\epsilon_{ij}^p\} = \{\dot{\epsilon}_{ij}^p\} dt \quad (25)$$

where $\dot{\epsilon}_{ij}^p$ is computed from the Malvern equation (Eq. 21).

The plastic strain is totaled by

$$\{\epsilon_{ij}^p\}^i = \{\epsilon_{ij}^p\}^{i-1} + \{d\epsilon_{ij}^p\}^i \quad (26)$$

The plastic strain rate, $\dot{\epsilon}_{ij}^p$, had been previously calculated by the Malvern flow law.

The plastic load vector, $\{Q\}^{i-1}$, is computed by

$$\{Q\}^{i-1} = \int_{vol} [B][D]\{\epsilon_{ij}^p\}^i d(vol) \quad (27)$$

where the B matrix and D matrix are described in Appendix A.

Next, the current external load vector is calculated by:

$$\{P\}^i = \{\dot{P}\}^i dt^i + \{P\}^{i-1} \quad (28)$$

where \dot{P} is the force rate vector (a known quantity).

The nodal displacements, $\{U\}^i$, are determined from:

$$\{U\}^i = [K]^{-1}(\{P\}^i + \{Q\}^{i-1}) \quad (29)$$

where K is the elastic stiffness matrix.

The current total strain $\{\epsilon_{ij}\}^i$ is evaluated from the strain-displacement equation,

$$\{\epsilon_{ij}\}^i = [B]\{U\}^i \quad (30)$$

The current stress, $\{\sigma\}$, can now be calculated from

$$\{\sigma_{ij}\}^i = [D](\{\epsilon_{ij}\}^i - \{\epsilon_{ij}^p\}^i) \quad (31)$$

The VISCO program incorporates a variable time step procedure to minimize computer central processor unit time usage. This time step change is more fully explained in later paragraphs. It is at this point in the program that the time step size is checked in terms of prescribed stress and strain change tolerances per time step. If these tolerances are not exceeded, the time step size may be increased for the next time step or left the same; if the tolerances are exceeded, the time step size is reduced and the iterative process is repeated in an effort to satisfy the stress and strain change tolerances. If the tolerances have been satisfied, the iterative process is repeated until the desired simulation time has been reached.

The computer algorithm built into VISCO for estimating the time step is based around the parameters P_σ and P_ϵ (Ref 7), which are defined as follows:

$$P_{\sigma} = \frac{\sigma_e^i - \sigma_e^{i-1}}{\sigma_e^{i-1} \sigma_{tol}} \quad (32)$$

where σ_{tol} is the stress tolerance, and

$$P_{\epsilon} = \frac{(d\epsilon_e^P)^i}{\epsilon_{total}^i \epsilon_{tol}} \quad (33)$$

where ϵ_{tol} is the strain tolerance, and

$$\epsilon_{total} = \sqrt{\epsilon_x^2 + \epsilon_y^2 + \frac{1}{2}\gamma_{xy}^2} \quad (34)$$

The superscript i refers to the time step. The parameters P_{σ} and P_{ϵ} are calculated for every element. One method that Hinnerichs suggested for changing the time step is:

$$dt^i = dt^{i-1}/P \quad (35)$$

where P is set equal to the largest value of P_{σ} or P_{ϵ} .

Another method that was suggested for altering the time step that avoids repetitive recalculations uses the following equations:

$$\begin{aligned} dt^i &= 0.8 dt^{i-1}/P && \text{if } P > 1 \\ dt^i &= dt^{i-1} && \text{if } 0.8 \leq P \leq 1 \\ dt^i &= 1.25 dt^{i-1} && \text{if } 0.65 \leq P \leq 0.8 \\ dt^i &= 1.5 dt^{i-1} && \text{if } P < 0.65 \end{aligned} \quad (36)$$

Eq. 36 reduces the time step more than Eq. 35 if P is greater than 1. If P is less than 1, Eq. 36 reduces the time step slower than Eq. 35. Hinnerichs employed Eq. 36 into the final form of VISCO.

Fracture Mechanics

Linear Elastic Fracture Mechanics (LEFM). Linear elastic fracture mechanics relates the stress field and displacements near a crack tip to the stress applied to the structure for various crack geometries. Elastic analysis is used. The term used to describe the elastic stress and deformation fields near a crack tip is the stress intensity factor, K . There are actually three different types of K , corresponding to the three modes of crack displacement; they are the opening mode, sliding mode, and tearing mode (Ref 10).

A mode I (opening) crack occurs when the stress is applied along the y-axis and the crack lies along the x-axis. The center cracked plate under consideration exhibits mode I behavior. The stress intensity factor, K_I , is given by:

$$K_I = \sigma \sqrt{\pi a} \left(\sec \frac{\pi a}{2b} \right)^{1/2} \quad (37)$$

where $2a$ is the crack length and $2b$ is the plate width. Eq. 37 is valid for $0.3 < a/b < 0.7$. Otherwise,

$$K_I = \sigma \sqrt{\pi a} \left(\frac{2b}{\pi a} \tan \frac{\pi a}{2b} \right)^{1/2} \quad (38)$$

Note that for the case of $a = 0.1367$ in. and $b = 0.500$ in., Eq. 37 is used. The stresses near the crack tip, σ_x , σ_y and τ_{xy} , are given in terms of K_I , a , radial distance r from the crack tip, and angular measure θ from the crack tip by (Ref 13):

$$\sigma_x = \frac{K_I}{\sqrt{2\pi r}} \cos \frac{\theta}{2} \left[1 - \sin \frac{\theta}{2} \sin \frac{3\theta}{2} \right] \quad (39)$$

$$\sigma_y = \frac{K_I}{\sqrt{2\pi r}} \cos \frac{\theta}{2} \left[1 + \sin \frac{\theta}{2} \sin \frac{3\theta}{2} \right]$$

$$\tau_{xy} = \frac{K_I}{\sqrt{2\pi r}} \sin \frac{\theta}{2} \cos \frac{\theta}{2} \sin \frac{3\theta}{2}$$

Note that for each of the values of stress, σ_x , σ_y , and τ_{xy} , there exists a $\frac{1}{\sqrt{r}}$ singularity near the crack tip. This means that the stresses approach infinity as one gets closer and closer to the crack tip.

The Crack Tip Element. The crack tip element accurately models the $\frac{1}{\sqrt{r}}$ singularity that results from linear elastic fracture mechanics. This element is formed by degenerating the eight-noded quadrilateral into a six-noded triangle with the midside nodes for the sides nearest the crack tip located at the quarter-chord point near the crack tip. Barsoum (Ref 2) and Henshell and Shaw (Ref 6) both describe the mechanism by which the $\frac{1}{\sqrt{r}}$ singularity is formed from the eight-noded quadrilateral.

Consider the quadrilateral in Fig. 7. Notice that the midside nodes nearest the crack tip have been placed at the $\frac{1}{4}$ chord point. The side 1-4 is now collapsed and the location of midside node 7 is adjusted such that it is at the $\frac{1}{4}$ chord position. The resulting six-noded triangle is shown in Fig. 8. In this case, the singularity is investigated along the x-axis, $\eta=0$.

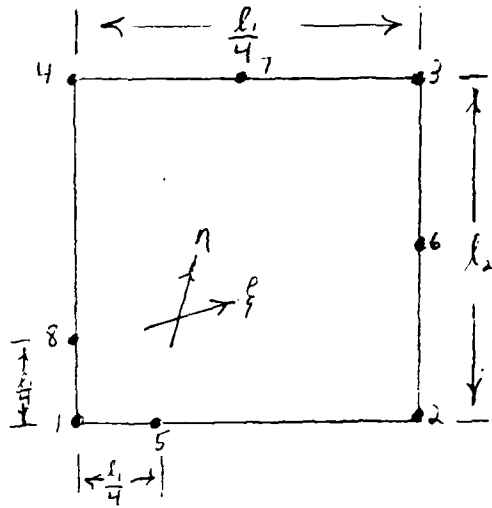


Figure 7. General 8-Noded Quadrilateral with Midside Nodes Moved to $\frac{1}{4}$ -Chord

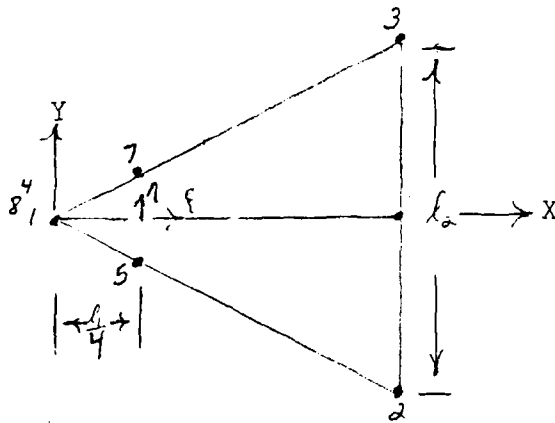


Figure 8. General Crack Tip Element

The equation used to determine x is given by:

$$x = \sum_{i=1}^8 N_i(\xi, \eta) x_i \quad (40)$$

N_i denotes the shape function for the eight-noded quadrilateral which is given in Eq. A-29. By using the values of x for each node, the equation for x as a function of ξ for $\eta=0$ becomes:

$$\begin{aligned} x = & -\frac{1}{4}(1+\xi)(1-\xi)l_1 - \frac{1}{4}(1+\xi)(1-\xi)l_1 + \frac{1}{2}(1-\xi^2)\frac{l_1}{4} \\ & + \frac{1}{2}(1+\xi)l_1 + \frac{1}{2}(1-\xi^2)\frac{l_1}{4} \end{aligned} \quad (41)$$

or,

$$x = (\xi^2 + 2\xi + 1)\frac{l_1}{4} \quad (42)$$

Therefore,

$$\xi = -1 + 2\sqrt{\frac{x}{l_1}} \quad (43)$$

Differentiating Eq. 42 results in

$$\frac{\partial x}{\partial \xi} = \frac{l_1}{2}(1+\xi) = \sqrt{\frac{x}{l_1}} \quad (44)$$

where the value of ξ in terms of x given by Eq. 43 has been substituted. Notice that $\frac{\partial x}{\partial \xi}$ equals zero at the crack tip ($x=0$). Now

$$\underline{\underline{\epsilon}} = \underline{\underline{J}}^{-1} \underline{\underline{B}}(\xi, \eta) \begin{pmatrix} u_i \\ v_i \end{pmatrix} \quad (45)$$

where

$$\det J = \frac{\partial(x, y)}{\partial(\xi, \eta)} \quad (46)$$

Therefore, Eq. 44 makes the Jacobian singular at $x=0$, $\xi=-1$. Considering only the displacements at nodes 1 and 6, the displacement u along the line 1-6 is given by:

$$u = \frac{1}{4}(\xi^2-1)u_1 + \frac{1}{2}(1+\xi^2)u_6 \quad (47)$$

The strain in the x direction then becomes:

$$\epsilon_x = \frac{\partial u}{\partial x} = \underline{J}^{-1} \frac{\partial u}{\partial \xi} = \frac{\partial \xi}{\partial x} \frac{\partial u}{\partial \xi} = \left(-\frac{1}{2} \sqrt{\frac{\ell}{x}} + 1\right)u_1 + \left(-\sqrt{\frac{\ell}{x}} + 2\right)u_6 \quad (48)$$

Therefore, a $\frac{1}{\sqrt{r}}$ strain singularity along the line 1-2 has been created by the use of the crack-tip singularity element. Since stress is proportional to strain, a $\frac{1}{\sqrt{r}}$ stress singularity also has been created. Since the Jacobian always goes to zero at the crack tip, one can choose any value of theta and there will be a $\frac{1}{\sqrt{r}}$ singularity for stress and strain along that r .

If the crack tip is surrounded by singularity elements (see Fig. 9), then one can choose any value of theta and have a $\frac{1}{\sqrt{r}}$ singularity for stress. Therefore, surrounding the crack tip with singularity elements effectively simulates the $\frac{1}{\sqrt{r}}$ singularity from the theory of linear elastic fracture mechanics.

Plasticity within the Singularity Elements. Any finite element will depict plastic action when the effective stress within the element has reached the yield stress. When this occurs, the stresses and strains within the element can be determined only through the iterative plastic analysis described previously. Linear elastic fracture mechanics

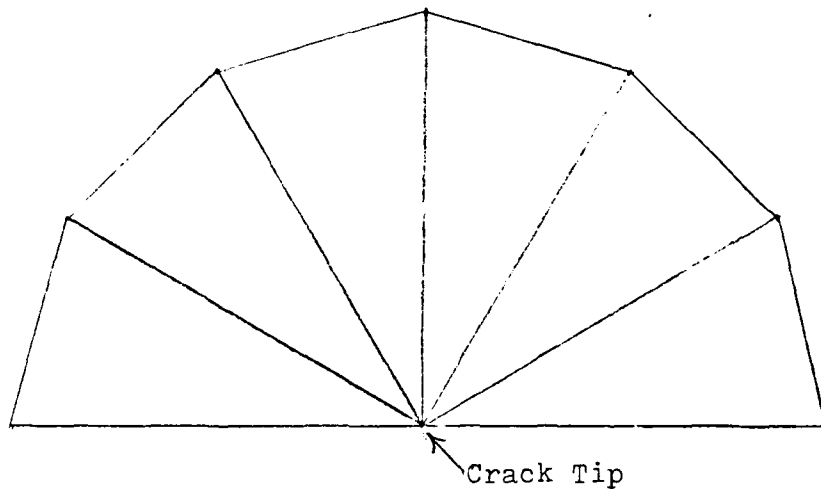


Figure 9. Crack Tip Surrounded with Crack
Tip Elements

can no longer be used to determine the stresses near the crack tip. In other words, the total stress will not increase as a function of $\frac{1}{\sqrt{r}}$ as one approaches the crack tip. Eventually, the effective stress for the elements near the crack tip will reach the maximum value that is permitted for the material under plasticity, which for IN-100 is taken as 164.0 ksi (1130.1 MPa)..

The crack tip singularity element performs irregularly in the crack tip region when the yield stress is reached due to the fact that the element is being forced to obey the $\frac{1}{\sqrt{r}}$ singularity rule even when it no longer applies. Therefore, spurious values of the stresses and strains for the crack tip element in plasticity should be seen in the finite element computer analysis.

IV. Results and Discussion

Time Independence vs. Time Dependence

The JALESE finite element program performs a time-independent, elastic-plastic analysis and uses the Prandtl-Reuss equations to determine plastic strain. The VISCO finite element program, on the other hand, performs a time-dependent, elastic-viscoplastic analysis and uses a time-dependent equation to determine plastic strain such as the Malvern flow law and Norton's law for creep. When solving plasticity problems using JALESE, one first had to input a small elastic load and the program then multiplied the load until one element became plastic. Then it was necessary to input small increments of load in order to arrive at a plastic solution. When using the VISCO program, one had to input the total desired load and a rate at which the load was to be applied. The program used a time-stepping procedure to increment the load and compute the plastic strain (see the section on Viscoplastic Solution Procedure in the Theoretical Formulation).

The time-dependent solution procedure used in VISCO was adapted for time-independent problems by first setting the creep coefficient equal to zero (Ref 8). Next, γ_p was assigned a non-zero positive value which produced a steady state solution. Finally, the load was applied quickly; therefore, a high force rate, such as 20% of the load per second, was used.

Mesh Arrangement

The first objective of the present research was to verify that the VISCO and JALESE programs were working. This was accomplished by testing a uniaxial specimen using a minimum number of elements. If the resulting plot of stress versus strain matched the uniaxial curve, the program was determined to be verified. For the constant strain triangle in the VISCO program, only two elements were used (see Fig. 10). The JALESE program was tested with two three-noded triangles and one eight-noded quadrilateral (see Fig. 11). The triangle available in the JALESE program is not a constant strain triangle but a four-noded quadrilateral condensed down to a triangle. It uses the shape functions and Gaussian integration schemes that a quadrilateral uses and not the simple functions and integration that the CST of the VISCO program uses.

For each of the test cases, the effective stress was plotted against the effective strain. The results were found to correspond very closely to the uniaxial stress-strain curve for IN-100. Since this satisfied the verification criterion, the programs were held to be in working condition.

The next task that had to be accomplished before the comparison tests could be run was to devise a suitable finite element mesh. For the constant strain triangle, the mesh that was used was identical to the one presented by Hinnerichs (Ref 7). This mesh will be discussed in later

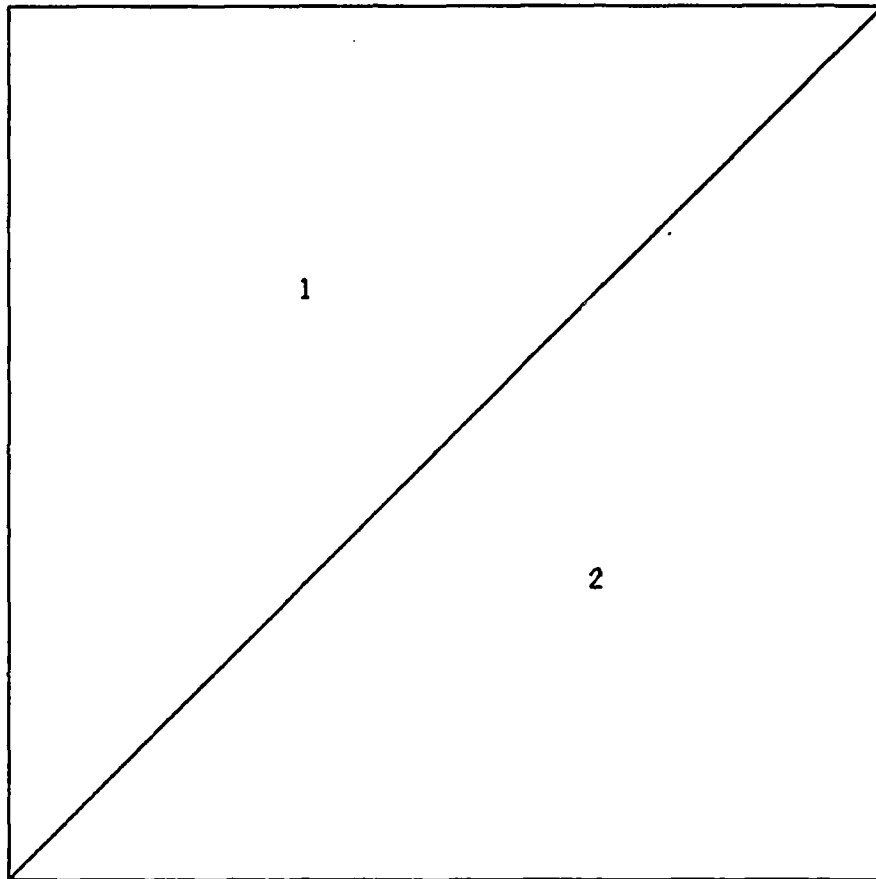


Figure 10. Two Triangular Elements Uniaxial Verification Mesh

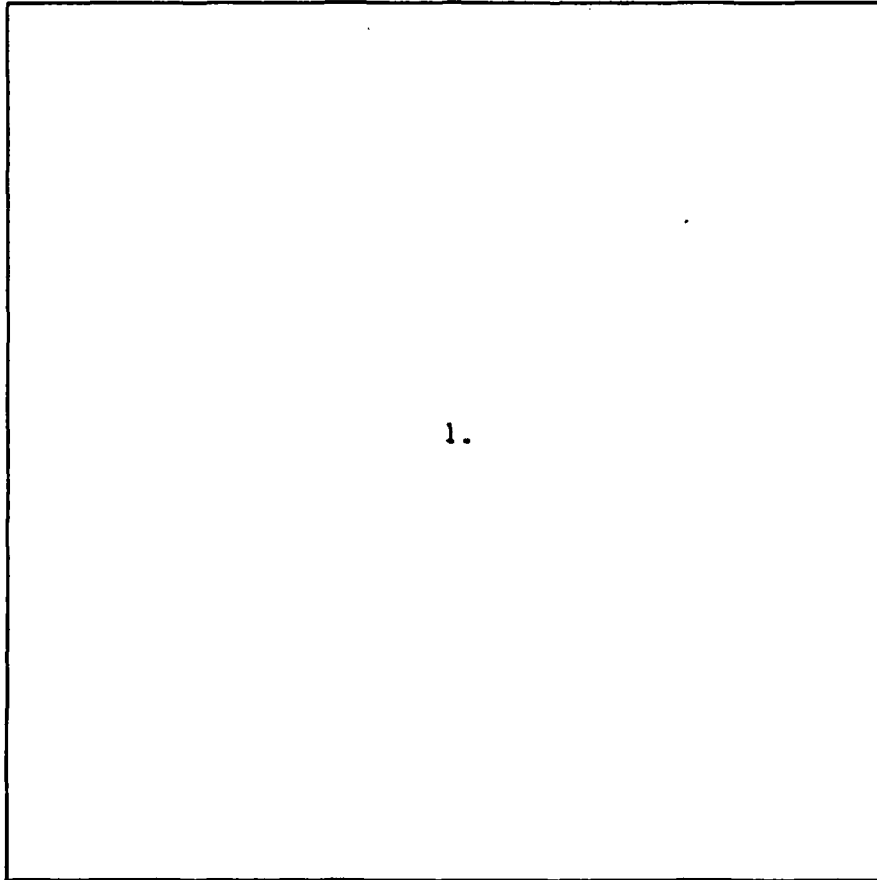


Figure 11: One Eight-Noded Element Uniaxial Verification Mesh

paragraphs. For the 8-noded and crack tip elements, it was necessary to slowly develop a finite element mesh by first devising a very coarse mesh using only 95 nodes, 170 degrees of freedom and 26 elements for the crack tip element (see Fig. 12), and 107 nodes, 192 degrees of freedom and 28 elements for the 8-noded element (see Fig. 13). The elastic stress intensity factor for each of these cases was determined, and the results were compared to the stress intensity factor for the constant strain triangle, fine mesh given in Hinnerichs as shown subsequently (Ref 7). The results were also compared with the theoretical stress intensity factor obtained from linear elastic fracture mechanics.

Once it had been verified that the very coarse mesh patterns were giving fairly accurate linear elastic answers, it then became necessary to devise the refined mesh patterns for the crack tip element mesh and the 8-noded element mesh. Barsoum (Ref 2) states that a mesh pattern that propagates radially from the crack tip works the best for elastic analysis because a radial pattern allows one to easily change element size. Such a radial pattern was used in the fine meshes. The same mesh pattern was used for elastic and plastic analysis since the mesh could not be altered in the middle of the program run. The mesh patterns are illustrated in Figs. 14-16. The crack tip region ($\frac{r}{a} \leq 0.005$) meshes are shown in Figs. 17-19.

Since the results of the eight-noded and crack tip element runs were to be compared with results from the constant strain triangle, it was necessary to keep the number

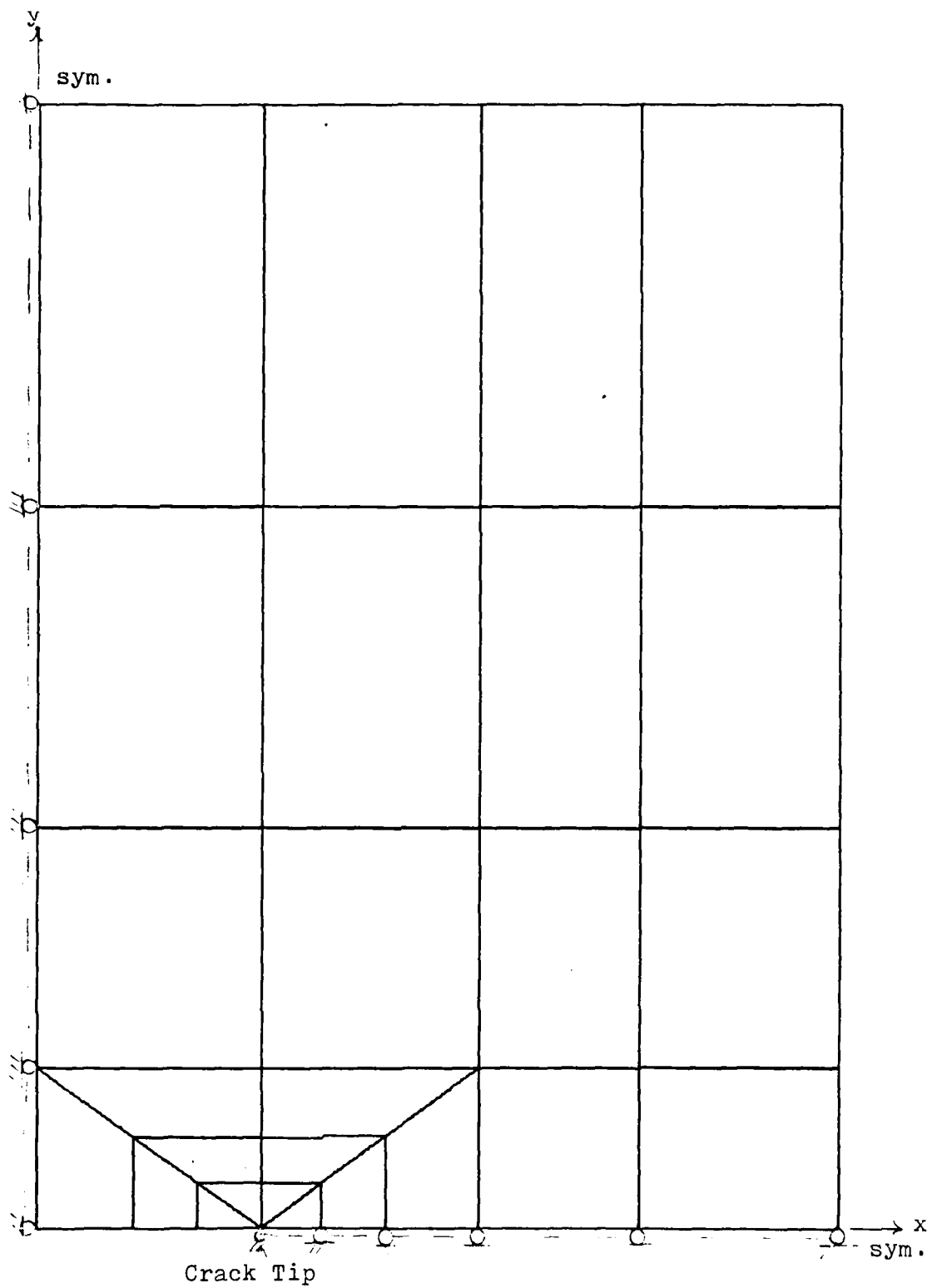


Figure 12. Crack Tip Element Test Mesh

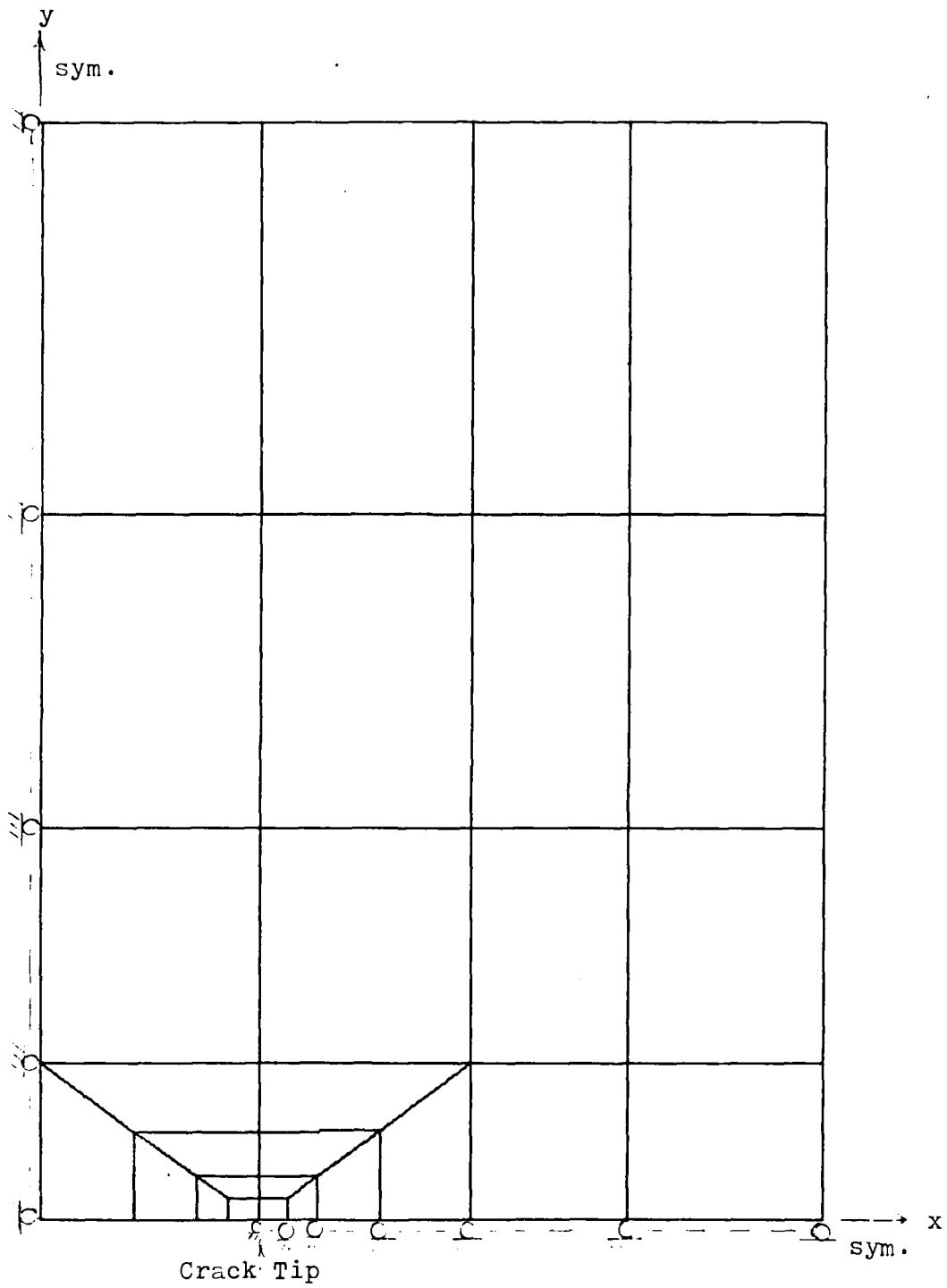


Figure 13. Eight-Noded Element Test Mesh

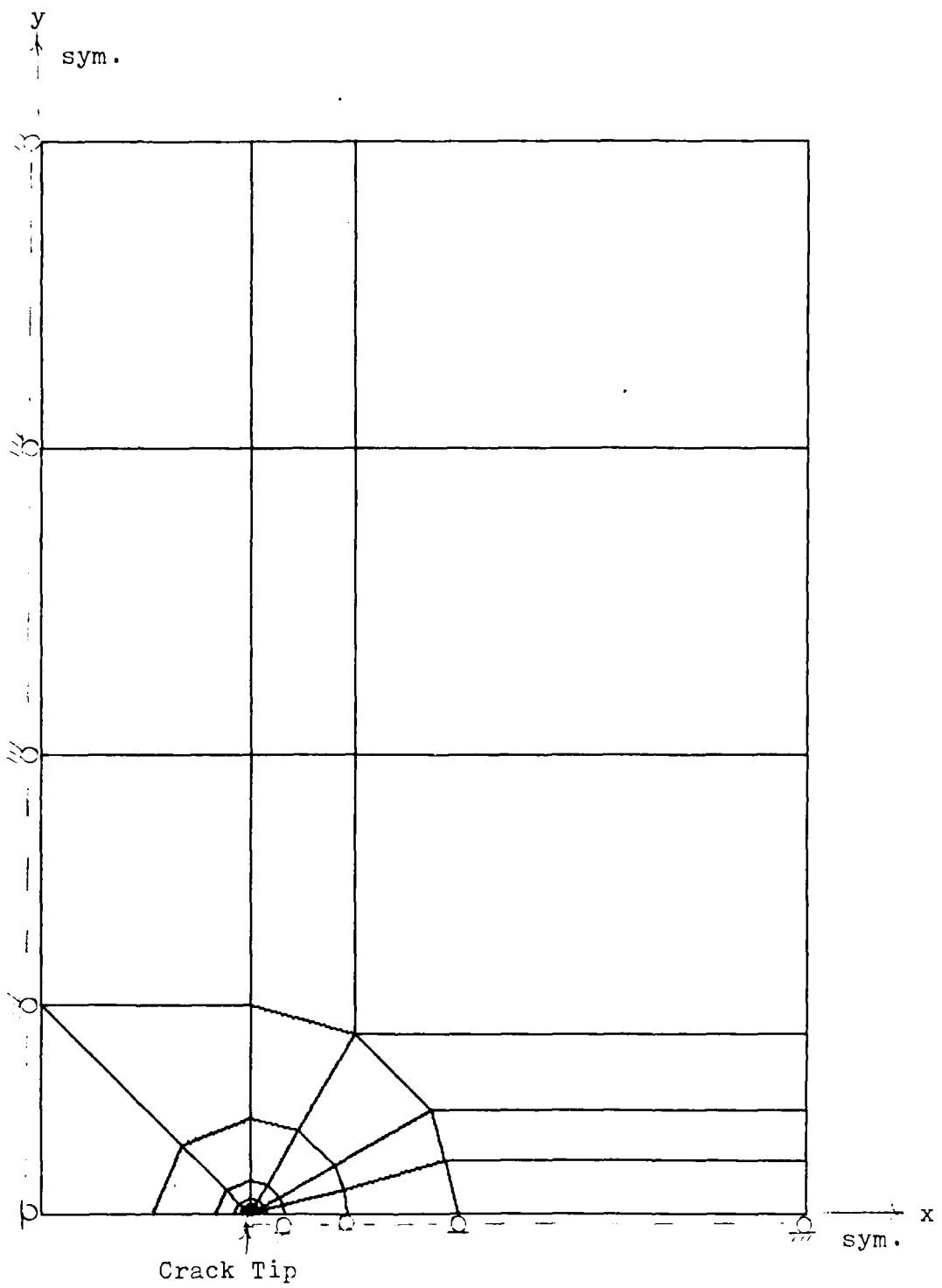


Figure 14. Crack Tip Element Fine Mesh

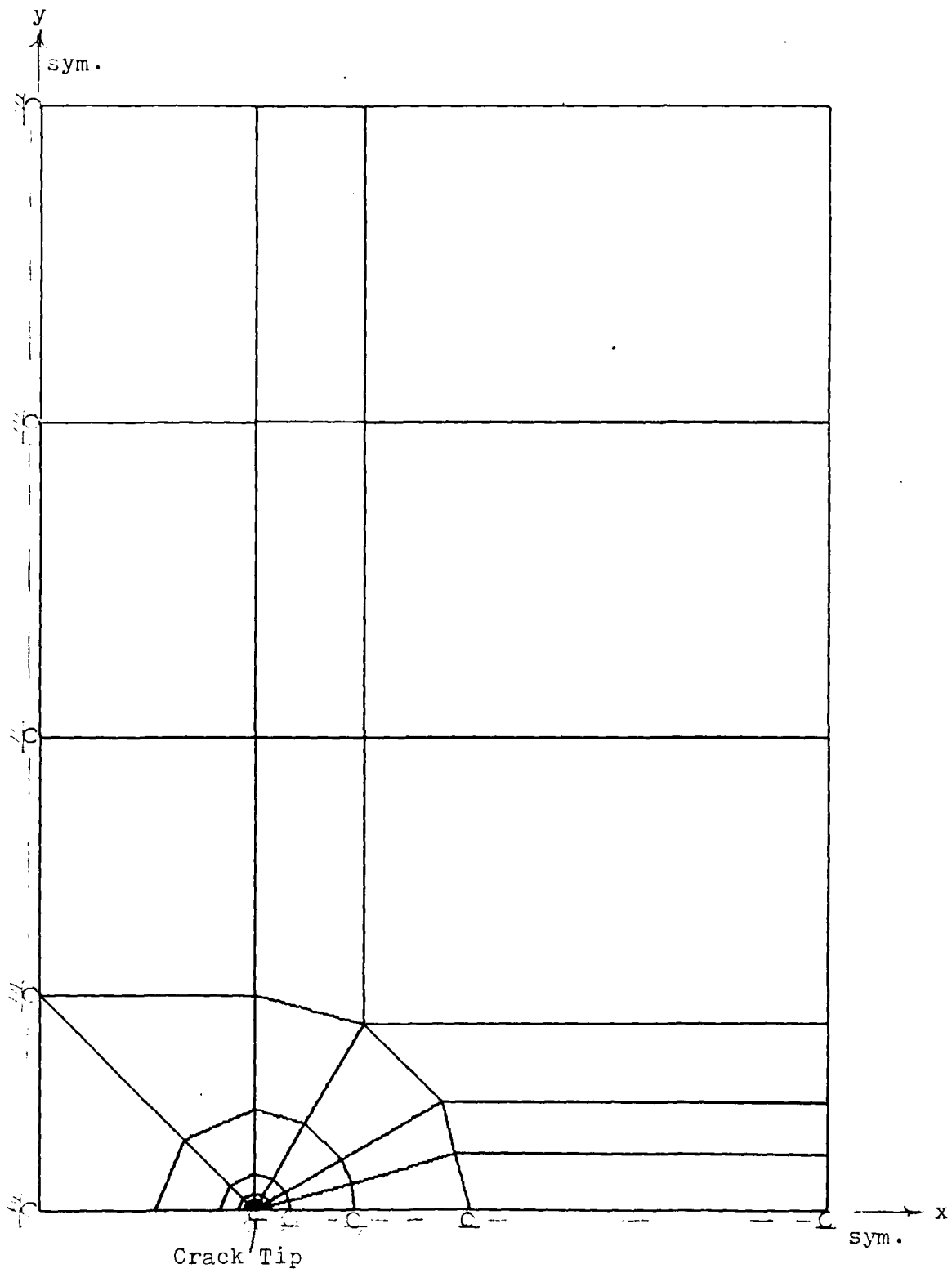


Figure 15. 8-Noded Element Fine Mesh

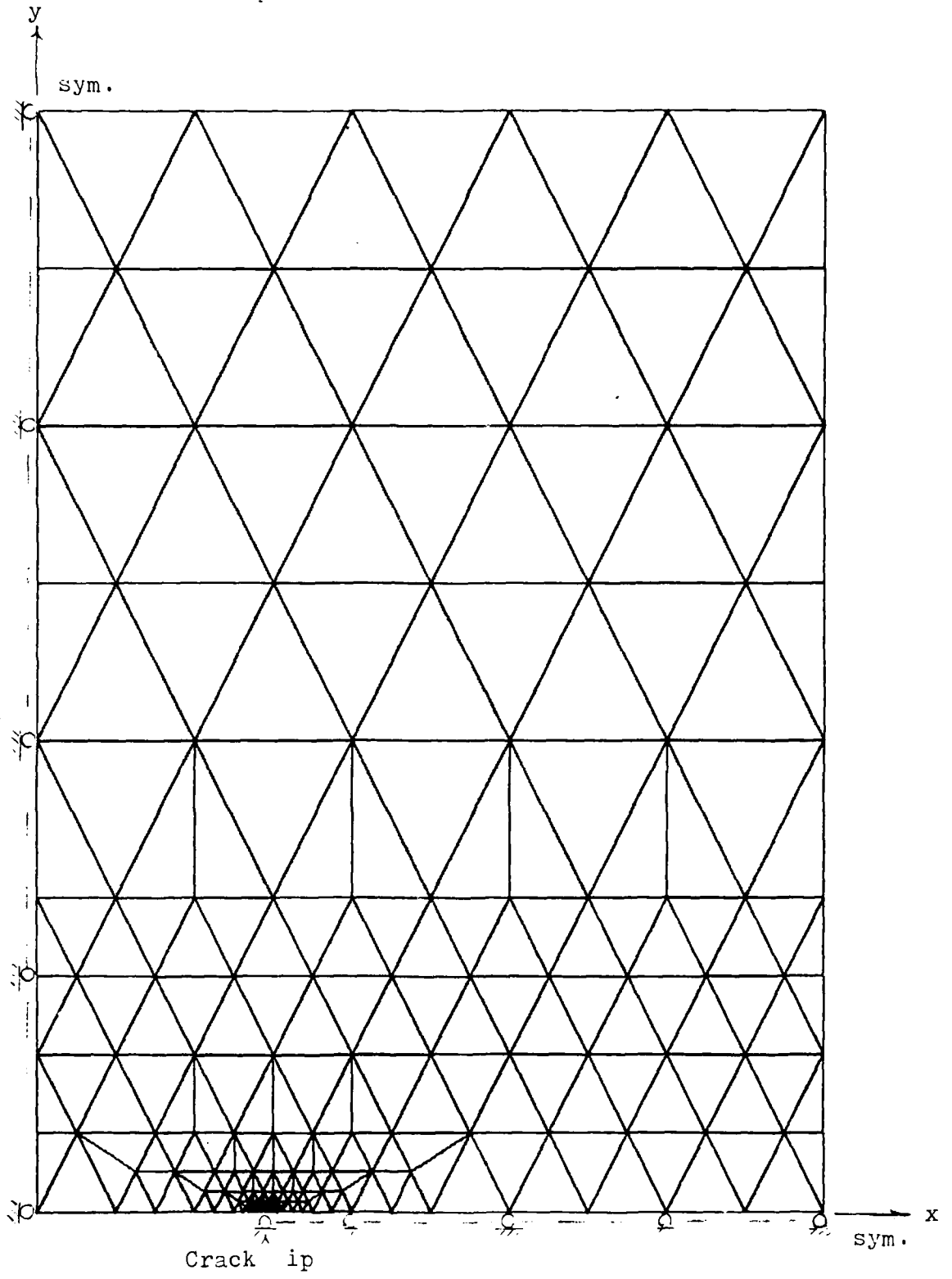


Figure 16. CST Fine Mesh

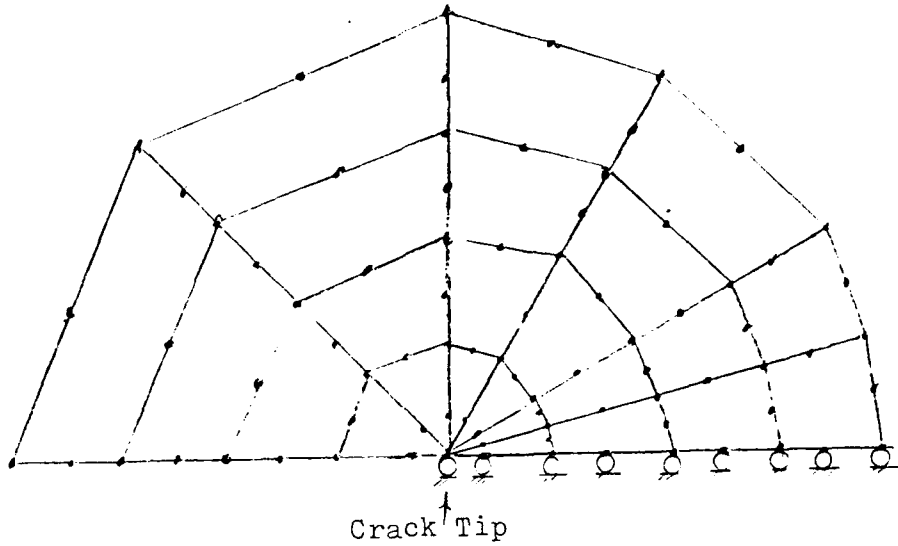


Figure 17. Crack Tip Region - Crack Element,
Fine Mesh

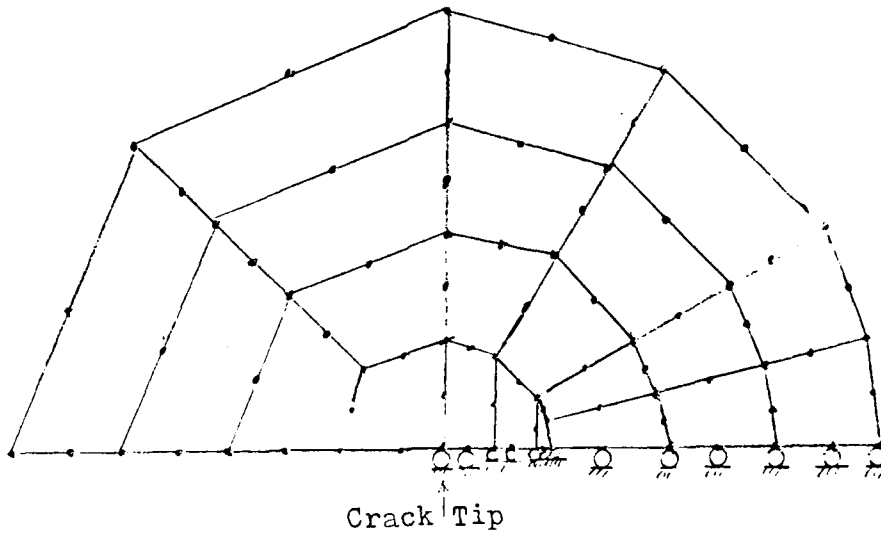


Figure 18. Crack Tip Region - 8-Noded Element
Fine Mesh

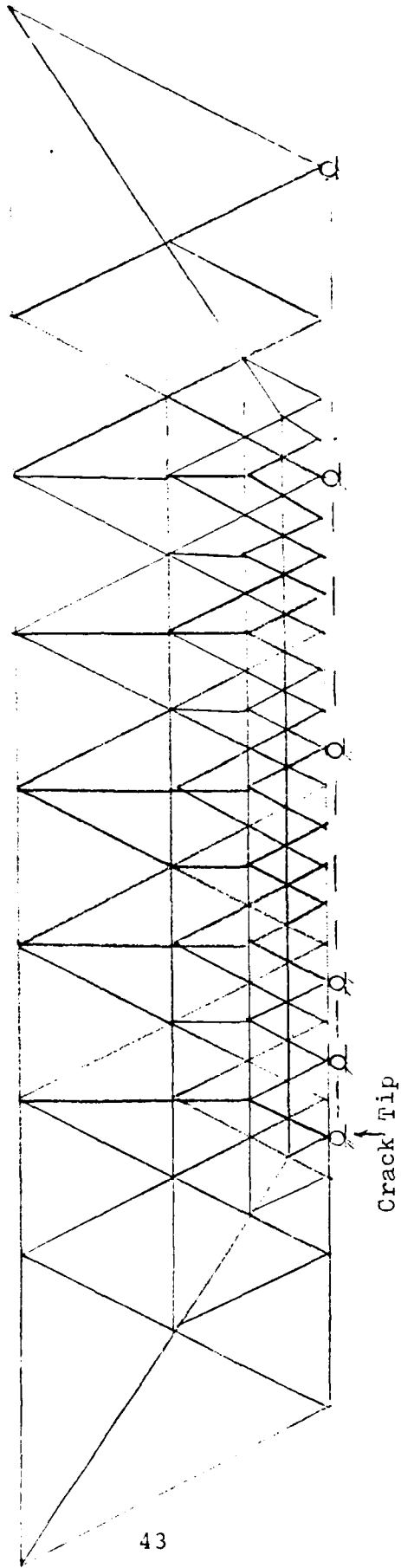


Figure 19. Crack Tip Region - CST, Fine Mesh

of degrees of freedom in the various regions the same. By doing this, one is able to compare each type of element to their primary characteristics. The number of degrees of freedom is the important parameter because the number of displacement equations to be solved equals the number of degrees of freedom. Equal degrees of freedom in given regions isolates the effect of element types as discussed subsequently. Therefore, for comparable results, it is important that the number of degrees of freedom in each test case be kept the same.

Table I shows the number of degrees of freedom in each region. Notice that overall, the crack tip element mesh had 60 elements, 205 nodes and 382 degrees of freedom, the eight-noded element mesh had 58 elements, 207 nodes, and 382 degrees of freedom, and the constant strain triangle mesh had 355 elements, 211 nodes, and 378 degrees of freedom. The crack tip element mesh and the eight-noded element mesh had exactly the same number of degrees of freedom and the constant strain triangle mesh had only 1% fewer degrees of freedom.

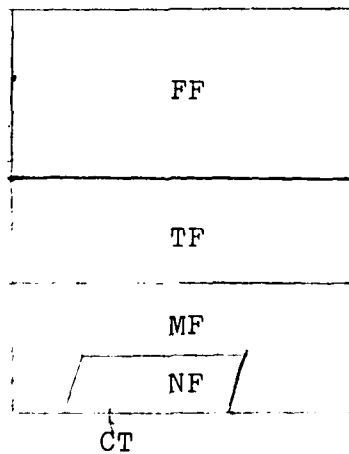
The two most important regions for which the number of degrees of freedom must be under close scrutiny are the far field region, for this is where the stresses are applied, and the crack tip region, since this is where the most important stress analysis will occur. In the crack tip region, the crack tip element mesh and the eight-noded element mesh had exactly the same number of degrees of

TABLE I

Regions and Degrees of Freedom, Fine Meshes

region see sketch below	r/a (approx.)	no. of d.o.f. (approx.)		
		crack el.	8-noded	CST
crack tip (CT)	0.05	153	153	151
near field (NF)	$0.05 < r/a < 0.5$	113	113	125
mid field (MF)	$0.5 < r/a < 1.0$	57	57	37
transition field (TF)	$1.0 \leq r/a \leq 2.0$	8	8	12
far field (FF)	$2.0 \leq r/a \leq 4.0$	53	53	59

fine mesh type	Totals		
	no. of elements	no. of nodes	no. of d.o.f.
crack tip element	60	205	382
8-noded element	58	207	382
CST	355	211	378



freedom, and the constant strain triangle mesh had only 4% more degrees of freedom. In the far field region, the crack tip element mesh and the eight-noded element mesh had the same number of degrees of freedom, and the constant strain triangle mesh had only 10% more degrees of freedom. Large differences occur in the intermediate regions. This is unavoidable. The reductions in element size for the eight-noded and crack tip element meshes occurred differently than for the constant strain triangle mesh.

After the tests with the fine meshes were completed, a coarse mesh in which the number of degrees of freedom in the crack tip region was halved was tried for the crack tip element and the eight-noded element meshes. The crack tip region arrangement for the coarse meshes are shown in Fig. 20 and 21. The coarse meshes were used to validate the convergence of fine mesh solutions.

Elastic Analysis-Stress Intensity Factor

The stress intensity factor describes the magnitude of the elastic stress field in the crack tip region (Ref 10). K_I was defined in Eq. 37. The relation between K_I and stress for any r or angle θ is given in Eq. 39.

Chan (Ref 4) gives a nondimensionalized form of the elastic stress intensity factor. This may be written as:

$$\bar{K}_I = \frac{K_I}{\sigma_\infty \sqrt{a}} \quad (49)$$

For the center-cracked plate with $a=0.1367$ in. and $b=0.5$ in., \bar{K}_I is equal to 1.86.

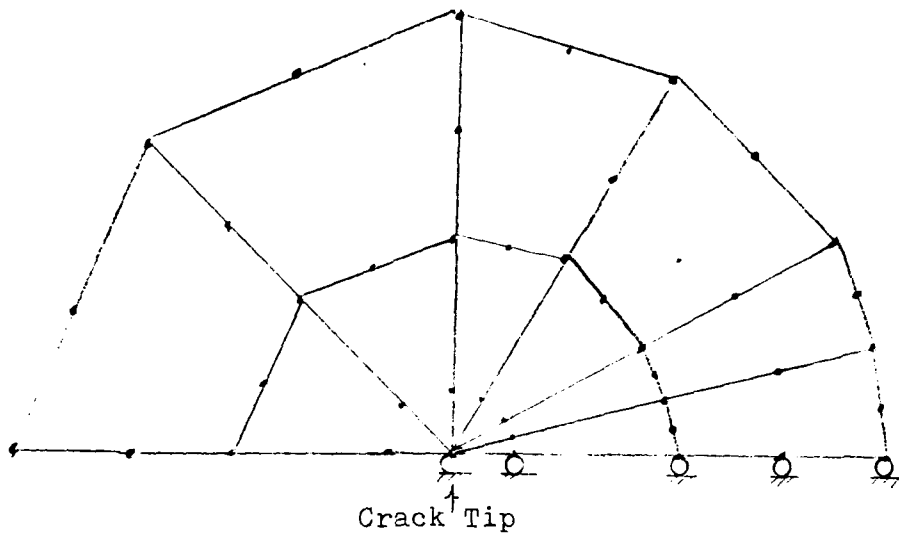


Figure 20. Crack Tip Region - Crack Element,
Coarse Mesh

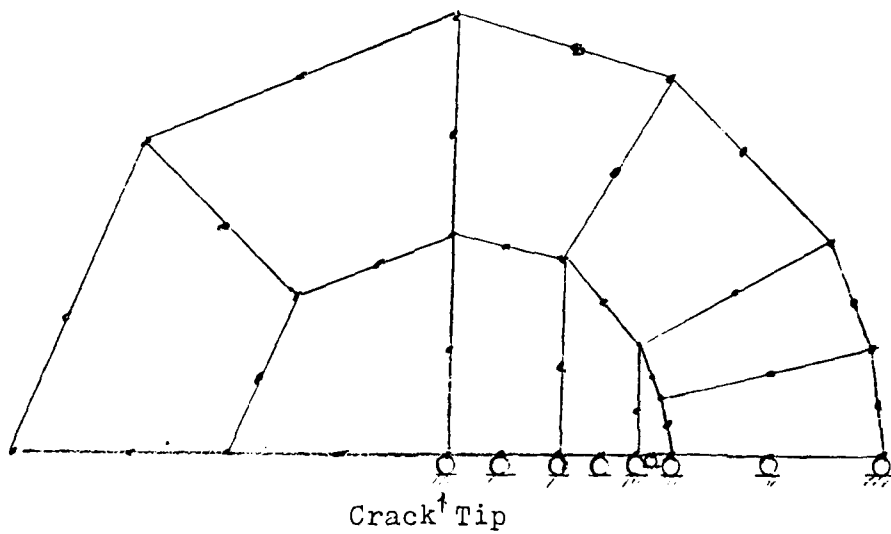


Figure 21. Crack Tip Region - 8-Noded Element,
Coarse Mesh

Numerical Evaluation of K_I . K_I was calculated numerically from the elastic finite element solutions. A radial line was drawn from the crack tip at a small angle, which was taken to be 7.5° . In order to determine K_I , an elastic analysis was first performed with the finite element problem. Values of σ_y were taken at several stations of r in the crack tip region. For each value of σ_y , K_I was determined by the following equation, which is a form of Eq. 39:

$$K_I = \sigma_y \sqrt{2\pi r} \left[\cos \frac{\theta}{2} (1 + \sin \frac{\theta}{2} \sin \frac{3\theta}{2}) \right]^{-1} \quad (50)$$

The value of K_I obtained was nondimensionalized by dividing it by σ_∞ (the applied stress). The resulting nondimensionalized stress intensity factor, K_I , was then plotted against its value of r/a . This was done for all of the points in the crack tip region. The resulting curve of \bar{K}_I vs. r/a was extrapolated to the \bar{K}_I axis ($r/a=0$). This was the elastic value of the nondimensionalized stress intensity factor for the problem.

The graphs of nondimensionalized stress intensity factor versus r/a are presented in Fig. 22 and Fig. 23. Table II presents the extrapolated value of the nondimensionalized stress intensity factor for each mesh.

From Table II, it is shown that the constant strain triangle and the eight-noded fine mesh both generate the same value of \bar{K}_I that was calculated using linear elastic fracture mechanics. The eight-noded element in a fine mesh and the constant strain triangle in a fine mesh, therefore,

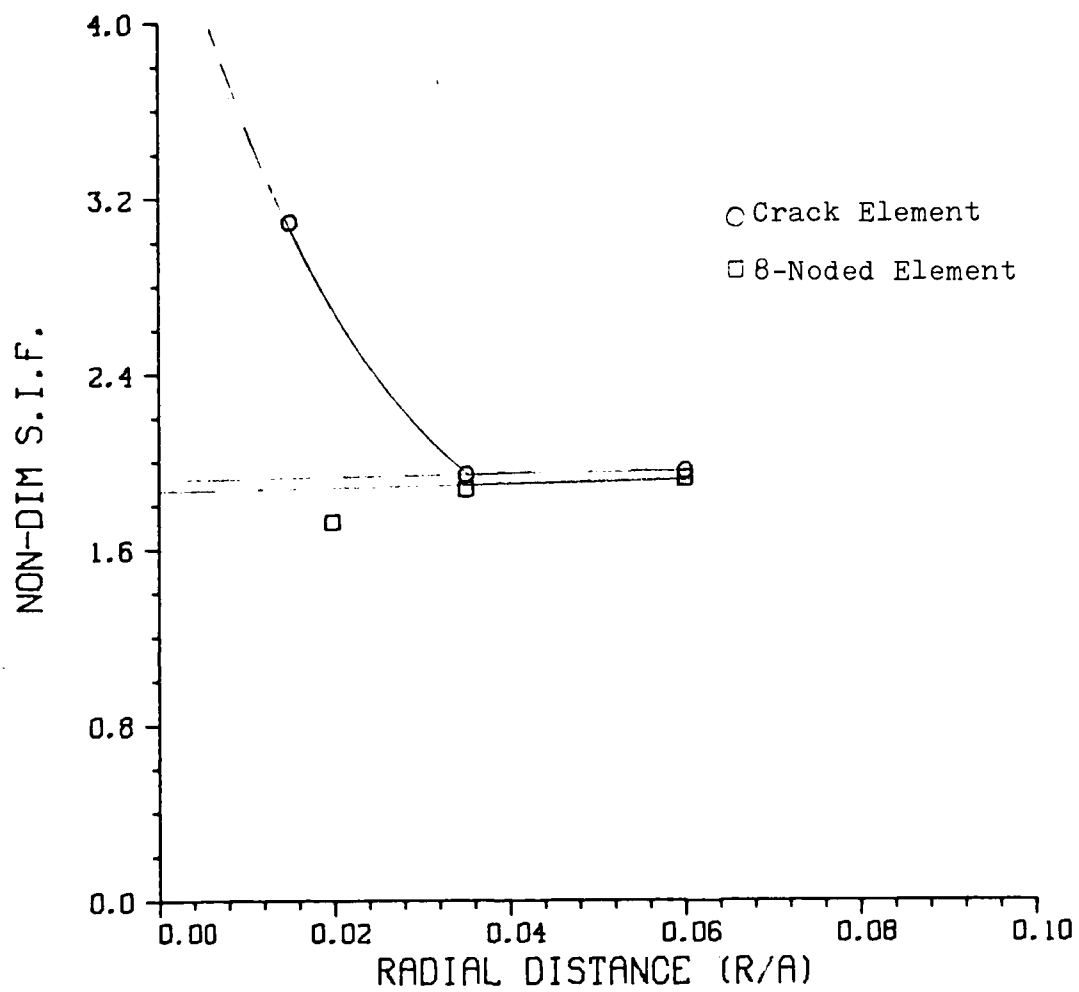


Figure 22. Elastic Analysis (\bar{K}_I), Coarse Meshes

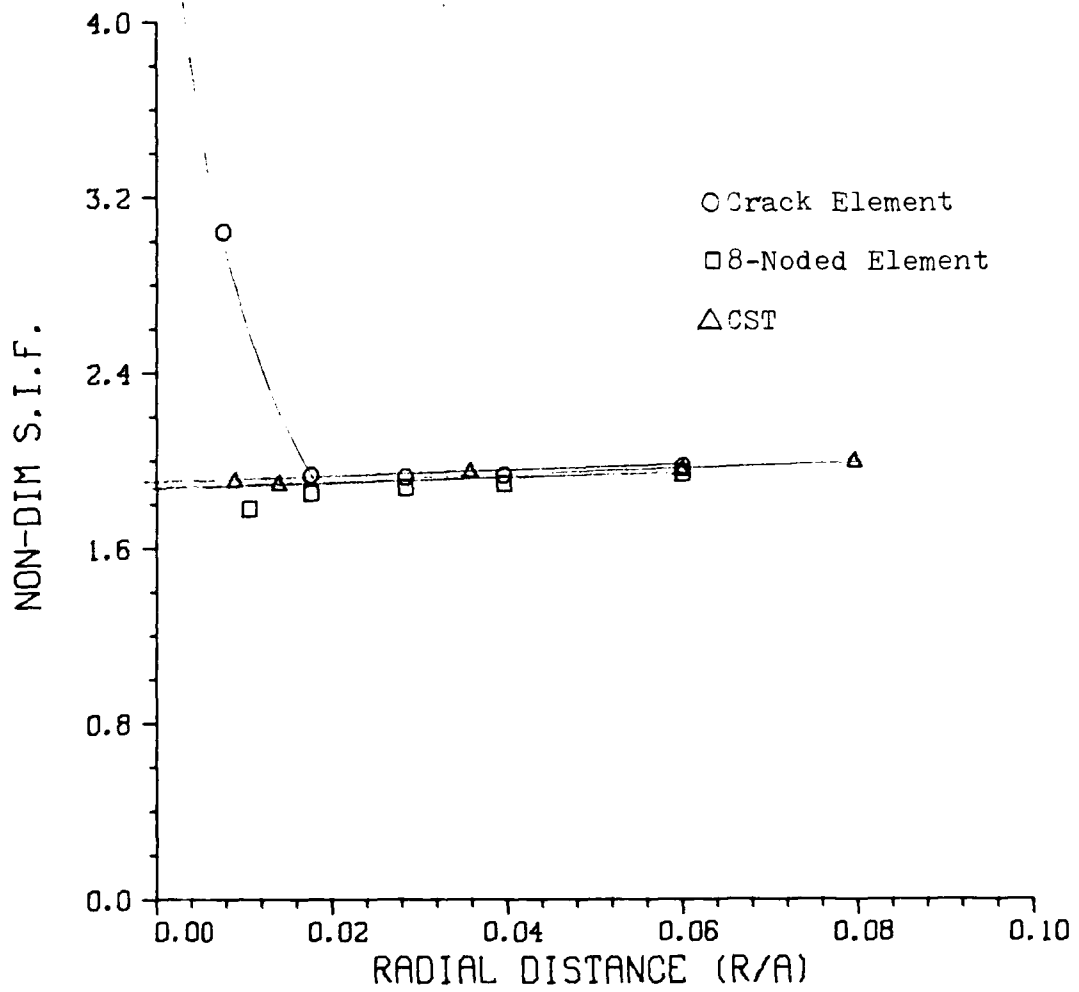


Figure 23. Elastic Analysis (\bar{K}_I), Fine Meshes

TABLE II

Elastic Analysis, Values of \bar{K}_I for Fine and Coarse Meshes

type of element and mesh	\bar{K}_I
crack tip element - coarse	2.34
8-noded element - coarse	1.95
crack tip element - fine	1.95
8-noded element - fine	1.86
CST - fine	1.86

were the best elements for solving the elastic problem. It is noted from Fig. 22 and Fig. 23 that the crack tip element does effectively simulate the $\frac{1}{\sqrt{r}}$ singularity, \bar{K}_I becomes very large near the crack tip. However, the extrapolated values of \bar{K}_I for this element were not as close to the K_I values for the constant strain triangle and the eight-noded element. The crack tip singularity element did not perform as well elastically as Barsoum predicted (Ref 2). This was true both for the fine and coarse meshes.

There was a 20% difference between the values of K_I for the crack element fine mesh and the crack element coarse mesh. The K_I values for the eight-noded fine and coarse meshes also differed by 20%. Therefore, the coarse mesh elastic solutions converged to the fine mesh elastic solutions.

Plastic Analysis

Two different values of loading were used for the plastic analysis; 10.896 Klb (48.465 kN) and 16.060 Klb (71.435 kN). The applied stresses therefore were 36.320 ksi (250.29 MPa) and 53.533 ksi (368.91 MPa). These loadings corresponded to values of K of 25.0 ksi $\sqrt{\text{in}}$ (27.4 MPa $\sqrt{\text{m}}$) and 36.8 ksi $\sqrt{\text{in}}$ (40.41 MPa $\sqrt{\text{m}}$). As stated in Appendix B, the loadings had to be applied as equivalent nodal forces. This procedure is outlined in Appendix B.

The comparison criteria for the plastic analysis were plastic regions, profiles of σ_e vs. r/a for several angles,

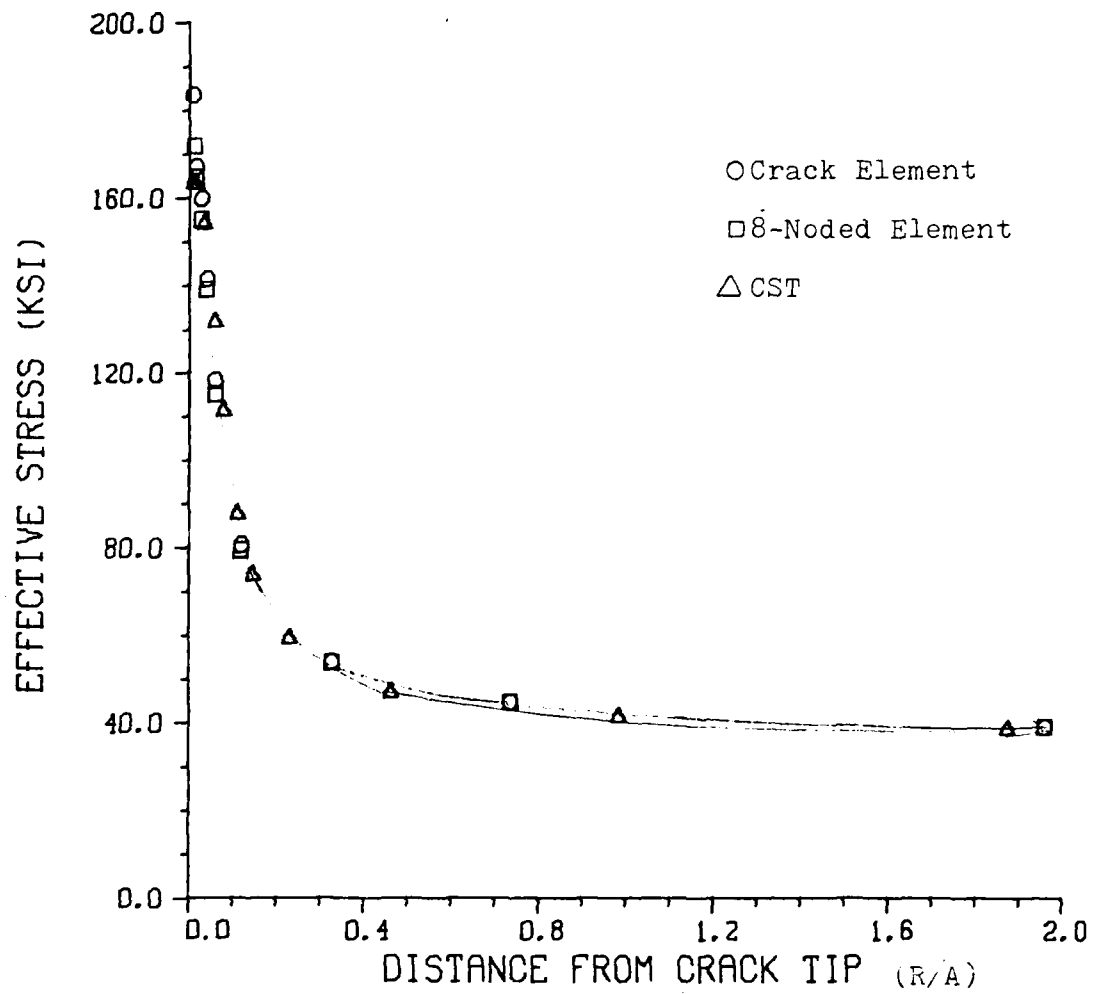


Figure 24. Stress Profiles, $\theta = 7.5^\circ$,
 $P = 10.896 \text{ klb}$

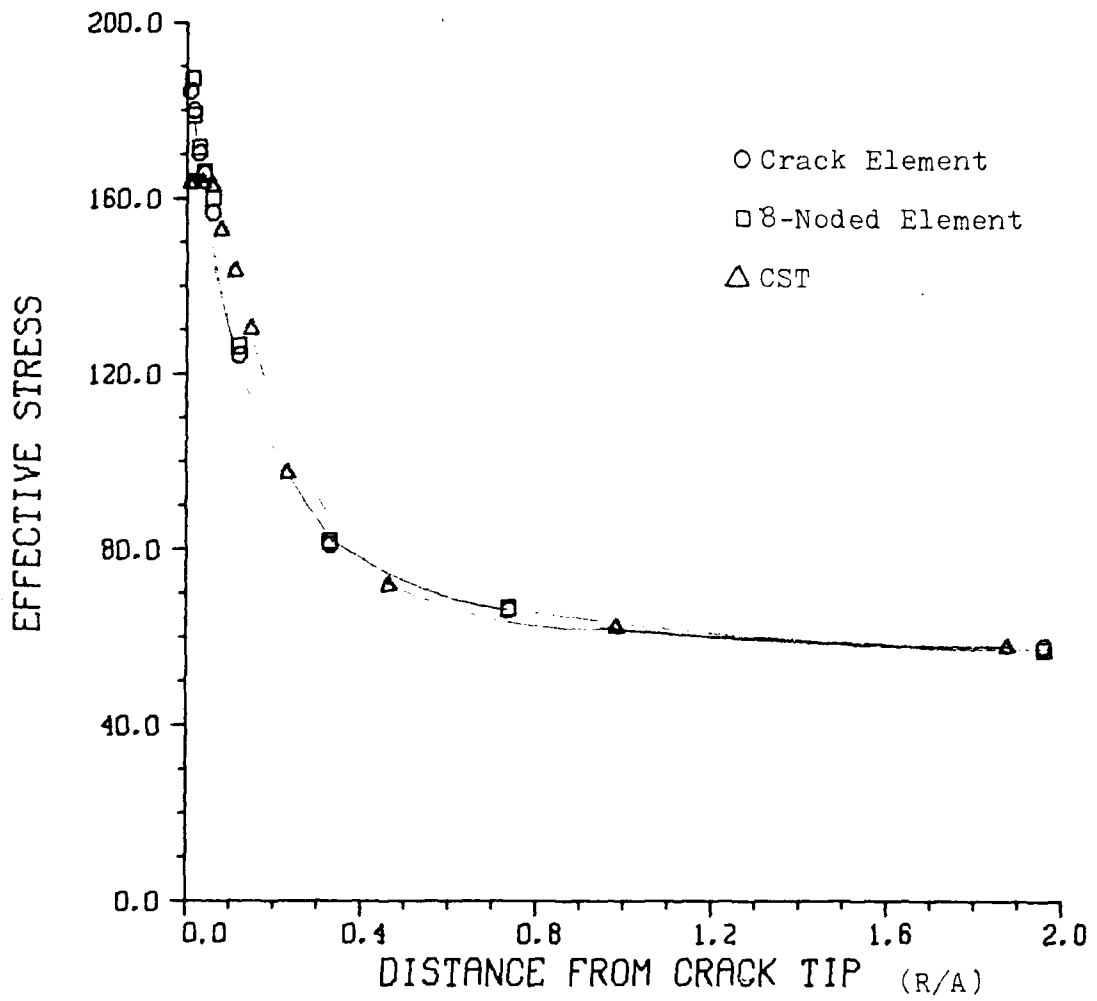


Figure 25. Stress Profiles, $\theta = 7.5^\circ$,
 $P = 16.060$ klb

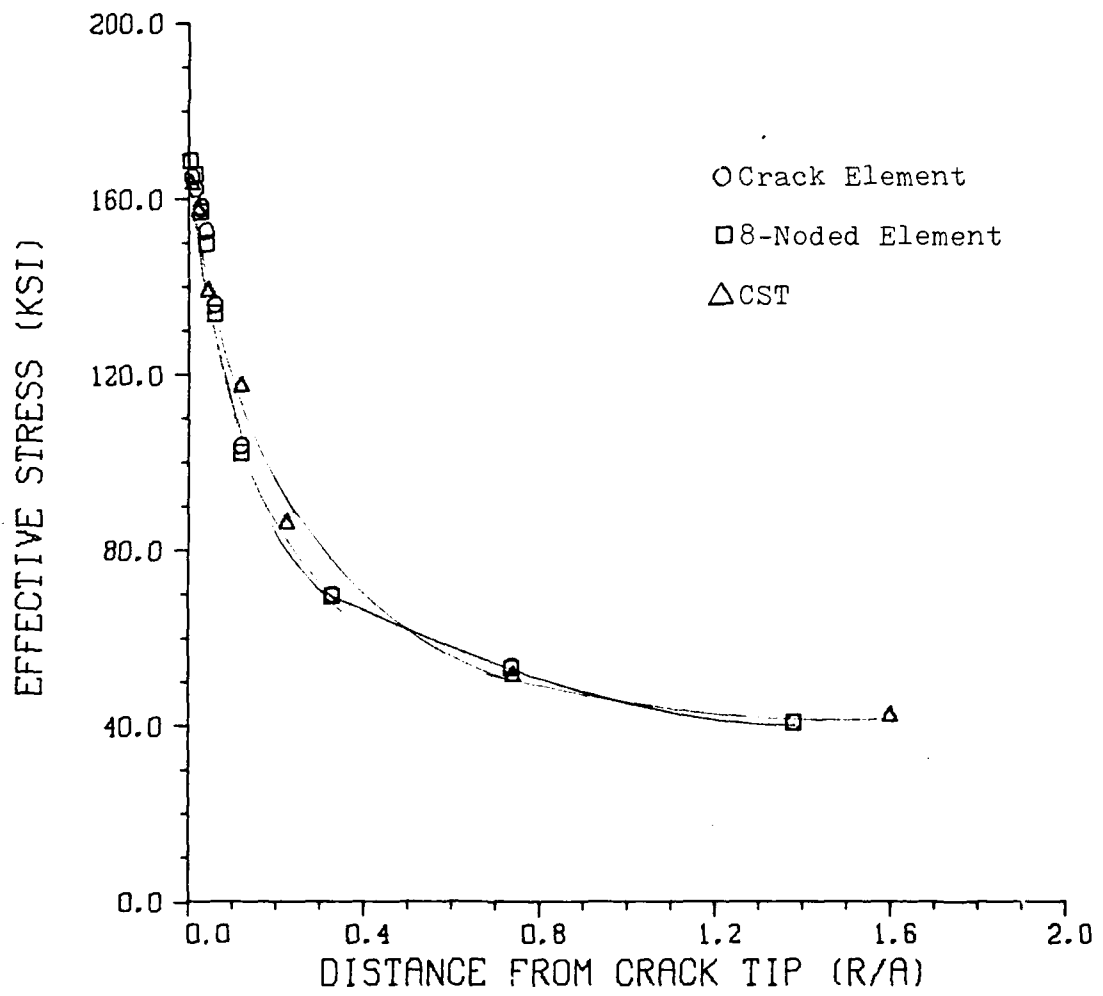


Figure 26. Stress Profiles, $\theta = 45^\circ$,
 $P = 10.896 \text{ klb}$

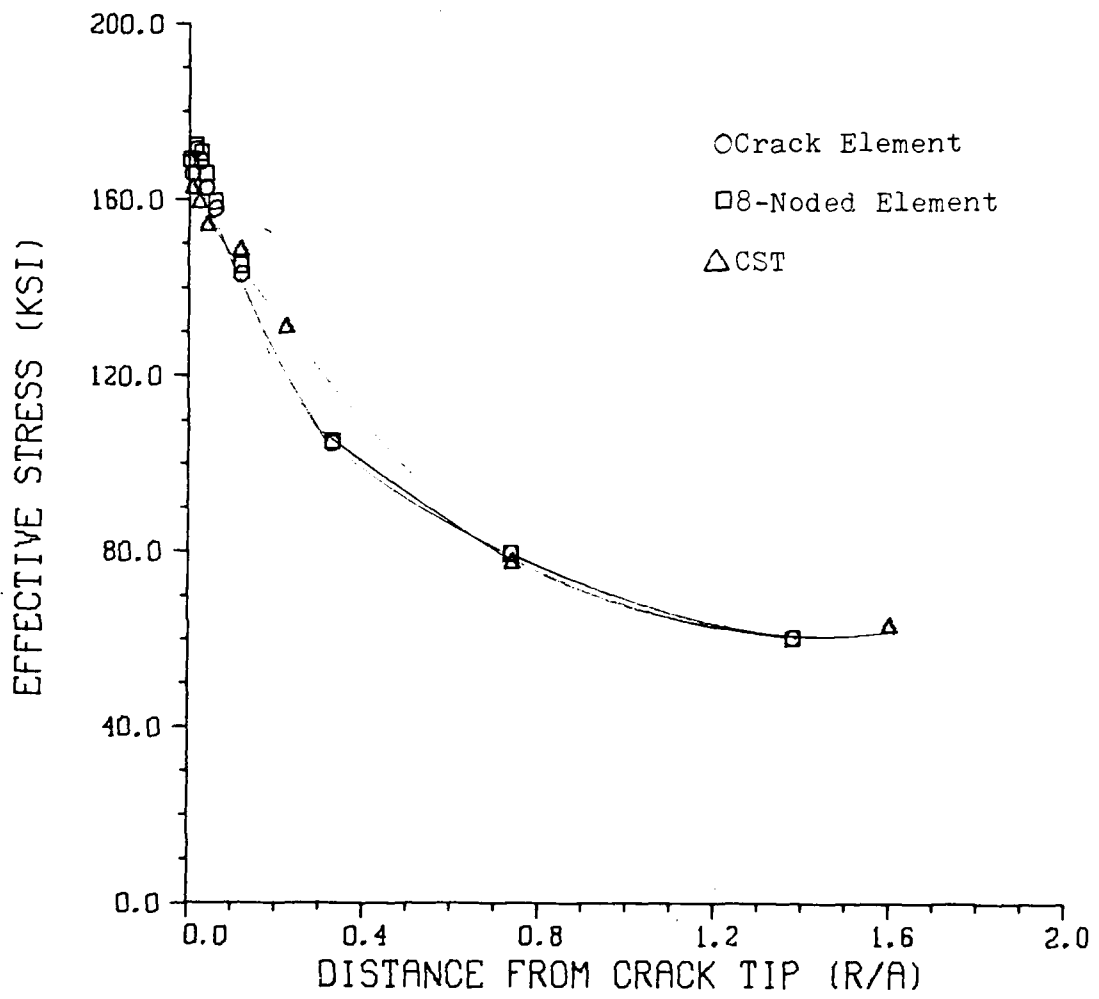


Figure 27. Stress Profiles, $\theta = 45^\circ$,
 P = 16.060 klb

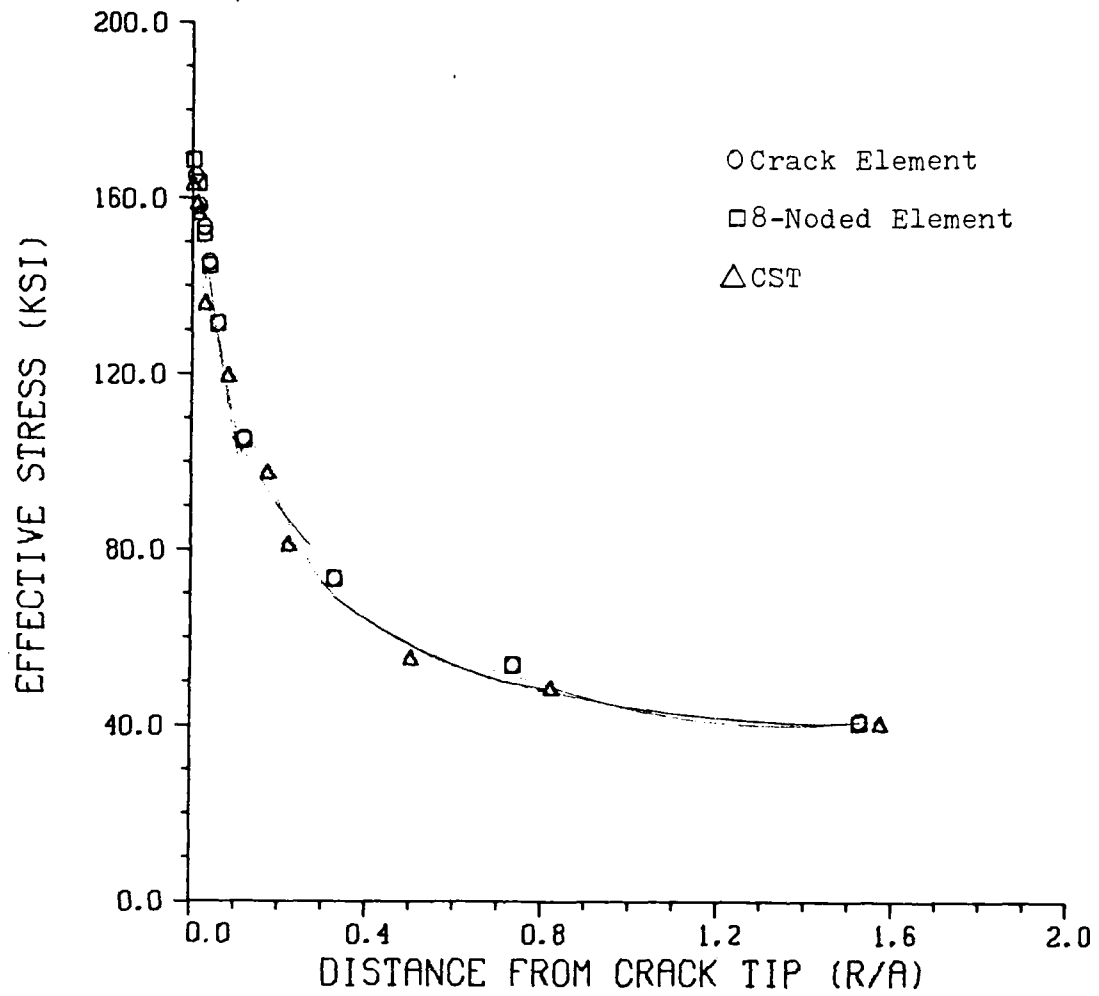


Figure 28. Stress Profiles, $\theta = 75^\circ$,
 P = 10.896 klb

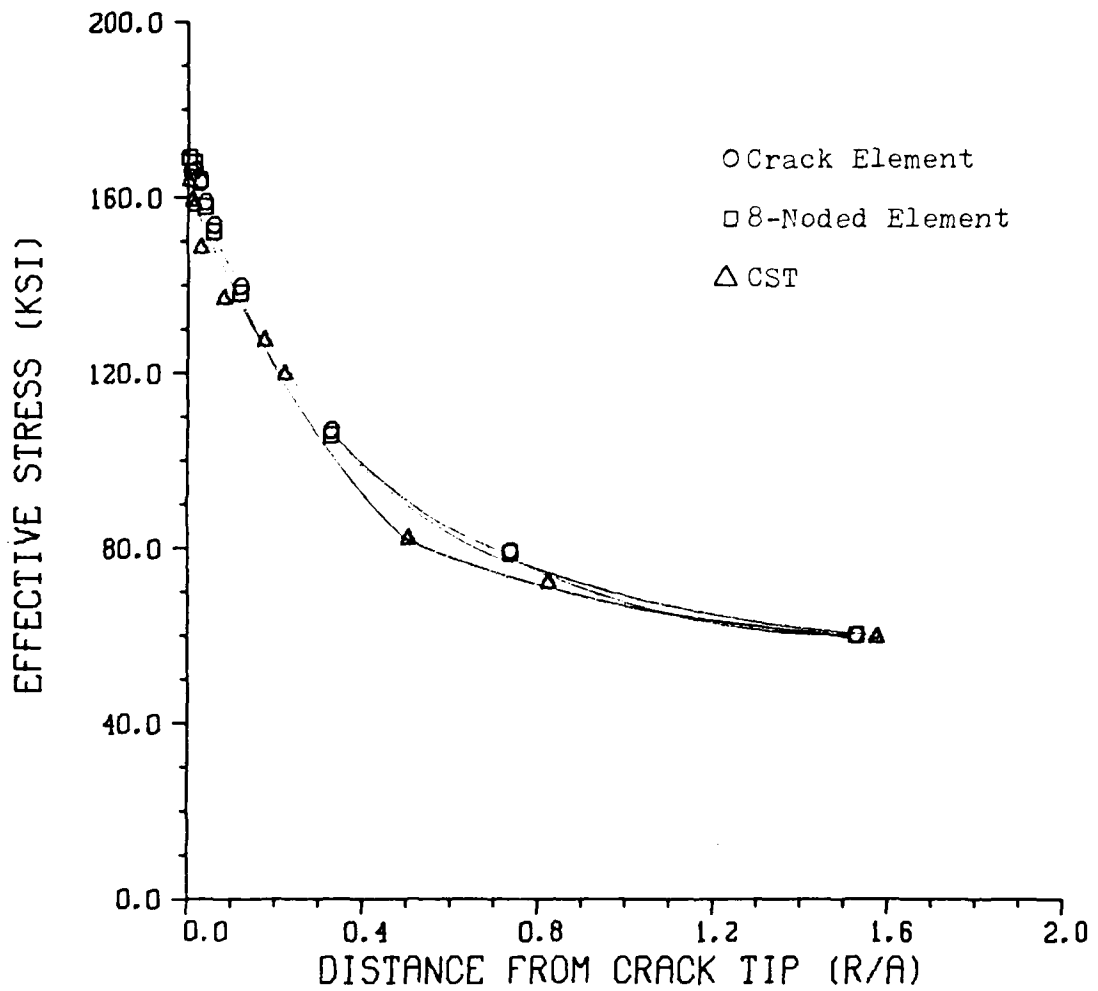


Figure 29. Stress Profiles, $\theta = 75^\circ$,
 P = 16.060 klb

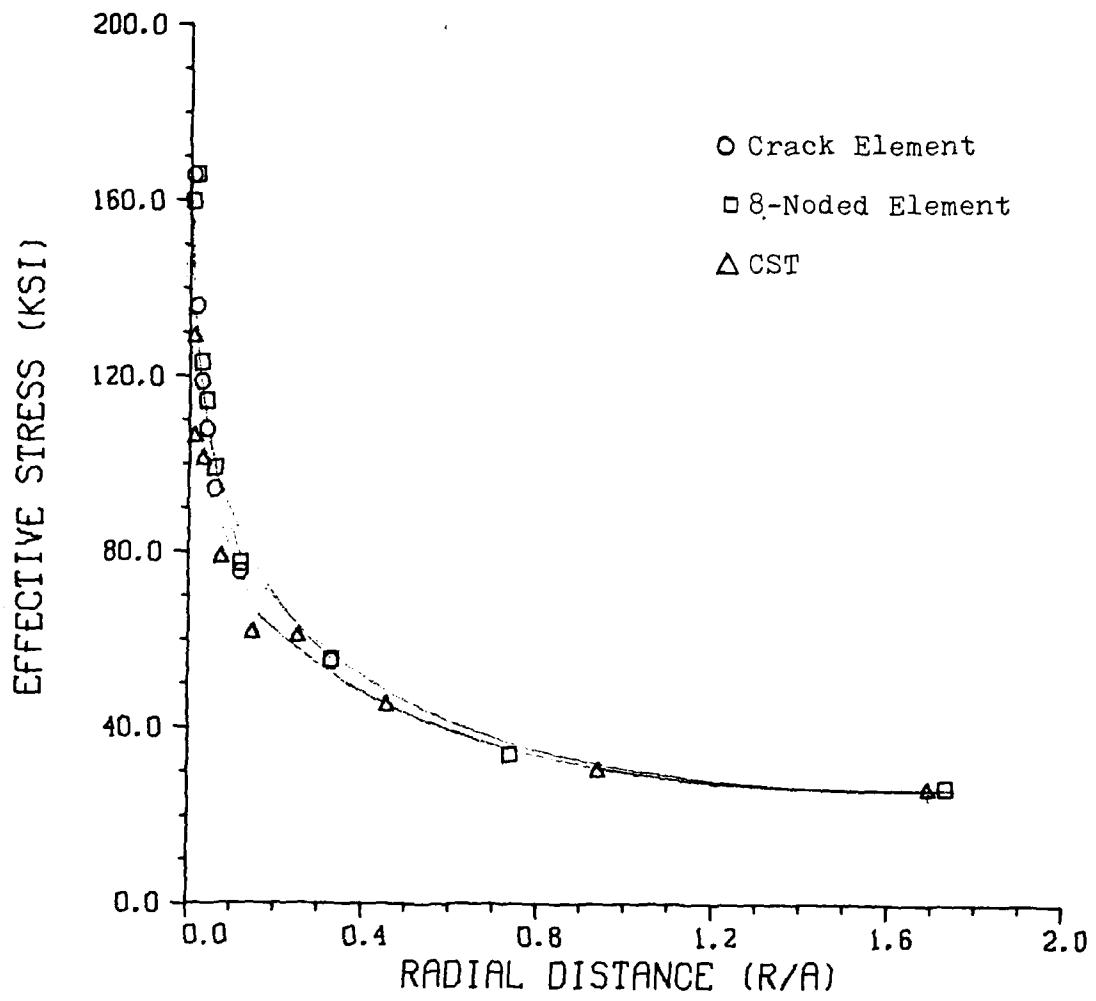


Figure 30. Stress Profiles, $\theta = 112.5^\circ$,
 $P = 10.896 \text{ klb}$

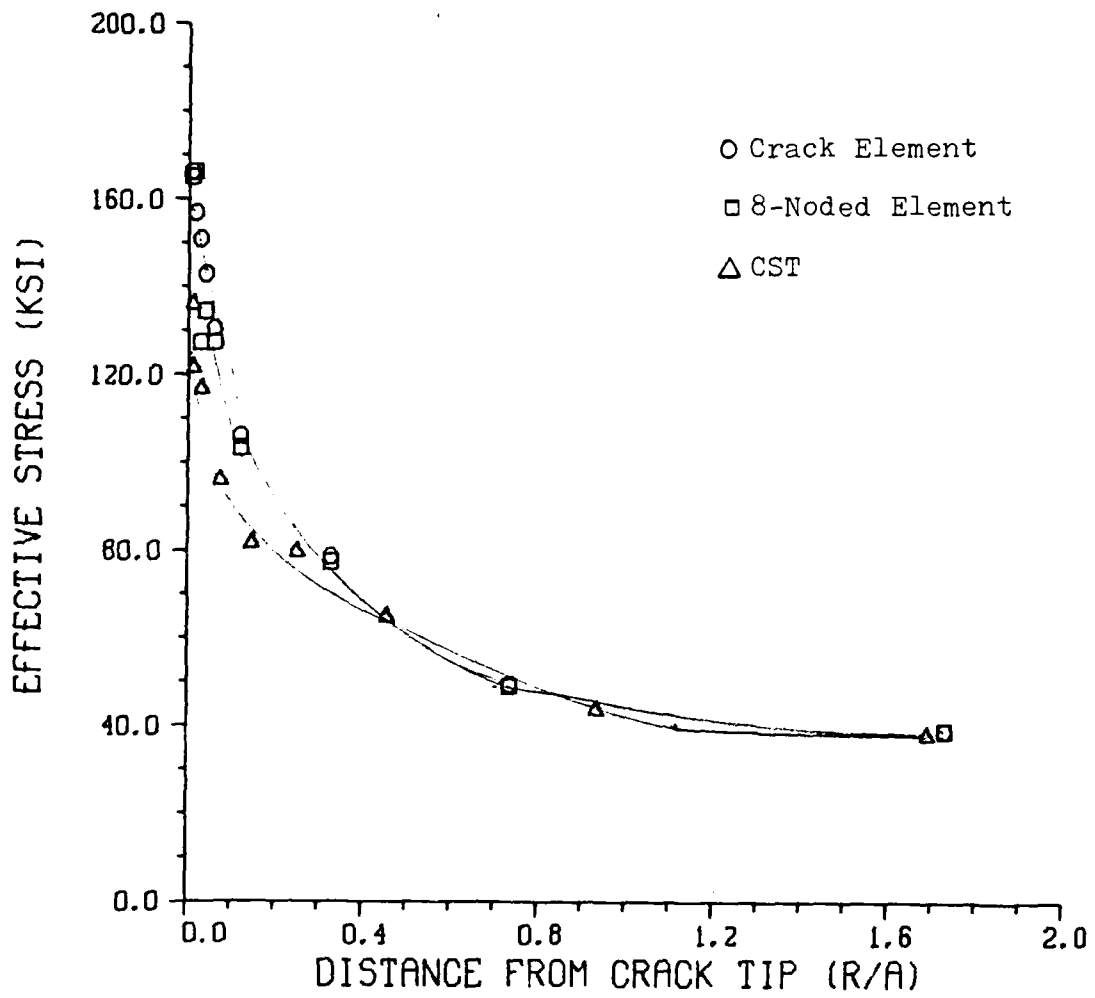


Figure 31. Stress Profiles, $\theta=112.5^\circ$,
 $P = 16.060 \text{ klb}$

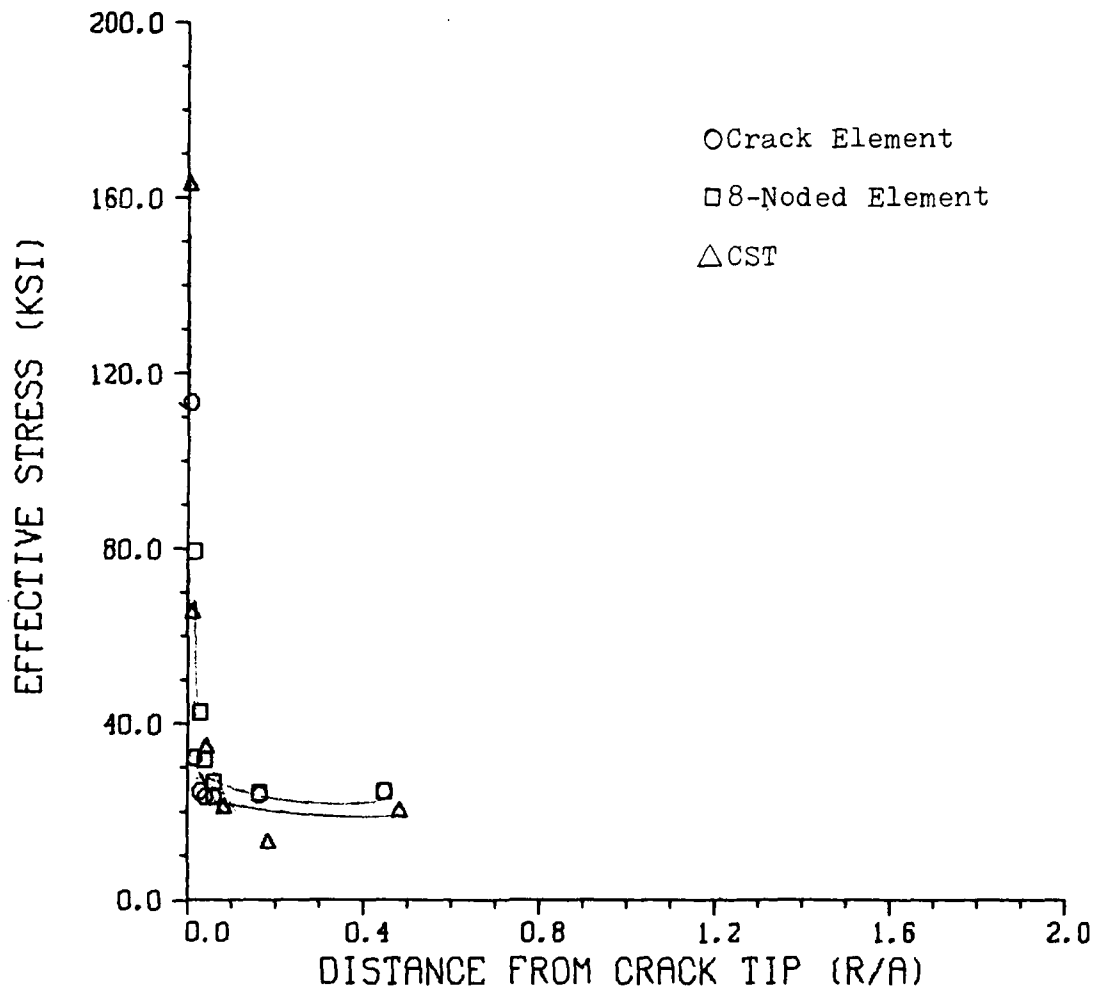


Figure 32. Stress Profiles, $\theta = 157.5^\circ$,
 $P = 10.896 \text{ klb}$

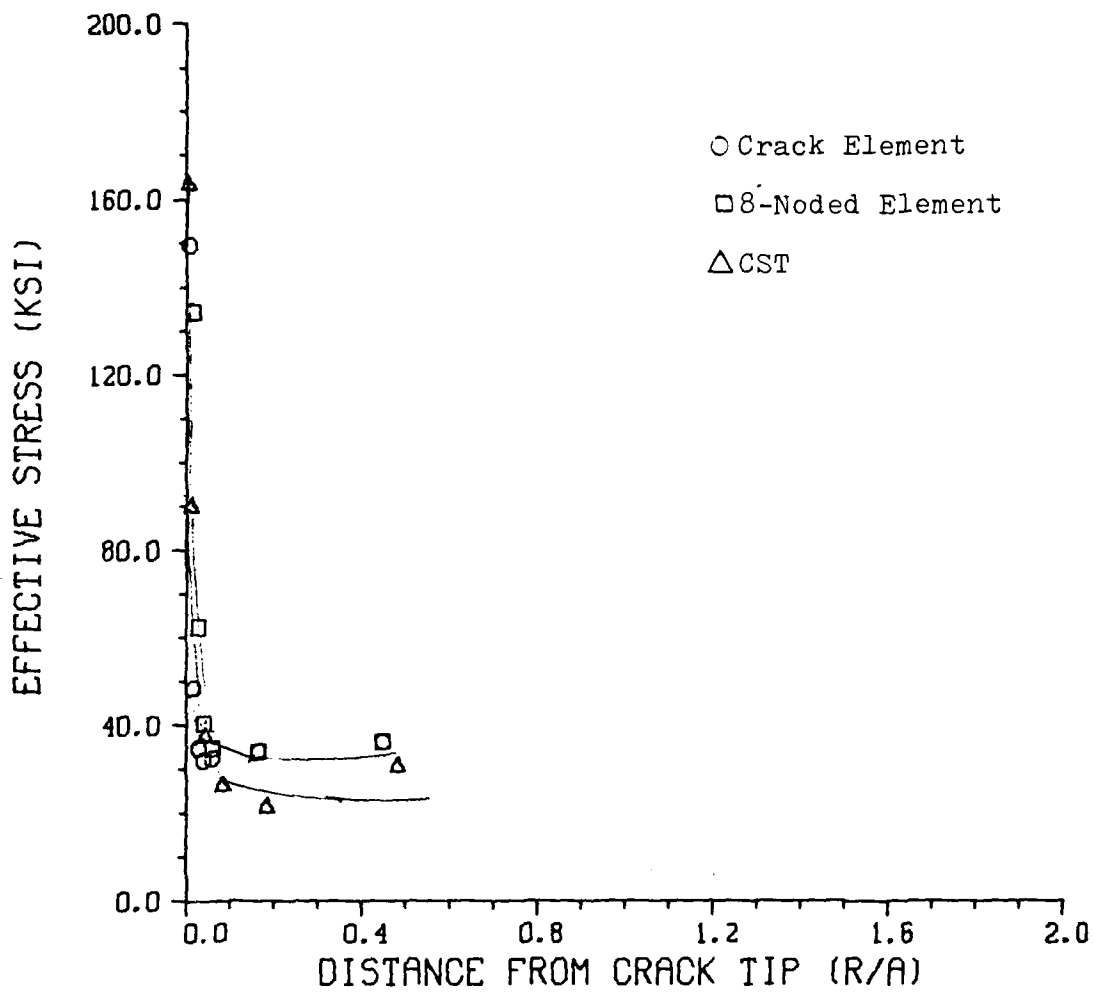


Figure 33. Stress Profiles, $\theta = 157.5^\circ$,
 $P = 16.060 \text{ klb}$

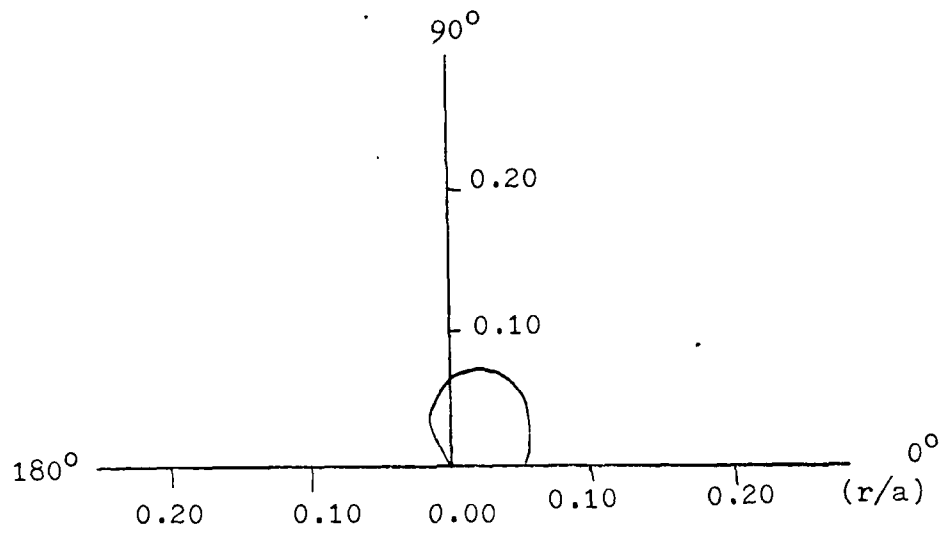


Figure 34. Plastic Region, Crack Element,
Fine Mesh, P = 10.896 klb

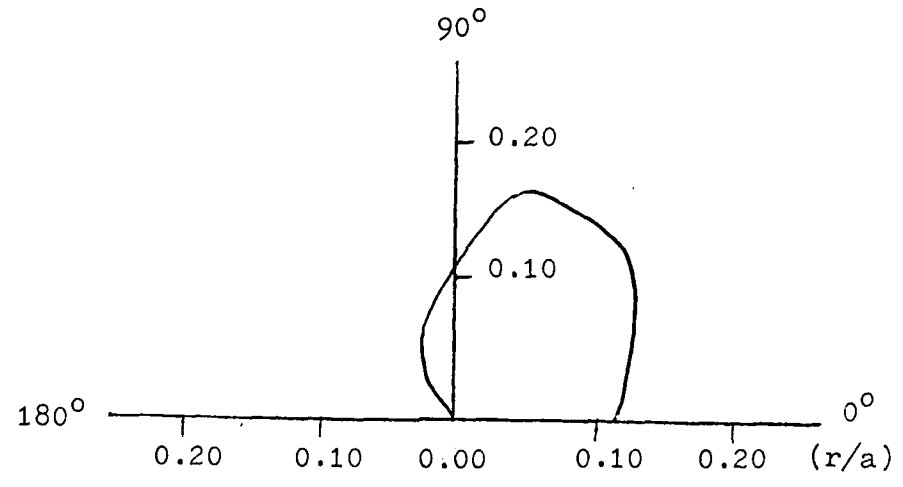


Figure 35. Plastic Region, Crack Element,
Fine Mesh, P = 16.060 klb

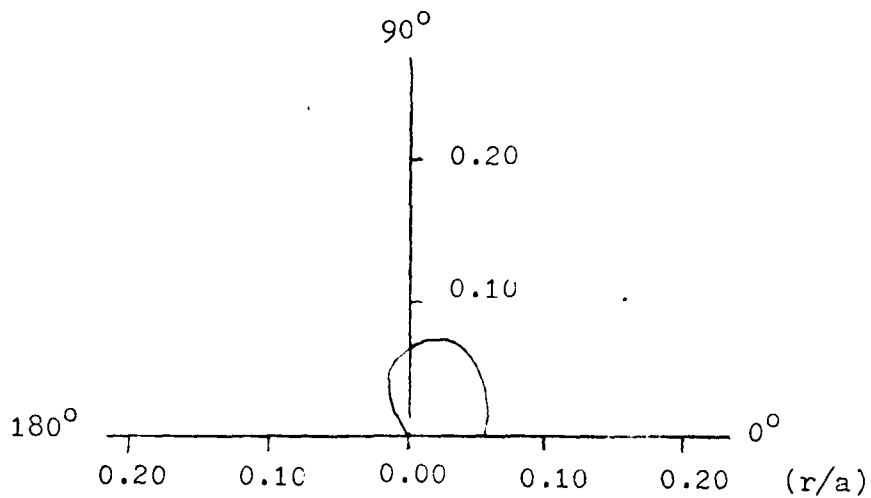


Figure 36. Plastic Region, 8-Noded Element,
Fine Mesh, $P = 10.896$ klb

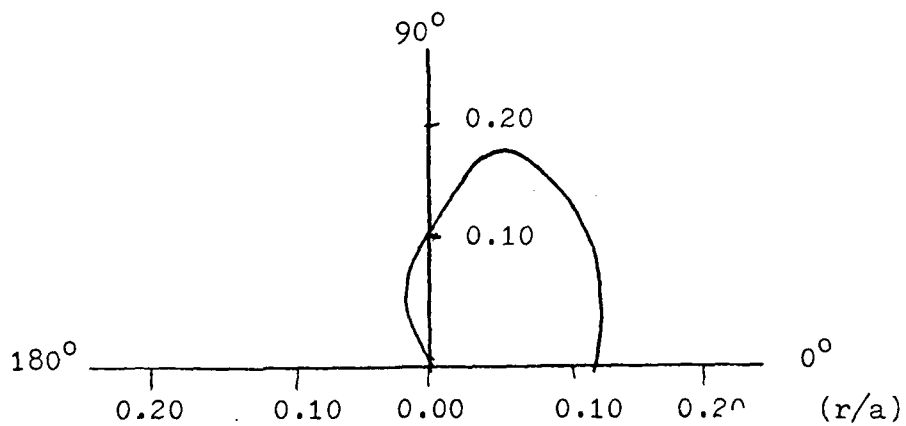


Figure 37. Plastic Region, 8-Noded Element,
Fine Mesh, $P = 16.060$ klb

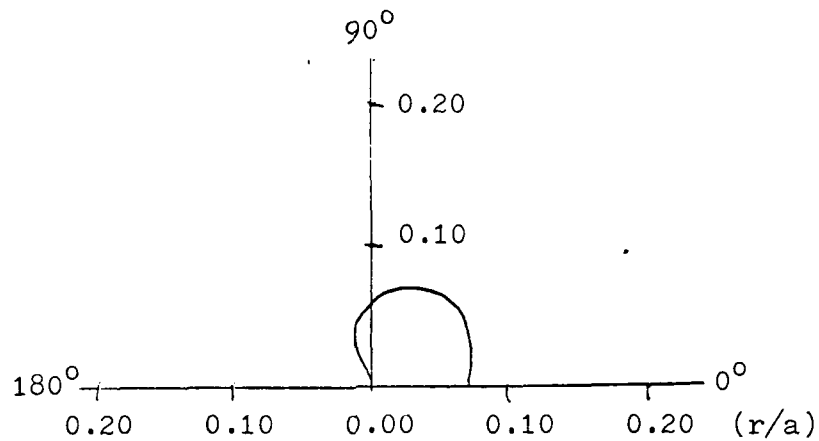


Figure 38. Plastic Region, CST,
Fine Mesh, P = 10.896 klb

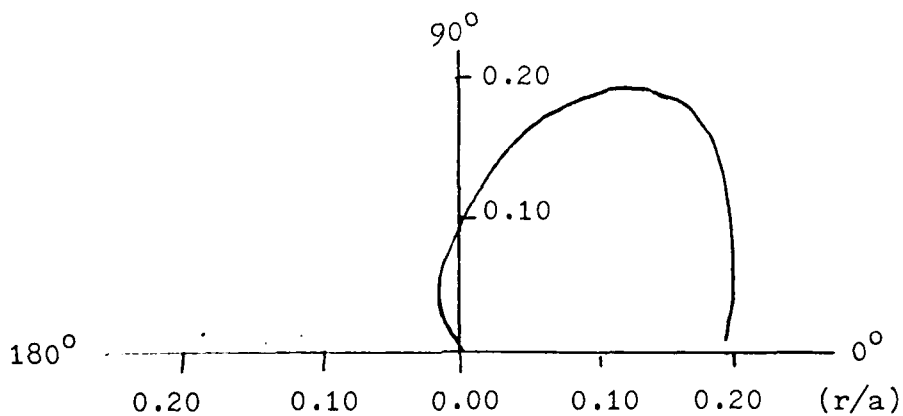


Figure 39. Plastic Region, CST,
Fine Mesh, P = 16.060 klb

and effective stress profiles. An element was determined to have gone plastic if its effective stresses had exceeded the yield stress. This is simply a restatement of the von Mises yield criterion.

The stress profiles shown as σ_e vs. r/a at various angles θ are shown in Fig. 24 through Fig. 33. The plastic regions are shown in Fig. 34 through Fig. 39.

The diagrams of the plastic region show that the constant strain triangle mesh had the largest region of plasticity at both load levels. The plastic regions for the other elements covered roughly the same areas. It is not surprising that the CST mesh would show the greatest amount of plasticity; the constant strain triangle is more flexible than either the crack-tip singularity element or the eight-noded quadrilateral.

The stress profiles show that the crack-tip singularity element generated extraordinarily high stresses at the crack tip. Figure 40 and Fig. 41 show the curves of x-displacement vs. distance from the crack tip for each type of element at the two different loadings. The slope of these curves near the crack tip was determined, and this value was divided by the crack length to obtain $\partial y/\partial x$, which is ϵ_x , or the strain in the x-direction. The results were compiled in Table III. It is noted that the crack-tip singularity element exhibited strains that were an order of magnitude greater than either the eight-noded quadrilateral or the constant-strain triangle. Since the singularity

TABLE III

Strains Near the Crack Tip, $\theta=0^\circ$, Fine Meshes

load (klb)	fine mesh type	ϵ_x near crack tip
10.896	crack tip element	40.0×10^{-3}
10.896	8-noded element	9.52×10^{-3}
10.896	CST	3.55×10^{-3}
16.060	crack tip element	60.92×10^{-3}
16.060	8-noded element	7.75×10^{-3}
16.060	CST	3.98×10^{-3}

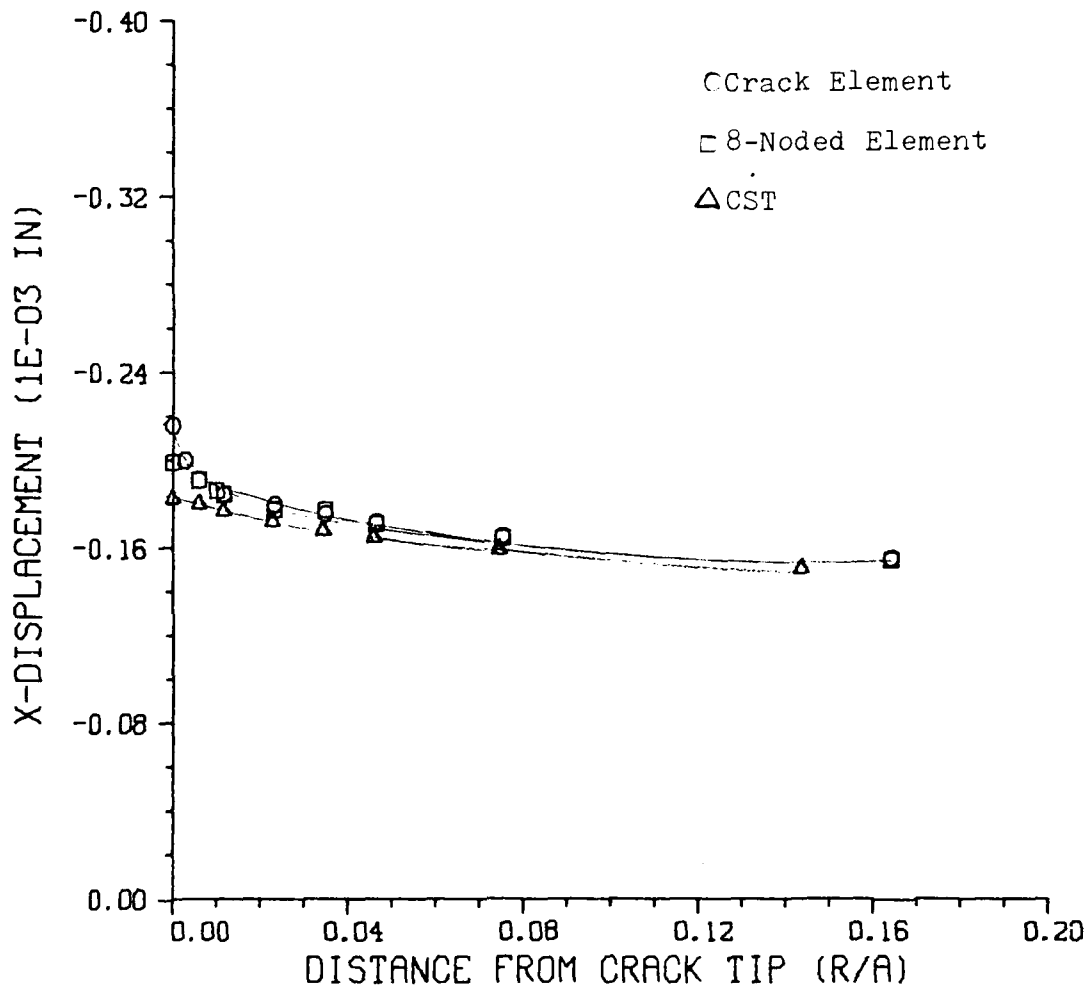


Figure 40. Displacement Profiles, $\theta = 0^\circ$,
 $P = 10.896$ klb

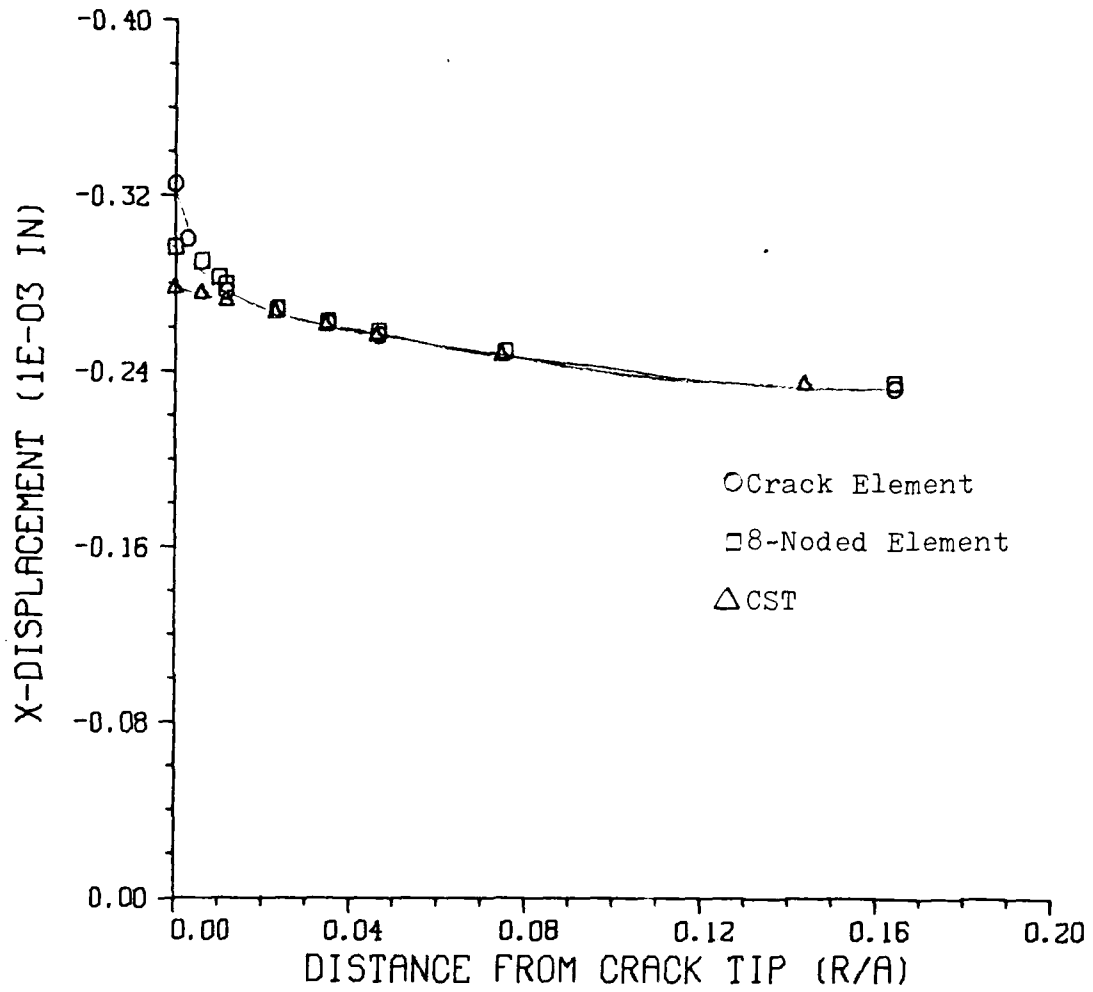


Figure 41 . Displacement Profiles, $\theta = 0^\circ$,
 $P = 16.060$ klb

that is characteristic of the crack tip element creates high levels of stress near the crack tip, and since stress is related to strain, the $\frac{1}{\sqrt{r}}$ singularity forces the crack tip element to behave with unnatural stiffness in the plastic regime.

It also should be noted that the eight-noded element produced strains that were about three times greater than the strains in the CST near the crack tip. This is due to the fact that higher order elements are naturally stiffer than the constant strain triangle.

The stress profiles show that though the eight-noded element produced stresses that were higher than the constant strain triangle, it was not as far off as was the crack tip element. The eight-noded element gave stresses that were within 15% of the stress values of the CST, except in the elements nearest the crack tip. This further demonstrates that the eight-noded element was stiffer than the constant strain triangle, but it was not as stiff as the singularity element.

Each of the finite element modelings accurately displayed the stresses near the stress-free boundary at $\theta=180^\circ$. At $\theta=157.5^\circ$ (Fig. 32 and Fig. 33), very high stresses were shown in the element nearest the crack tip. The stresses rapidly dropped off away from the crack tip. In the region of $0.1 \leq r/a \leq 0.6$, the eight-noded element meshes showed markedly higher stresses than the CST or crack element meshes. This occurred because there were two elements near

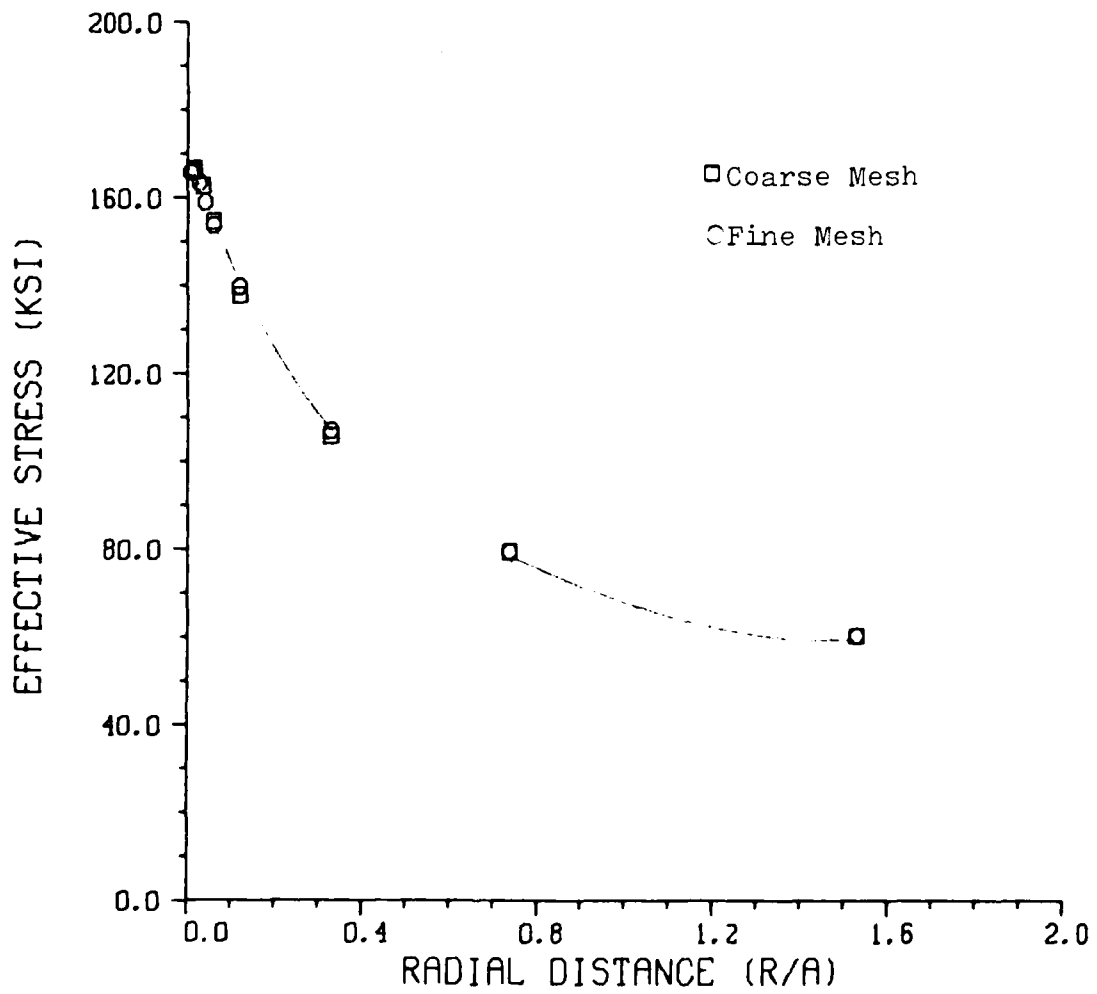


Figure 42. Convergence of Coarse to Fine Mesh, Crack Tip Element Mesh

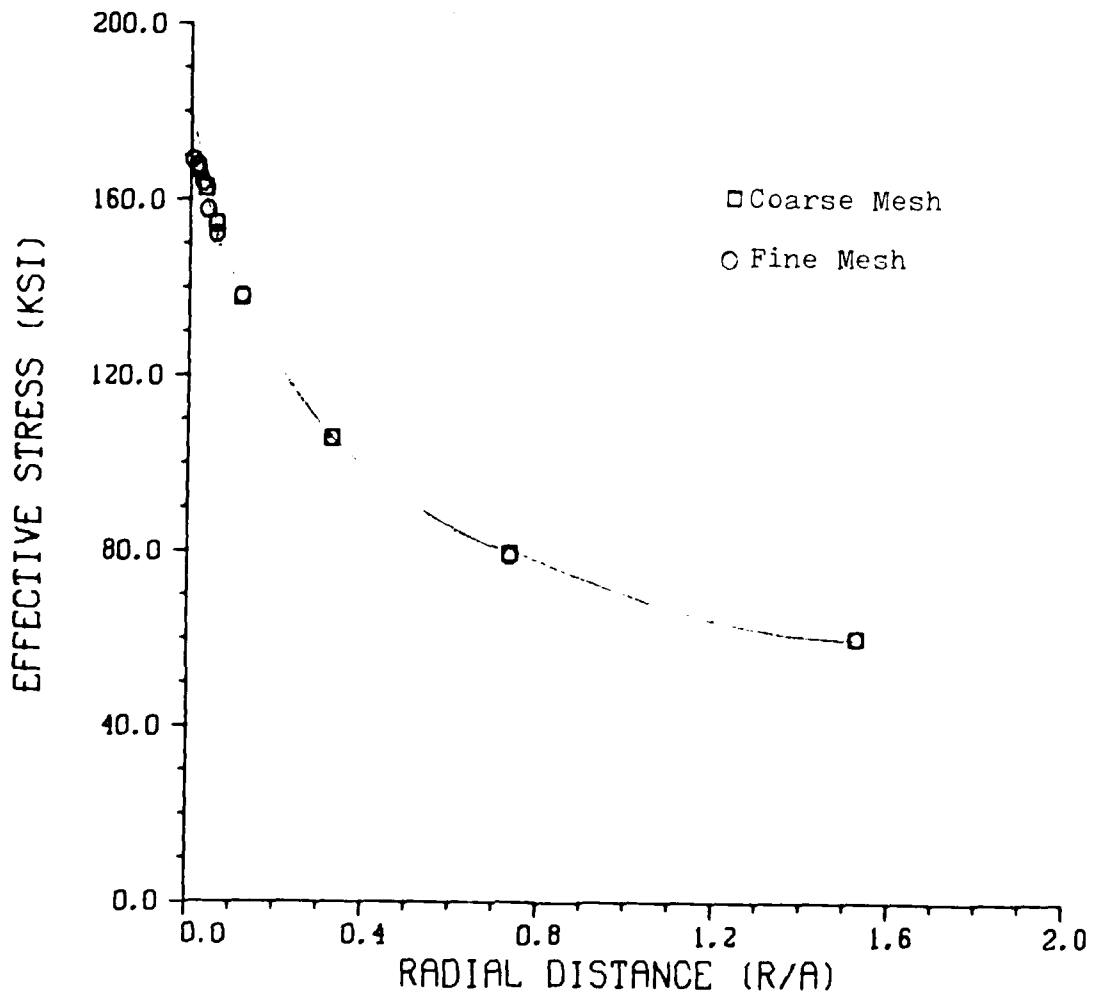


Figure 43. Convergence of Coarse to Fine Mesh
8-Noded Element Mesh

the crack tip for the crack element mesh and several elements near the crack tip for the CST mesh, while there was only one element near the crack tip for the eight-noded mesh. Therefore, it was easier for the CST and crack element meshes to adjust to the stress-free boundary than the eight-noded element mesh.

Figure 42 and Fig. 43 show the convergence of the coarse meshes to the fine meshes. For $r/a > 0.70$, the coarse mesh and the fine mesh for both types of elements each gave identical results. However, for $r/a \leq 0.7$, the coarse meshes gave stresses that ranged from three to seven percent higher than the fine meshes.

The diagrams of the plastic region show that the constant strain triangle produced the largest area of plasticity. Since the number of degrees of freedom in each mesh was kept the same and the number of degrees of freedom in the crack tip region was kept the same, the larger region of plasticity in the constant strain triangle mesh was caused by the fact that the constant strain triangle was not as stiff as either the eight-noded element or the crack tip element, and not because one mesh was inherently more restrained than another. Because of its close agreement elastically with linear elastic fracture mechanics and because of its lower stiffness, the constant strain triangle is preferred over the eight-noded element and the crack tip element for modeling elastic-plastic problems.

The higher-order elements do have some advantages, however. Since a mesh involving the higher-order elements has fewer elements than the constant strain triangle mesh, it requires less work on the part of the user to input the mesh for the higher-order elements. The eight-noded rectangular program also requires that only corner nodes be input while the constant strain program requires that the user supply the coordinates of all of the nodes. Since less cards are punched for the higher-order element mesh than for the constant strain triangle mesh, there is less chance of error; and since there are fewer cards for the isoparametric elements, it is easier to check the mesh. Overall, one would produce results more quickly by using higher-order elements than by using the constant strain triangle in terms of elapsed time from the start to the finish of the problem. However, it appears the elastic-plastic resulting stresses will be more realistic if one uses the constant strain triangular element rather than the eight-noded element or crack-tip singularity element.

Computational Comparisons

The last comparison to be made involves the difference in computer resources required between the two programs. A test case was set up. A uniaxial specimen was divided into two triangular elements acting under a uniaxial load of 134.0 ksi (923.4 MPa). The JALESE and VISCO programs were then used for comparison. Triangular elements were chosen because both programs incorporated triangular elements. However, the triangular elements used in the JALESE

program were not constant strain triangles but degenerated four-noded rectangles. Once again, the creep coefficient was set equal to zero and the load was applied very quickly. The results are shown in Table IV.

The JALESE program used 30% more central processor time than the VISCO program in the test cases. This occurred because the JALESE program utilizes Gaussian quadrature to perform the integration necessary to obtain the stiffness matrix while the VISCO program, which incorporates a constant strain triangle, can evaluate the integrals exactly since only constants are integrated. The JALESE program also required 32300 (octal) more core memory to load than the VISCO program. This is because the VISCO program stores the K matrix in a more efficient manner. The greater usage of core memory and central processor time slowed down the turnaround time of JALESE as compared to VISCO. It also makes the JALESE runs more expensive than the VISCO runs.

If the default value of stress and strain tolerance (0.001) was used with the crack tip element, fine mesh, in the JALESE program, the iterative initial stress solution for the plastic strains would not converge. The stress tolerance had to be increased to 0.005 in order to obtain a solution. Since the program only printed out four significant figures for the stress and strain solution, this change of the tolerance did not make a significant difference.

TABLE IV

Computational Resource Usage Comparisons,
Two Triangular Elements, Uniaxial Test,
JALESE and VISCO

Program Name	CM required (octal words)	CP usage (seconds)	IO time (seconds)	Cost (dollars)
JALESE	205100	5.560	25.424	1.04
VISCO	152600	4.273	25.678	0.94

It also should be noted that though it was easier to input data into the JALESE program, it was harder to obtain the desired levels of stress using JALESE over VISCO. JALESE required that the user supply incremental units of loading after plasticity has been achieved. When using VISCO, the total desired load was inputted in one data card. VISCO used time increments to increment the load.

V. Conclusions

It appears that for at least the center cracked plate, the best element to use for elastic-plastic analysis was the constant strain triangle. Elastically, the constant strain triangle gave results that agreed exactly with linear elastic fracture mechanics. The eight-noded quadrilateral also performed well elastically; its results also agreed with linear elastic fracture mechanics predictions. The crack tip singularity element, however, did not give accurate elastic results despite its unique ability to simulate the singularity that occurs in the crack tip region.

Plastically, the constant strain triangle performed much better than either the eight-noded quadrilateral or the crack tip singularity element. The constant strain triangle, in a mesh with the same number of degrees of freedom as the other elements, exhibited larger plastic regions and more realistic stresses near the crack tip. This was verified by Hinnerichs by comparisons made with experimental measurements (Ref 7). The eight-noded quadrilateral gave erroneously high stresses near the crack tip because of its inherent stiffness. The crack-tip singularity element gave even higher stresses because of its imposed singularity. This singularity made the crack tip elements unnaturally stiff. They did not model plasticity very well.

Though the eight-noded quadrilateral element and the crack-tip singularity element meshes were easier to input

and check than the constant strain triangle element mesh, it was easier to obtain the desired stress level using the triangle because the program that was used for the triangular element incremented with time viscoplastically and not with user-supplied load increments. The VISCO program that incorporated the constant strain triangle viscoplastically required less core memory space and less computer process or time than the JALESE program that contained the higher-order element approach.

The constant strain triangle also modeled the stress-free region better than either the eight-noded element or the crack tip element. The constant strain triangle with its great flexibility material-wise provided a very accurate model of the elastic and plastic strains near the crack tip.

One recommendation for future work is that a time dependency be incorporated into the JALESE program and that the comparisons be made viscoplastically. Creep should be studied in addition to the instantaneous plastic strains. A constant strain triangle should also be incorporated into the JALESE program so that the comparisons could all be made with one computer program. Another suggested future project is that crack growth comparisons should be made.

In summary, the eight-noded and crack-tip singularity elements presented in JALESE perform well elastically, with the crack element being slightly less accurate. The plastic results of the crack element and the eight-noded

element are disappointing. The constant strain triangle, with its great simplicity for understanding, provides extremely accurate answers in the elastic and plastic regimes. Though some extra work is required to set up the mesh, it is well worth it in order to obtain comparable accuracy with faster computer turnaround time.

Bibliography

1. Ahmad, Jalese and V. Papaspyropoulos. "Two-Dimensional Elastic-Plastic Finite Element Analysis of Fracture Specimens with Crack Growth Modeling," draft report on a two-dimensional elastic-plastic finite element code developed by the authors, Battelle Columbus Laboratories, Columbus, Ohio, 30 May 1981.
2. Barsoum, Roshdy S. "On the Use of Isoparametric Finite Elements in Linear Fracture Mechanics," International Journal for Numerical Methods in Engineering, Vol. 10, pp 25-37 (1976).
3. Bisplinghoff, Raymond L., James W. Mar, and Theodore H. Pian. Statics of Deformable Solids, Reading, Massachusetts: Addison-Wesley Publishing Company, Inc., 1965.
4. Chan, S. K., I. S. Tuba, and U. K. Wilson. "On the Finite Element Method in Linear Fracture Mechanics," Journal of Engineering Fracture Mechanics, Vol. 2, pp 1-17 (1970).
5. Cooke, Robert D. Concepts and Applications of Finite Element Analysis, New York: John Wiley and Sons, Inc., 1974.
6. Henshell, R. D. and K. G. Shaw. "Crack Tip Finite Elements are Unnecessary," International Journal for Numerical Methods in Engineering, Vol. 9, pp 495-507 (1975).
7. Hinnerichs, Terry D. Viscoplastic and Creep Crack Growth Analysis by the Finite Element Method, (Ph.D. dissertation, Air Force Institute of Technology), Materials Laboratory, Air Force Wright Aeronautical Laboratories, Air Force Systems Command, Wright-Patterson Air Force Base, Ohio, 1980.
8. Hinnerichs, Terry P. "The 'VISCO' Finite Element Computer Program," unpublished users guide to the VISCO program, 1980.
9. Mendelson, Alexander. Plasticity: Theory and Applications, New York: The MacMillan Company, 1968.
10. Rolfe, Stanley T. and John M. Barsom. Fracture and Fatigue Control on Structures, Englewood Cliffs, New Jersey: Prentice-Hall, Inc., 1977.

11. Saada, Adel S. Elasticity: Theory and Applications, New York: Pergamon Press, Inc., 1974.
12. Tong, Pin and John N. Rossettos. Finite Element Method, Cambridge, Massachusetts: The MIT Press, 1977.
13. Zienkiewicz, O. C. The Finite Element Method (Third Edition), London: McGraw-Hill Book Company, Ltd., 1977.
14. Zienkiewicz, O. C. and I. C. Corneau. "Visco-Plasticity Solution by Finite Element Process," Archives of Mechanics, Vol. 24, pp 873-889 (1972).
15. Zienkiewicz, O. C., S. Valliapan, and I. P. King. "Elastic-Plastic Solutions of Engineering Problems 'Initial Stress', Finite Element Approach," International Journal for Numerical Methods in Engineering, Vol. 1, pp 75-100 (1969).

Appendix A: The Finite Element Method

Introduction

The basic philosophy of the finite element is that an approximate solution for a problem too complex to be solved exactly can be found by dividing the field of interest into a number of discrete regions and, by the use of simple functions, solve for the desired quantities in each region (Ref 13). For continuous structures, this involves dividing the system into a finite number of elements which are interconnected at a discrete number of nodal points . their boundaries. Displacement functions are chosen which satisfy the elemental boundary conditions and continuous forces or stresses are modeled as concentrated forces at the nodes. By using the equations of structural analysis, the forces, strains, stresses, and nodal displacements for each element are calculated. The global solution is found by appropriately combining the elemental solutions.

Constant Strain Triangle

One element that is used in structural analysis is the three-noded triangle, which is also called the constant strain triangle. A typical triangular element along with its nodal displacements is shown in Fig. A-1. The nodes are numbered counterclockwise as i , j , and k .

The displacements within the element are uniquely determined from the six values of nodal displacement. For

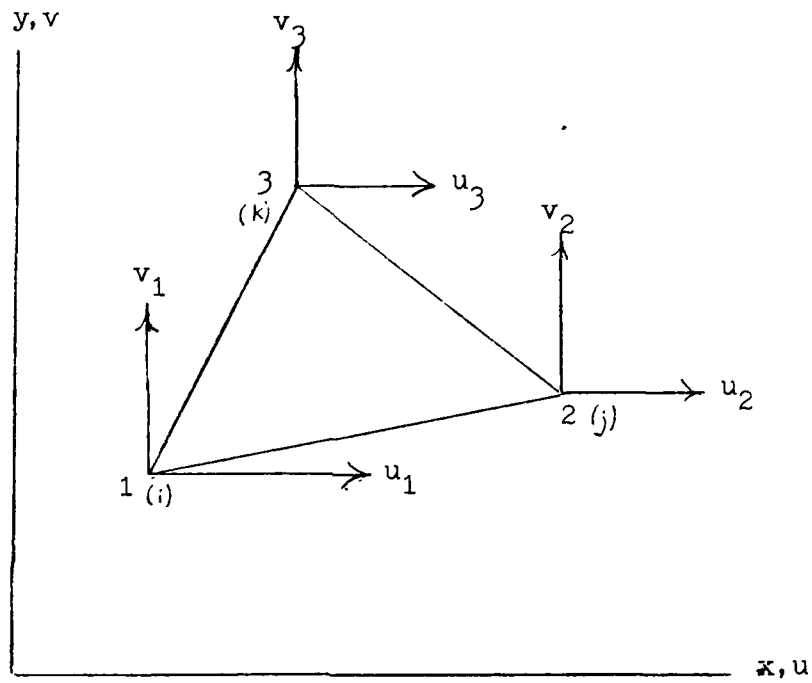


Figure A-1. Triangular Element and Nodal Displacements in x-y Space

the constant strain triangle, the function which does this is linear (Ref 5) and is given by:

$$\begin{aligned} u &= \alpha_1 + \alpha_2 x + \alpha_3 y \\ v &= \alpha_4 + \alpha_5 x + \alpha_6 y \end{aligned} \tag{A-1}$$

The constants are easily computed and are given by

$$\begin{pmatrix} \alpha_1 \\ \alpha_2 \\ \alpha_3 \end{pmatrix} = \frac{1}{2\Delta} \begin{bmatrix} a_i & a_j & a_k \\ b_i & b_j & b_k \\ c_i & c_j & c_k \end{bmatrix} \begin{pmatrix} u_i \\ u_j \\ u_k \end{pmatrix} \tag{A-2}$$

and

$$\begin{pmatrix} \alpha_4 \\ \alpha_5 \\ \alpha_6 \end{pmatrix} = \frac{1}{2\Delta} \begin{bmatrix} a_i & a_j & a_k \\ b_i & b_j & b_k \\ c_i & c_j & c_k \end{bmatrix} \begin{pmatrix} v_i \\ v_j \\ v_k \end{pmatrix} \tag{A-3}$$

where Δ represents the area of the triangle. The coefficients a_i , b_i , and c_i and the area 2Δ are given in terms of the nodal coordinates x_i and y_i by

$$\begin{aligned} a_i &= x_j y_k - x_k y_j \\ b_i &= y_j - y_k \\ c_i &= x_k - x_j \end{aligned} \quad 2\Delta = \begin{vmatrix} 1 & x_i & y_i \\ 1 & x_j & y_j \\ 1 & x_k & y_k \end{vmatrix} \tag{A-4}$$

a_j , b_j , c_j and a_k , b_k , c_k are obtained by a cyclic permutation of the indices in Eq. A-4. One finally obtains:

$$\begin{aligned} u &= \frac{1}{2\Delta} [(a_i + b_i x + c_i y) u_i + (a_j + b_j x + c_j y) u_j + (a_k + b_k x + c_k y) u_k] \\ v &= \frac{1}{2\Delta} [(a_i + b_i x + c_i y) v_i + (a_j + b_j x + c_j y) v_j + (a_k + b_k x + c_k y) v_k] \end{aligned} \tag{A-5}$$

Eq. A-5 may be written in standard form as:

$$\underline{u} = \begin{pmatrix} u \\ v \end{pmatrix} = \underline{N} \underline{a}^e = [\underline{N}_i, \underline{N}_j, \underline{N}_m] \underline{a}^e \quad (\text{A-6})$$

\underline{a}^e represents a listing of the nodal displacements for a particular element and the shape functions, N_i , N_j , and N_k , are given by

$$N_i = \frac{(a_i + b_i x + c_i y)}{2\Delta} \quad (\text{A-7})$$

etc.

The strain at any point within the element may be defined in terms of the nodal displacements derivatives by:

$$\underline{\epsilon} = \begin{pmatrix} \epsilon_x \\ \epsilon_y \\ \gamma_{xy} \end{pmatrix} = \begin{pmatrix} \frac{\partial u}{\partial x} \\ \frac{\partial u}{\partial y} \\ \frac{\partial u}{\partial y} + \frac{\partial u}{\partial x} \end{pmatrix} \quad (\text{A-8})$$

Writing Eq. A-8 in terms of the nodal displacements and coordinates and taking the appropriate derivatives results in:

$$\underline{\epsilon} = \underline{B} \underline{a}^e \quad (\text{A-9})$$

where \underline{u} is the generalized nodal displacement vector written as

$$\underline{a}^T = (u_i \ v_i \ u_j \ v_j \ u_k \ v_k)^T \quad (\text{A-10})$$

and

$$\underline{\underline{B}} = \frac{1}{2\Delta} \begin{bmatrix} b_i & 0 & b_j & 0 & b_k & 0 \\ 0 & c_i & 0 & c_j & 0 & c_k \\ c_i & b_i & c_j & b_j & c_k & b_k \end{bmatrix} \quad (\text{A-11})$$

Elastic Analysis

For linear elastic, isotropic materials, the relationship between the stresses, $\underline{\sigma}$, strains, $\underline{\epsilon}$, initial stresses, $\underline{\sigma}_0$, and initial strains, $\underline{\epsilon}_0$, is given by (Ref 13)

$$\underline{\sigma} = \begin{pmatrix} \sigma_x \\ \sigma_y \\ \sigma_{xy} \end{pmatrix} = \underline{\underline{D}}[\underline{\epsilon} - \underline{\epsilon}_0] + \underline{\sigma}_0 \quad (\text{A-12})$$

where $\underline{\underline{D}}$ is the elasticity matrix containing the appropriate material properties. For plane stress $\underline{\underline{D}}$ is given by:

$$\underline{\underline{D}} = \frac{E}{1-\nu^2} \begin{bmatrix} 1 & \nu & 0 \\ \nu & 1 & 0 \\ 0 & 0 & \frac{1-\nu}{2} \end{bmatrix} \quad (\text{A-13})$$

For plane strain, $\underline{\underline{D}}$ is given by

$$\underline{\underline{D}} = \frac{E(1-\nu)}{(1+\nu)(1-2\nu)} \begin{bmatrix} 1 & \nu/1-\nu & 0 \\ \nu/1-\nu & 1 & 0 \\ 0 & 0 & \frac{1-2\nu}{2(1-\nu)} \end{bmatrix} \quad (\text{A-14})$$

Note that for plane stress, $\sigma_{zz} = \sigma_{zx} = \sigma_{zy} = 0$, while for plane strain, $\epsilon_{zz} = \epsilon_{zx} = \epsilon_{zy} = 0$ and

$$\sigma_x = \sigma(\sigma_x + \sigma_y) \quad (\text{A-15})$$

As stated previously, before any finite element analysis can be performed, the applied loads, which include the applied stresses and any body forces, must be modeled as equivalent nodal forces. For the applied stresses,

$$\underline{\bar{\sigma}} = \begin{pmatrix} \bar{\sigma}_x \\ \bar{\sigma}_y \\ \bar{\sigma}_{xy} \end{pmatrix} \quad (A-16)$$

and body forces,

$$\underline{b} = \begin{pmatrix} b_x \\ b_y \end{pmatrix} \quad (A-17)$$

the equivalent nodal forces,

$$\underline{q}^e = \begin{pmatrix} q_i^e \\ q_j^e \end{pmatrix} \quad (A-18)$$

where

$$q_i^e = \begin{pmatrix} U_i \\ V_i \end{pmatrix} \quad (A-19)$$

with components U_i and V_i corresponding to the directions of u and v displacements, are given by:

$$\underline{q}^e = \int_v \underline{B}^T \underline{\sigma} d(\text{vol}) - \int_v \underline{N}^T \underline{b} d(\text{vol}) \quad (A-20)$$

The generalized equation for the elastic response of the structure is derived from the principle of virtual work (Ref 13) and can be written as:

$$\underline{\underline{K}} \underline{U} = \underline{P} + \underline{Q} \quad (\text{A-21})$$

$\underline{\underline{K}}$ is called the elastic stiffness matrix, \underline{U} is the generalized displacement vector, \underline{P} represents the externally applied load vector, and \underline{Q} is the force vector caused by initial stresses and initial strains. \underline{Q} is used both for time-independent and time-dependent problems.

The stiffness matrix can be represented as:

$$\underline{\underline{K}} = \int_V \underline{\underline{B}}^T \underline{\underline{D}} \underline{\underline{B}} d(\text{vol}) \quad (\text{A-22})$$

The global stiffness matrix is obtained by evaluating the stiffness matrix for each element and summing over the whole structure. The equivalent nodal forces due to the initial stresses are given by

$$\underline{Q}\underline{\sigma}_0 = \int_V \underline{\underline{B}}^T \underline{\sigma}_0 d(\text{vol}) \quad (\text{A-23})$$

The equivalent nodal forces due to the initial strains may be expressed as:

$$\underline{Q}\underline{\epsilon}_0 = \int_V \underline{\underline{B}}^T \underline{\underline{D}} \underline{\epsilon}_0 d(\text{vol}) \quad (\text{A-24})$$

Note that the equivalent nodal forces due to the applied stresses, which is the first integral in Eq. A-20, can be written as:

$$\underline{Q}\underline{\sigma} = \underline{\underline{K}} \underline{a}^e \quad (\text{A-25})$$

Once the nodal displacements have been evaluated, the stresses at any point of the element can be found by combining Eqs. A-9 and A-12 to obtain:

$$\underline{\sigma} = \underline{D} \underline{B} \underline{a}^e - \underline{D} \underline{\epsilon}_0 - \sigma_0 \quad (\text{A-26})$$

where \underline{a}^e is the nodal displacement vector. The stress recovery matrix is defined as:

$$\underline{S}_e = \underline{D} \underline{B} \quad (\text{A-27})$$

Biquadratic Quadrilateral

It has been shown that for a three-noded triangle, a linear interpolation function for the displacements is chosen. Since the strains are a function of the first derivative of the displacements, the strains are constant throughout the triangle. This is why the three-noded element is called a constant strain triangle. The approximation of constant strain in an element is valid if and only if the element is relatively small. For larger elements, a higher-order interpolation function must be selected.

Consider the distorted eight-noded element shown in Fig. A-2. While the constant strain triangle had nodes only at the vertices, this element has one node in the middle of each side. The interpolation function chosen to model the element displacements is second order, and this allows the element to have curved sides. The same interpolation function that models the displacements is also chosen to model the shape of the element. Elements for which this is done belong to the family of isoparametric elements (Ref 5). The interpolation function may also be referred to as a shape function.

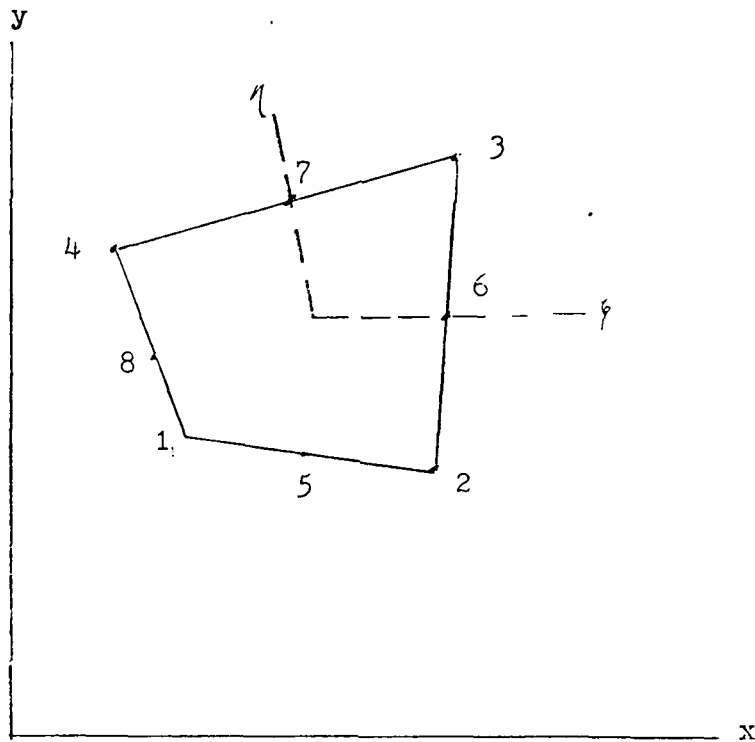


Figure A-2. Distorted Isoparametric Element in x-y Space

To thoroughly describe an isoparametric, a nonorthogonal local coordinate system is drawn. This has been done to the element in Fig. A-2. The element drawn in the local system is shown in Fig. A-3.

For the equation:

$$\underline{u} = \underline{N} \underline{a}^e \quad (\text{A-28})$$

the shape functions N_i may be given as (Ref 12)

$$\begin{aligned} N_i &= \frac{1}{4}(1+\xi\xi_i)(1+\eta\eta_i)(\xi\xi_i+\eta\eta_i-1) & i = 1,2,3,4 \\ &= \frac{1}{2}(1-\xi^2)(1+\eta\eta_i) & i = 5,7 \\ &= \frac{1}{2}(1-\eta^2)(1+\xi\xi_i) & i = 6,0 \end{aligned} \quad (\text{A-29})$$

where (ξ_i, η_i) represent the coordinates of node i in the local system.

The shape of the element, expressed as the coordinate points (x,y) , may be written in terms of the shape functions and the coordinates of the nodes as:

$$\begin{pmatrix} x \\ y \end{pmatrix} = \begin{bmatrix} N_1 & 0 & N_2 & 0 & N_3 & 0 & N_4 & 0 \\ 0 & N_1 & 0 & N_2 & 0 & N_3 & 0 & N_4 \end{bmatrix} \begin{pmatrix} x_1 \\ y_1 \\ x_2 \\ y_2 \\ x_3 \\ y_3 \\ x_4 \\ y_4 \end{pmatrix} \quad (\text{A-30})$$

The displacements within the element, u and v , may be written in terms of the nodal displacements as:

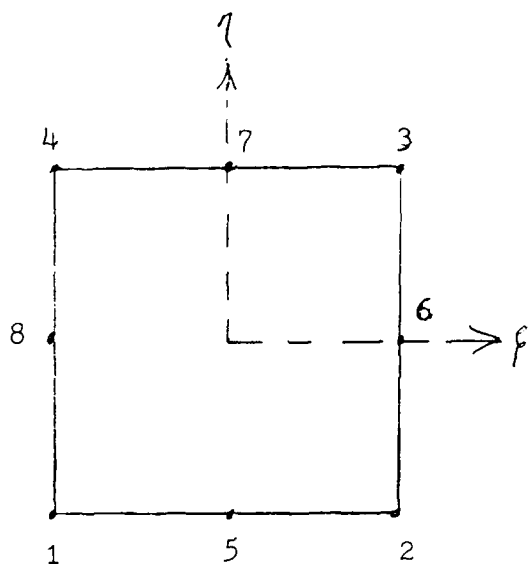


Figure A-3. 8-Noded Isoparametric Element
in ξ - η Space

$$\begin{pmatrix} u \\ v \end{pmatrix} = \begin{bmatrix} N_1 & 0 & N_2 & 0 & N_3 & 0 & N_4 & 0 \\ 0 & N_1 & 0 & N_2 & 0 & N_3 & 0 & N_4 \end{bmatrix} \begin{pmatrix} u_1 \\ v_1 \\ u_2 \\ v_2 \\ u_3 \\ v_3 \\ u_4 \\ v_4 \end{pmatrix} \quad (\text{A-31})$$

In shortened notation, Eqs. A-30 and A-31 may be written as:

$$\begin{pmatrix} x \\ y \end{pmatrix} = \begin{bmatrix} \underline{N} & 0 \\ 0 & \underline{N} \end{bmatrix} \begin{pmatrix} \underline{x}_i \\ \underline{v}_i \end{pmatrix} \quad (\text{A-32})$$

and

$$\begin{pmatrix} u \\ v \end{pmatrix} = \begin{bmatrix} \underline{N} & 0 \\ 0 & \underline{N} \end{bmatrix} \begin{pmatrix} \underline{u}_i \\ \underline{v}_i \end{pmatrix} \quad (\text{A-33})$$

The strain-displacement relation can be expressed as

$$\underline{\epsilon} = \begin{pmatrix} \epsilon_x \\ \epsilon_y \\ \gamma_{xy} \end{pmatrix} = \begin{bmatrix} 1 & 0 & 0 & 0 \\ 0 & 0 & 0 & 1 \\ 0 & 1 & 1 & 0 \end{bmatrix} \begin{pmatrix} u,x \\ u,y \\ v,x \\ v,y \end{pmatrix} \quad \text{where } u,x = \frac{\partial u}{\partial x} \\ u,y = \frac{\partial u}{\partial y} \quad \text{etc.} \quad (\text{A-34})$$

The derivatives with respect to x and y must be converted into derivatives with respect to ξ and η . This is done through the use of the Jacobian.

Recall that the Jacobian is defined as (Ref 12):

$$\underline{J} = \begin{bmatrix} x',_{\xi} & y',_{\xi} \\ x',_{\eta} & y',_{\eta} \end{bmatrix} \quad (\text{A-35})$$

where $x',_{\xi} = \frac{\partial x}{\partial \xi}$, $x',_{\eta} = \frac{\partial x}{\partial \eta}$, etc.

The determinant of the Jacobian $|J|$, is then given by:

$$|J| = \begin{vmatrix} x',_{\xi} & y',_{\xi} \\ x',_{\eta} & y',_{\eta} \end{vmatrix} = x',_{\xi} y',_{\eta} - x',_{\eta} y',_{\xi} \quad (\text{A-36})$$

The inverse of the Jacobian, J^* , can be expressed as:

$$J^* = \begin{bmatrix} J^*_{11} & J^*_{12} \\ J^*_{21} & J^*_{22} \end{bmatrix} = \frac{1}{|J|} \begin{bmatrix} y',_{\eta} & -y',_{\xi} \\ -x',_{\eta} & x',_{\xi} \end{bmatrix} \quad (\text{A-37})$$

By the chain rule,

$$\begin{pmatrix} ()',_{\xi} \\ ()',_{\eta} \end{pmatrix} = \begin{bmatrix} x',_{\xi} & y',_{\xi} \\ x',_{\eta} & y',_{\eta} \end{bmatrix} \begin{pmatrix} ()',_{x} \\ ()',_{y} \end{pmatrix} = \underline{J} \begin{pmatrix} ()',_{x} \\ ()',_{y} \end{pmatrix} \quad (\text{A-38})$$

where the empty parentheses denote a vacant operator.

Therefore,

$$\begin{pmatrix} ()',_{x} \\ ()',_{y} \end{pmatrix} = \underline{J^*} \begin{pmatrix} ()',_{\xi} \\ ()',_{\eta} \end{pmatrix} \quad (\text{A-39})$$

By the use of Eq. A-39, Eq. A-34 can be written as:

$$\underline{\varepsilon} = \begin{bmatrix} 1 & 0 & 0 & 0 \\ 0 & 0 & 0 & 1 \\ 0 & 1 & 1 & 0 \end{bmatrix} \begin{bmatrix} J_{11}^* & J_{12}^* & 0 & 0 \\ J_{21}^* & J_{22}^* & 0 & 0 \\ 0 & 0 & J_{11}^* & J_{12}^* \\ 0 & 0 & J_{21}^* & J_{22}^* \end{bmatrix} \begin{pmatrix} u, \xi \\ u, \eta \\ v, \xi \\ v, \eta \end{pmatrix} \quad (\text{A-40})$$

Differentiating Eq. A-33 and applying it to Eq. A-40 results in:

$$\underline{\varepsilon} = \begin{bmatrix} J_{11}^* & J_{12}^* & 0 & 0 \\ 0 & 0 & J_{21}^* & J_{22}^* \\ J_{21}^* & J_{22}^* & J_{11}^* & J_{12}^* \end{bmatrix} \begin{bmatrix} \underline{N}, \xi & 0 \\ \underline{N}, \eta & 0 \\ 0 & \underline{N}, \xi \\ 0 & \underline{N}, \eta \end{bmatrix} \begin{pmatrix} \underline{u}_i \\ \underline{v}_i \end{pmatrix} \quad (\text{A-41})$$

Differentiating Eq. A-32 and applying the results to Eq. A-37 gives for the inverse of the Jacobian:

$$\underline{J}^* = \frac{1}{|J|} \begin{bmatrix} \underline{N}, \eta \underline{y}_i & -\underline{N}, \xi \underline{y}_i \\ -\underline{N}, \eta \underline{x}_i & \underline{N}, \xi \underline{x}_i \end{bmatrix} \quad (\text{A-42})$$

Since $\underline{\varepsilon} = \underline{B} \underline{a}_e$, the matrix is the product of the first two matrices in Eq. A-41. Using Eq. A-42 gives:

$$\underline{B} = \frac{1}{|J|} \begin{bmatrix} \underline{N}, \eta \underline{y}_i & -\underline{N}, \xi \underline{y}_i & 0 & 0 \\ 0 & 0 & -\underline{N}, \eta \underline{x}_i & -\underline{N}, \xi \underline{x}_i \\ -\underline{N}, \eta \underline{x}_i & \underline{N}, \xi \underline{x}_i & \underline{N}, \eta \underline{y}_i & -\underline{N}, \xi \underline{y}_i \end{bmatrix} \begin{bmatrix} \underline{N}, \xi & 0 \\ \underline{N}, \eta & 0 \\ 0 & \underline{N}, \xi \\ 0 & \underline{N}, \eta \end{bmatrix} \quad (\text{A-43})$$

Matrix multiplication results in

$$\underline{B} = \frac{1}{|J|} \begin{bmatrix} \underline{N}_{,\eta} \underline{Y}_i \underline{N}_{,\xi} - \underline{N}_{,\xi} \underline{Y}_i \underline{N}_{,\eta} & 0 \\ 0 & -\underline{N}_{,\eta} \underline{x}_i \underline{N}_{,\xi} + \underline{N}_{,\xi} \underline{x}_i \underline{N}_{,\eta} \\ -\underline{N}_{,\eta} \underline{x}_i \underline{N}_{,\xi} + \underline{N}_{,\xi} \underline{x}_i \underline{N}_{,\eta} & \underline{N}_{,\eta} \underline{Y}_i \underline{N}_{,\xi} - \underline{N}_{,\xi} \underline{Y}_i \underline{N}_{,\eta} \end{bmatrix} \quad (\text{A-44})$$

By vector multiplication identity,

$$\underline{N}_{,\eta} \underline{Y}_i = \underline{Y}_i^T \underline{N}_{,\eta}^T \quad (\text{A-45})$$

Therefore,

$$\underline{N}_{,\eta} \underline{Y}_i \underline{N}_{,\xi} = \underline{Y}_i^T \underline{N}_{,\eta}^T \underline{N}_{,\xi} \quad (\text{A-46})$$

Defining the vector \underline{Q} as:

$$\underline{Q} = \underline{N}_{,\eta}^T \underline{N}_{,\xi} - \underline{N}_{,\xi}^T \underline{N}_{,\eta} \quad (\text{A-47})$$

(note that $\underline{Q}^t = -\underline{Q}$, that is, \underline{Q} is antisymmetric)

Therefore,

$$\underline{Y}_i^T \underline{Q} = \underline{N}_{,\eta} \underline{Y}_i \underline{N}_{,\xi} - \underline{N}_{,\xi} \underline{Y}_i \underline{N}_{,\eta} \quad (\text{A-48})$$

The B matrix may now be expressed as:

$$\underline{B} = \frac{1}{|\sigma|} \begin{bmatrix} \underline{Y}_i^T \underline{Q} & 0 \\ 0 & -\underline{x}_i^T \underline{Q} \\ -\underline{x}_i^T \underline{Q} & \underline{Y}_i^T \underline{Q} \end{bmatrix} \quad (\text{A-49})$$

The determinant of J may be rewritten as:

$$|J| = \underline{x}_{,\xi} \underline{y}_{,\eta} - \underline{x}_{,\eta} \underline{y}_{,\xi} = \underline{x}_i^T \underline{N}_{,\xi}^T \underline{N}_{,\eta} \underline{y}_i - \underline{x}_i^T \underline{N}_{,\eta}^T \underline{N}_{,\xi} \underline{y}_i \quad (\text{A-50})$$

Using Q, Eq. A-50 can be taken to be:

$$|J| = -\underline{x}_i^T \underline{Q} \underline{y}_i \quad (A-51)$$

Let

$$\underline{\lambda}_x = -\underline{y}_i^T \underline{Q} \quad (A-52)$$

$$\underline{\lambda}_y = -\underline{x}_i^T \underline{Q}$$

Therefore,

$$\underline{B} = \frac{1}{|J|} \begin{bmatrix} \lambda_x & 0 \\ 0 & \lambda_y \\ \lambda_y & \lambda_x \end{bmatrix} \quad (A-53)$$

where

$$|J| = \lambda_y \underline{y}_i \quad (A-54)$$

The stiffness matrix \underline{K} can be determined to be

$$\underline{K} = t \iint \underline{B}^T \underline{D} \underline{B} \, dx dy \quad (A-55)$$

where t is the thickness of the element, assumed to be a constant. By the use of the transformation rule,

$$dx dy = |J| d\xi d\eta \quad (A-56)$$

the stiffness matrix can be expressed as:

$$\underline{K} = t \int_{-1}^1 \int_{-1}^1 \underline{B}^T \underline{D} \underline{B} |J| d\xi d\eta \quad (A-57)$$

Let

$$\underline{\underline{D}} = \begin{bmatrix} D_{11} & D_{12} & D_{13} \\ D_{12} & D_{22} & D_{23} \\ D_{13} & D_{23} & D_{33} \end{bmatrix} \quad (\text{A-58})$$

Then the quantity B^TDB can be written as:

$$\underline{\underline{B}}^T \underline{\underline{D}} \underline{\underline{B}} = \frac{1}{|J|^2} \begin{bmatrix} D_{11}\chi_x^T\chi_x + D_{33}\chi_y^T\chi_y & D_{12}\chi_x^T\chi_y + D_{13}\chi_x^T\chi_x \\ +D_{13}(\chi_x^T\chi_y + \chi_y^T\chi_x) & +D_{23}\chi_y^T + D_{33}\chi_y^T\chi_x \\ D_{12}\chi_y^T\chi_x + D_{13}\chi_x^T\chi_x & D_{22}\chi_y^T\chi_y + D_{33}\chi_x^T\chi_x \\ +D_{23}\chi_y^T\chi_y + D_{33}\chi_x^T\chi_y & +D_{23}(\chi_y^T\chi_x + \chi_x^T\chi_y) \end{bmatrix} \quad (\text{A-59})$$

It is the quantity B^TDB that must be integrated in order to evaluate the stiffness matrix, K . While B^TDB for the three-noded triangle contains only constant terms, making the integration for $\underline{\underline{K}}$ trivial, B^TDB for the eight-noded quadrilateral is composed of variables in ξ and η . The integration for K is no longer a simple matter and a numerical integration scheme must be used. The method of integration most widely used is Gaussian quadrature.

The Gaussian quadrature integration rule in one dimension (Ref 13) states that the integral:

$$I = \int_{-1}^1 f(\xi) d\xi \quad (\text{A-60})$$

can be evaluated by:

$$\int_{-1}^1 f(\xi) d\xi = \sum_{i=1}^n H_i f(\xi_i) \quad (\text{A-61})$$

H_i denotes an appropriate "weight" for each value of ξ_i evaluated. The location of the sampling points, ξ_i , is chosen such that the error associated with the numerical integration is minimized. The order of the error is $2n$, where n is the number of integration stations chosen (order of the integration).

In two dimensions, the Gaussian quadrature integration rule becomes (Ref 13):

$$I = \int_{-1}^1 \int_{-1}^1 f(\xi, \eta) d\xi d\eta = \sum_{i=1}^n \sum_{j=1}^n H_i H_j f(\xi_j, \eta_i) \quad (A-62)$$

Thus, if

$$f(\xi, \eta) = \underline{\underline{B}}^T \underline{\underline{D}} \underline{\underline{B}} |J| \quad (A-63)$$

then

$$K = t \int_{-1}^1 \int_{-1}^1 f(\xi, \eta) d\xi d\eta = t \sum_{i=1}^n \sum_{j=1}^n H_i H_j f(\xi_j, \eta_i) \quad (A-64)$$

The locations of ξ and η are chosen symmetrical to the axes system.

The order of integration needed to accurately determine K is determined by analyzing the order of $\det J$ (Ref 5). For a plane quadratic element of constant thickness $\det J$ contains ξ^3 and η^3 terms. Therefore, only a 2nd order (2 x 2) Gauss rule, where the error is on the order of $2n$, or 4, is all that is required. However, when one uses low

order integration rules, zero energy deformation modes may develop (Ref 5). Consider an eight-noded rectangle using a second order (2 x 2) Gauss rule. Let the element be represented in ξ - η space and let the nodal degrees of freedom be assigned the values:

$$\begin{aligned}
 -u_1 &= u_3 = u_5 = -u_7 = v_1 = v_3 = -v_5 = -v_7 = 1 \\
 -v_2 &= -u_7 = v_6 = u_8 = \frac{1}{2} \\
 u_2 &= v_4 = u_6 = v_8 = 0
 \end{aligned}
 \tag{A-65}$$

(See Fig. A-4 for a representation of the element and the displacements.)

At the Gauss points, $\xi=\eta=\pm 0.5774$, all of the strains are zero. Since the Gauss points represent the element when its stiffness matrix is formed, the element offers no resistance at all to this particular deformation mode. This implies that the resulting stiffness matrix will be singular. If a zero-energy mode appears, it is usually superimposed on the deformation modes formed from actual nodal displacements.

This particular zero-energy mode is not compatible with the same mode in an adjacent element. The global assembly, therefore, will not have this zero-energy mode and the global stiffness matrix will not be singular. However, zero-energy modes that are compatible may be formed (Ref 5). These are detected by computing the eigenvalues of the global stiffness matrix. For a structure free of rigid body motion, there will be as many zero-energy

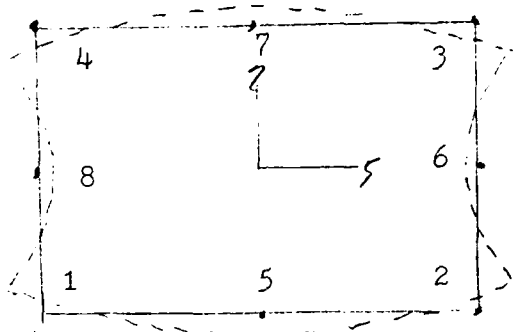


Figure A-4. Zero Energy Mode for an 8-Noded Isoparametric Element

modes as there are zero eigenvalues in the global stiffness matrix.

By selecting a third-order Gaussian quadrature, one avoids all of the zero-energy modes by eliminating the extraneous strains. The JALESE program makes use of a third-order Gaussian quadrature in performing the integration necessary to evaluate K . Figure A-5 shows the eight-noded element in ξ - η space with its Gaussian integration stations. Table A-I, which is Table 8.1 from Ref 13, shows the location of the Gaussian integration stations and their associated weight functions for each order, n .

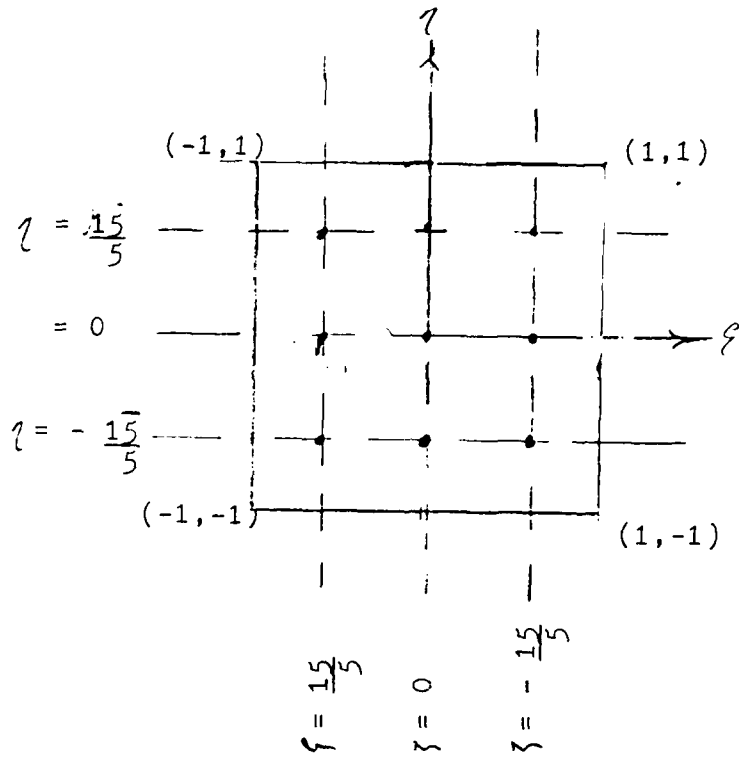


Figure A-5. Gaussian Integration Stations of an 8-Noded Isoparametric Element in ξ - ζ Space ($n=3$).

$$\int_{-1}^1 f(x) dx = \sum_{j=1}^n H_j f(a_j),$$

$\pm a$	n	H
0	$n = 1$	2.00000 00000 00000
0.57735 02691 89626	$n = 2$	1.00000 00000 00000
0.77459 86692 41483 0.00000 00000 00000	$n = 3$	0.55555 55555 55556 0.88888 88888 88889
0.86113 63115 94053 0.33998 10435 84856	$n = 4$	0.34785 48451 37454 0.65214 51548 62546
0.90617 98459 38664 0.53846 93101 05683 0.00000 00000 00000	$n = 5$	0.23692 68850 56189 0.47862 86704 99366 0.56888 88888 88889
0.93246 95142 03152 0.66120 93864 66265 0.23861 91860 83197	$n = 6$	0.17132 44923 79170 0.36076 15730 48139 0.46791 39345 72691
0.94910 79123 42759 0.74153 11855 99394 0.40584 51513 77397 0.00000 00000 00000	$n = 7$	0.12948 49661 68870 0.27970 53914 89277 0.38183 00303 05119 0.41795 91836 73469
0.96028 98564 97536 0.79666 64774 13627 0.52553 24099 16329 0.18343 46424 95650	$n = 8$	0.10122 85362 90376 0.22238 10344 53374 0.31370 66458 77887 0.36268 37833 78362
0.96816 02395 07626 0.83603 11073 26636 0.61337 14327 00590 0.32425 34234 03809 0.00000 00000 00000	$n = 9$	0.08127 43883 61574 0.18064 81606 94857 0.26061 06964 02935 0.31234 70770 40003 0.33023 93550 01260
0.97390 65285 17172 0.86506 33666 88985 0.67940 95682 99024 0.43339 53941 29247 0.14887 43389 81631	$n = 10$	0.06667 13443 08688 0.14945 13491 50581 0.21908 63625 15982 0.26926 67193 09996 0.29552 42247 14753

Table A-I. Weight Coefficients and Abscissae for Gaussian Quadrature (Ref 13)

Appendix B: Calculation of Equivalent Nodal Forces

The expression for the calculation of the equivalent nodal forces due to applied loading and body forces is:

$$\underline{q}^e = \int_{\text{vol}} \underline{B}^T \underline{\sigma} d(\text{vol}) - \int_{\text{vol}} \underline{N}^T \underline{b} d(\text{vol}) \quad (\text{B-1})$$

where \underline{q}^e denotes the equivalent nodal force vector, \underline{B} is the matrix that relates strain to nodal displacements, \underline{N} is the interpolation function vector, \underline{b} is the nodal force vector, and $\underline{\sigma}$ are the externally applied stresses.

Gravity and centrifugal "force" are two types of body forces. There are no body forces for the problem in this work. (Gravitational effects are neglected.) For an element at the boundary subject to a distributed loading q , virtual work considerations result in the equivalent nodal forces, $\underline{F}^{\text{eq}}$, to be expressed as:

$$\underline{F}^{\text{eq}} = \int_s \underline{q} \underline{N}^T ds \quad (\text{B-2})$$

where ds represents the incremental path length.

For the constant strain triangle, the calculation of the equivalent nodal forces becomes straightforward. Only the integration of constants is necessary, and, for a constant distributed load of magnitude q , the equivalent nodal forces become:

$$\underline{F}^{\text{eq}} = \underline{q} \ell \quad (\text{B-3})$$

where l is the length of surface that the load covers. This calculation is performed for each element and the loads at the nodes are summed. Figure B-1 illustrates an example of the calculation of the equivalent nodal force for a constant strain triangle.

For an eight-noded quadrilateral, integration must be performed to obtain the equivalent nodal forces. Consider the eight-noded quadrilateral boundary element under a constant distributed load, q , given in Fig. B-2.

The interpolation function, N_i , for the eight-noded quadrilateral is given by:

$$\begin{aligned} N_i &= \frac{1}{4}(1+\xi_i\xi)(1+\eta_i\eta)(\xi\xi_i+\eta\eta_i-1) & i = 1,2,3,4 \\ N_i &= \frac{1}{2}(1-\xi^2)(1+\eta\eta_i) & i = 5,7 \\ N_i &= \frac{1}{2}(1+\xi\xi_i)(1-\eta^2) & i = 6,8 \end{aligned} \quad (B-4)$$

At node point 3, $(\xi, \eta) = (1, 1)$ and

$$N_3 = \frac{1}{4}(1+\xi)(1+\eta)(\xi+\eta-1) \quad (B-5)$$

Along the upper surface, $\eta=1$. Therefore,

$$N_3 = \frac{1}{2}(\xi^2+\xi) \quad (B-6)$$

At node point 4, $(\xi, \eta) = (-1, 1)$ and

$$N_4 = \frac{1}{4}(1-\xi)(1+\eta)(-\xi+\eta-1) \quad (B-7)$$

Along the upper surface, $\eta=1$. Therefore,

$$N_4 = \frac{1}{2}(\xi^2-\xi) \quad (B-8)$$

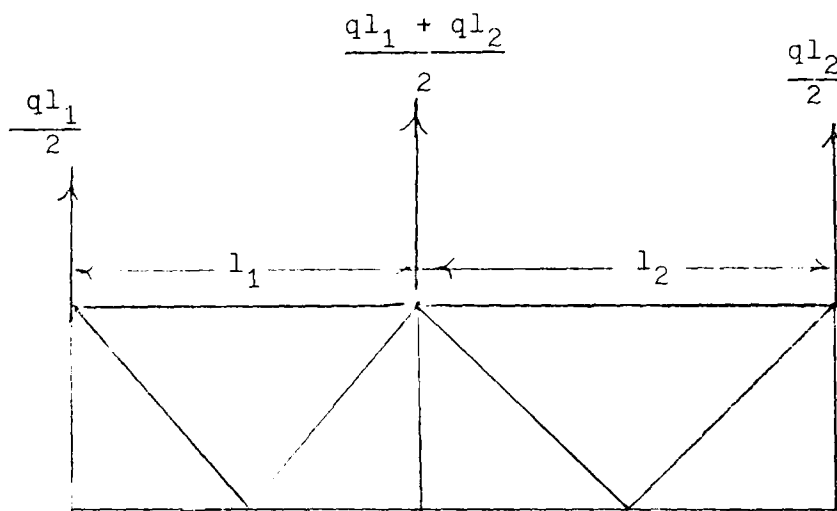


Figure B-1. Example of the Calculation of Equivalent Nodal Forces For the CST

At node point 7, $(\xi, \eta) = (0, 1)$. Along the upper surface, $\eta=1$. Therefore,

$$\begin{aligned} N_7 &= \frac{1}{2}(1-\xi^2)(1+\eta) \\ &= (1-\xi^2) \end{aligned} \quad (\text{B-9})$$

Now

$$\underline{F}^{eq} = \int q \underline{N}^T ds = \ell \int_{-1}^1 q \underline{N}^T ds \quad (\text{B-10})$$

where ℓ = length of element. Substitution results in:

$$\begin{pmatrix} F^{3eq} \\ F^{4eq} \\ F^{7eq} \end{pmatrix} = \ell q \int_{-1}^1 \begin{pmatrix} \frac{1}{2}(\xi^2 + \xi) \\ \frac{1}{2}(\xi^2 - \xi) \\ (1 - \xi^2) \end{pmatrix} d\xi \quad (\text{B-11})$$

Integration gives:

$$\begin{pmatrix} F^{3eq} \\ F^{4eq} \\ F^{7eq} \end{pmatrix} = q\ell \begin{pmatrix} \frac{1}{6} \\ \frac{1}{6} \\ \frac{4}{6} \end{pmatrix} \quad (\text{B-12})$$

Therefore, the equivalent nodal force is four times greater at the midside node than at the corner nodes.

As in the case for the constant strain triangle, the equivalent nodal forces are calculated for each element and the forces at the nodes are summed. An example of the calculation of equivalent nodal forces is shown in Fig. B-3.

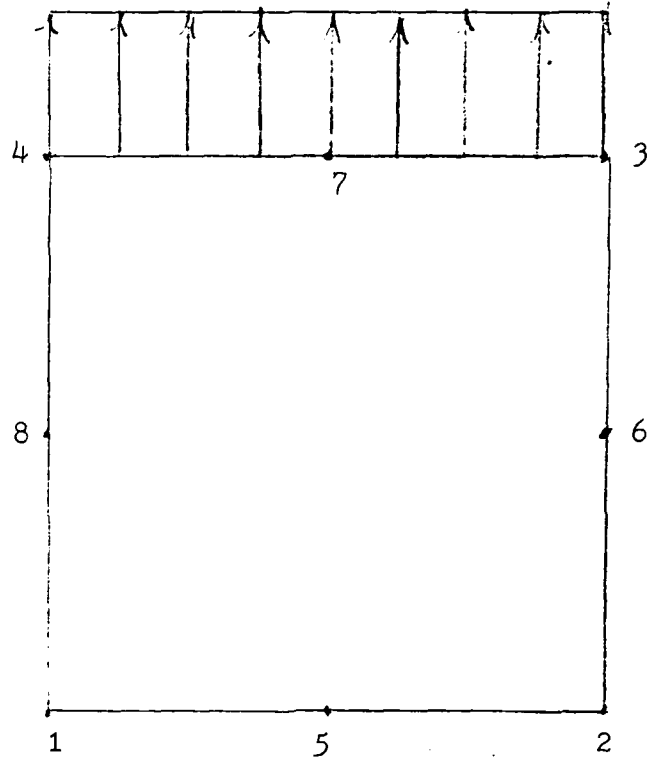
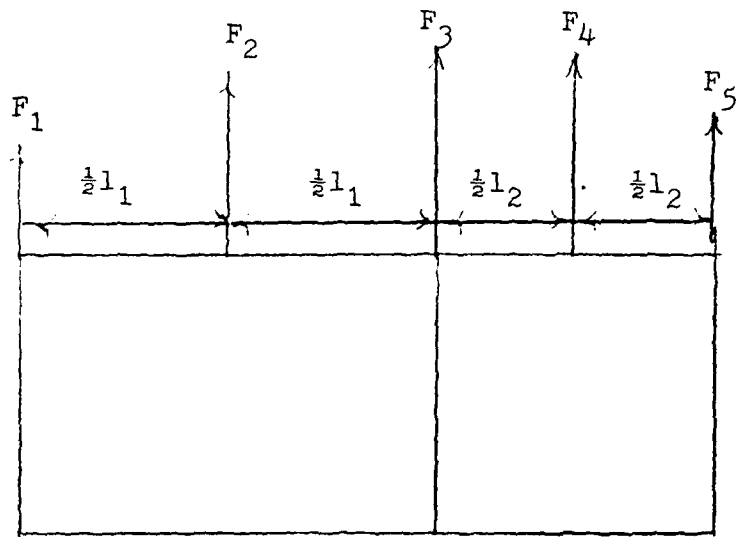


Figure B-2. 8-Noded Element at the Boundary Under Loading



$$\begin{aligned}
 F_1 &= 1/6 * (ql_1) \\
 F_2 &= 4/6 * (ql_1) \\
 F_3 &= 1/6 * (ql_1 + ql_2) \\
 F_4 &= 4/6 * (ql_2) \\
 F_5 &= 1/6 * (ql_2)
 \end{aligned}$$

Figure B-3. Example of the Calculation of Equivalent Nodal Forces for the 8-Noded Isoparametric Element

Appendix C: Users Guide for JALESE

The JALESE program is an elastic-plastic finite element code for plane stress or plane strain problems. Usage of the code is very straightforward. The data cards are punched up according to the users guide by Ahmad and Papaspyropoulos (Ref 1). There are some fine points to be noted, however, in the loading and execution of the problems.

Minimum usage of core memory space is of prime importance in achieving fast turnaround. In JALESE, the largest block of common memory is used by the stiffness matrix. The stiffness matrix array is called SK in JALESE and is stored in the block named NEW2. SK is a two by two array and is sized by SK (2*no. of nodes, 1 + semi-bandwidth) (half-bandwidth). Therefore, it is important that the user size the SK array for his particular problem.

To minimize the size of the stiffness array, it is important to keep the bandwidth small. This is accomplished by numbering the nodes appropriately. For a rectangular array, the best node numbering scheme is horizontal (left to right). If a radial "cobweb" array is used, it is best to number the nodes along the concentric curves. If a saw-tooth pattern is desired, extreme care must be used in formulating the mesh in order to avoid a large semi-bandwidth.

It has not been found worthwhile to attempt further reductions in core memory usage by reducing the size of

the blocks that contain the element connectivity, nodal location, uniaxial stress-strain curve definition points, etc. Much work is required to insure that the common blocks remain the same length from subroutine to subroutine. Eighty percent of the memory is used to store the stiffness matrix. This is where one should direct one's efforts to reduce core memory requirements.

Besides minimizing the size of the stiffness array, an efficient numbering scheme for the nodes that reduces the semi-bandwidth will also minimize computer processing time. The JALESE program uses Gaussian elimination to solve for the nodal displacements. If the semi-bandwidth is reduced, the computer will have fewer equations to solve.

It has been determined that the core memory (number of octal words) required to load the JALESE program in its published form is 270000. This is far too large to load on the CYBER 74 (CSB); however, it will load on the CYBER 175 (CSA). Unfortunately, the job will not be run until the evening shift and if the system is overloaded (which it usually is), the job will not be run until the weekend shift. In the current work, the JALESE program was modified by cutting down the size of the SK array and the program was loaded with a core memory size of 205100.

It was also determined that 200 seconds of central processor time and 75 seconds of input-output time had to be specified on the job control card. The exact amount of

processor and input-output time actually used can be determined by examining the dayfile at the end of the print-out. One could, therefore, reduce the time specifications for repeat runs and cut down turnaround time. It is advisable, however, to overspecify by 25%; if the computer is overloaded and the job is in the queues for a long time, more execution and IO time will be used.

If a particular problem has more than sixty elements, the stress and strain tolerances must be increased from the default value of 0.001. If the crack-tip singularity elements are used, one must alter the tolerance if more than fifty elements are used. If this is not done, the initial stress or strain solution technique will not converge to a solution. However, since the program only prints out four significant figures, changing the tolerance does not greatly alter the results.

The JALESE program as it is currently published does not have a plotting routine. The work with VISCO, which does have a plotting routine, showed that a plot of the mesh was very useful in debugging the input data. Therefore, a plotting subroutine was written for use with a modified JALESE program. This subroutine is listed in Fig. C-1. To use this subroutine, it is necessary to add a line of code that reads the variables SCAL and NSUP. This subroutine is compatible with the CALCOMP 565 plotter. It can be easily modified for use with the CALCOMP 1036 or CALCOMP 1038 plotters.

```

SUBROUTINE PLOTOUT(SCAL, NSUP)
COMMON/NEWL/NPUI, NLEEM, NBOUN, IR, NDOVC, NBAND, NFOUNS
COMMON/VINOT/NO(205,8)
COMMON/HUGLL/X(333), Y(333)
CALL FLOT(1., 1., -3)
CALL FACTOR(SCAL)
HGT = .1/SCAL
DO I=1, NLEEM
K1=NOD(I, 1)
K2=NOD(I, 2)
K3=NOD(I, 3)
K4=NOD(I, 4)
CALL FLOT(X(K1), Y(K1), +3)
CALL FLOT(X(K2), Y(K2), +2)
CALL FLOT(X(K3), Y(K3), +2)
CALL FLOT(X(K4), Y(K4), +2)
CALL FLOT(X(K1), Y(K1), +2)
CALL FLOT(X(K1), Y(K2), +3)
XD1=ABS(Y(K1)-X(K2))*SCAL
XD2=ABS(X(K3)-X(K2))*SCAL
XD3=ABS(X(K4)-Y(K3))*SCAL
XD4=ABS(X(K4)-X(K1))*SCAL
IF(NRUP.EQ.0)GOTO 499
IF(XD1.LT..25.AND.XD2.LT..25.AND.XD3.LT..1.AND.XD4.LT..25)
130 TO 199
XCENT=(X(K1)+X(K2)+X(K3)+X(K4))/4.-.1/SCAL
YCENT=(Y(K1)+Y(K2)+Y(K3)+Y(K4))/4.
RATIO=T
IF(RATIO.LT.1.)XCENT=XCENT+.1/SCAL
CALL NUMBER(XCENT, YCENT, HGT, RATIO, '.-1)
CONTINUE
CALL FACTOR(1.)
CALL FLOT(1.)
RETURN
END

```

Figure C-1. Plotting Subroutine for the JALESE Program

As an example, the following data cards for the two element uniaxial test case using IN-100 are shown. The user is urged to examine the user's guide (Ref 1).

Card 1: FORMAT 9I4, F20.10

NPRTY=1
NELEM=2
NPOIN=4
NBOUN=2
NCONC=2
NCPOIN=4
NQPTS=0
JPATHS=0
IREST=0
GTOL=0.001

Card 1' (used when plotting subroutine has been added to program)

FREE FORMAT

SCAL=11. (Scaling Factor for CALCOMP Plotter)
NSUP=1 (0 suppresses printout of element numbers)

Card 2: FORMAT 3F20.5, I4

E=26300.0
P=0.3
YST=130.0
NSSPT=4

Card 3: FORMAT 4F20.5

SRS(1)=130.0
SRN(1)=0.00494
SRS(2)=152.0
SRN(2)=0.00716

Card 4: FORMAT 4F20.5

SRS(3)=164.0
SRN(3)=0.01494
SRS(4)=164.0
SRN(4)=1.00000

Card 5: FORMAT 3I4

NF=1
NB(1)=1
NB(2)=1

Card 6: FORMAT 3I4

NF=2
NB(1)=1
NB(2)=0

Card 7: FORMAT I4, 2F20.5

NF=3
U(1)=0.150
U(2)=0.0

Card 8: FORMAT I4, 2F20.5

NF=4
U(1)=0.150
U(2)=0.0

Cards 9,10,11,12: FORMAT I4, 2F10.5

I=1
X(1)=0.0
Y(1)=0.0

I=2
X(2)=0.0
Y(2)=1.0

I=3
X(3)=1.0
Y(3)=0.0

I=4
X(4)=1.0
Y(4)=1.0

Cards 13,14: FORMAT 9I4, F10.5

NOD(1,1)=1
NOD(1,2)=3
NOD(1,3)=4
NOD(1,4)=4
NOD(1,5)=0
NOD(1,6)=0
NOD(1,7)=0
NOD(1,8)=0
NEP=1
THICK=0.3

NOD(2,1)=1
NOD(2,2)=4
NOD(2,3)=4
NOD(2,4)=2
NOD(2,5)=0
NOD(2,6)=0
NOD(2,7)=0
NOD(2,8)=0
NEP=1
THICK=0.3

Card 15: FORMAT I4, 2F20.10

N=3
FX=0.600
FY=0.0000

Card 16: FORMAT I4, 2F10.10

N=4
FX=0.600
FY=0.000

Cards 15 and 16 are repeated until the desired loading has been achieved. The data cards are terminated with a blank card.

To run the program, the following job control cards were used. Note that the version of the program used was called JALESELONGEST. The cards to activate the CALCOMP plotter calls are also shown. For more information on the CALCOMP plotter see the CALCOMP Plotter User's Guide.

HDG,CM207000,T200,I0100. M790098,GANS,55533
ATTACH,A,JALESELONGEST.
ATTACH,CCPLOT,CCPLOT56X,ID=LIBRARY,SN=ASD.
LIBRARY,CCPLOT.
FTN,I=A,B=DOG.
MAP,PART.
DOG,PL=10000.
7/8/9
Data Cards
7/8/9
6/7/8/9

VITA

Howard Dwight Gans was born on 29 March 1958 in Chicago, Illinois. He graduated with honors from Niles Township High School North in June 1976. He then attended the Massachusetts Institute of Technology in Cambridge, Massachusetts from which he was awarded the degree of Bachelor of Science in Aeronautics and Astronautics in June 1980. Upon graduation, he received a commission in the United States Air Force through the Reserve Officers Training Corps (ROTC) program, and was awarded the honor of Distinguished Graduate. In June 1980 he entered the School of Engineering, Air Force Institute of Technology, to pursue a masters degree in Aeronautical Engineering.

Permanent Address: 2812 Woodland Drive
Northbrook, IL 60062

Unclassified

SECURITY CLASSIFICATION OF THIS PAGE (When Data Entered)

REPORT DOCUMENTATION PAGE		READ INSTRUCTIONS BEFORE COMPLETING FORM
1. REPORT NUMBER AFIT/GAE/AA/81D-10	2. GOVT ACCESSION NO.	3. RECIPIENT'S CATALOG NUMBER
4. TITLE (and Subtitle) ELASTIC-PLASTIC FINITE ELEMENT MODEL COMPARISONS IN FRACTURE MECHANICS		5. TYPE OF REPORT & PERIOD COVERED MS Thesis
		6. PERFORMING ORG. REPORT NUMBER
7. AUTHOR(s) Howard D. Gans 2LT USAF		8. CONTRACT OR GRANT NUMBER(s)
9. PERFORMING ORGANIZATION NAME AND ADDRESS Air Force Institute of Technology (AFIT-EN) Wright-Patterson AFB, Ohio 45433		10. PROGRAM ELEMENT, PROJECT, TASK AREA & WORK UNIT NUMBERS
11. CONTROLLING OFFICE NAME AND ADDRESS		12. REPORT DATE December, 1981
		13. NUMBER OF PAGES 133
14. MONITORING AGENCY NAME & ADDRESS (if different from Controlling Office) Air Force Wright Aeronautical Laboratory AFWAL/MLLN Air Force Materials Laboratory Wright-Patterson AFB, Ohio 45433		15. SECURITY CLASS. (of this report) Unclassified
		15a. DECLASSIFICATION DOWNGRADING SCHEDULE
16. DISTRIBUTION STATEMENT (of this Report) Approved for public release; distribution unlimited		
17. DISTRIBUTION STATEMENT (of the abstract entered in Block 20, if different from Report) Approved for public release (NS) Distribution Statement: Approved for public release (NS)		
18. SUPPLEMENTARY NOTES Approved for public release; IAW AFR 190-17 Frederic C. Lynch, Major, USAF Director of Public Affairs 28 JAN 1982		
19. KEY WORDS (Continue on reverse side if necessary and identify by block number) Crack Tip Finite Element Models Elastic-Plastic Analysis Computational Comparisons		
20. ABSTRACT (Continue on reverse side if necessary and identify by block number) Stress near a crack tip in plasticity was analyzed using three different finite element modelings; a constant strain strain viscoplastic triangle, an eight-noded elastic-plastic quadrilateral and a crack tip elastic-plastic singularity element. The specimen under consideration was a center cracked plate made from IN-100. The half-crack length was 0.1367 in (3.472 mm). An elastic solution was formulated and two		

Unclassified

SECURITY CLASSIFICATION OF THIS PAGE (When Data Entered)

different loadings to generate plasticity were considered. Fine mesh and coarse mesh solutions for the higher order elements were generated and compared. Comparisons were made based on an equal number of degrees of freedom in two specific regions referred to as the near field and the far field regions.

It was determined that the elements whose elastic solutions conformed best to linear elastic fracture mechanics predictions were the constant strain triangle and the eight-noded quadrilateral in a fine mesh. The crack tip element did not perform as well as was expected. For the plastic analysis, the constant strain triangle exhibited the largest plastic region and gave the most accurate stress profiles. The eight-noded isoparametric element came within fifteen percent of the stress levels generated from the constant strain triangle. The stress singularity that is characteristic of the crack tip element forced that element to behave unnaturally stiff in plasticity.

Because it is not as stiff as either the crack tip element or the eight-noded element, the constant strain triangle offered the most accurate solutions. The CST solution required the least amount of computational resources. Though the isoparametric element mesh was easier to formulate and gave fairly accurate answers elastically and plastically, it was determined that the constant strain triangle in a fine mesh offered the best solution to elastic-plastic finite element problems for the center cracked plate.

Unclassified

SECURITY CLASSIFICATION OF THIS PAGE (When Data Entered)

END

DATE
FILMED

3-82

DTIC